NONLINEAR MODELING, IDENTIFICATION, AND COMPENSATION FOR
FRICTIONAL DISTURBANCES

By

CHARU MAKKAR

A THESIS PRESENTED TO THE GRADUATE SCHOOL
OF THE UNIVERSITY OF FLORIDA IN PARTIAL FULFILLMENT
OF THE REQUIREMENTS FOR THE DEGREE OF
MASTER OF SCIENCE

UNIVERSITY OF FLORIDA

2006

This work is dedicated to my parents for their unconditional love, unquestioned support and unshaken belief in me.

ACKNOWLEDGMENTS

TABLE OF CONTENTS

CHAPTER

APPENDIX

LIST OF TABLES

LIST OF FIGURES

Abstract of Thesis Presented to the Graduate School
of the University of Florida in Partial Fulfillment of the
Requirements for the Degree of Master of Science

NONLINEAR MODELING, IDENTIFICATION, AND COMPENSATION FOR
FRICTIONAL DISTURBANCES

By

Charu Makkar

May 2006

Chair: Warren E. Dixon
Major Department: Mechanical and Aerospace Engineering

For high-performance engineering systems, model-based controllers are
typically required to accommodate for the system nonlinearities. Unfortunately,
developing accurate models for friction has been historically challenging. Despite
open debates in Tribology regarding the continuity of friction, typical models
developed so far are piecewise continuous or discontinuous. Motivated by the fact
that discontinuous and piecewise continuous friction models can be problematic
for the development of high-performance controllers, a new model for friction is
proposed. This simple continuously differentiable model represents a foundation
that captures the major effects reported and discussed in friction modeling and
experimentation. The proposed model is generic enough that other subtleties such
as frictional anisotropy with sliding direction can be addressed by mathematically
distorting this model without compromising the continuous differentiability. From
literature, it is known that if the friction effects in the system can be accurately
modeled, there is an improved potential to design controllers that can cancel
the effects, whereas excessive steady-state tracking errors, oscillations, and limit
cycles can result from controllers that do not accurately compensate for friction.

A tracking controller is developed in Chapter 3 for a general Euler-Lagrange system based on the developed continuously differentiable friction model with uncertain nonlinear parameterizable terms. To achieve the semi-global asymptotic tracking result, a recently developed integral feedback compensation strategy is used to identify the friction effects on-line, assuming exact model knowledge of the remaining dynamics. A Lyapunov-based stability analysis is provided to conclude the tracking and friction identification results. Experimental results illustrate the tracking and friction identification performance of the developed controller.

The tracking result in Chapter 3 is further extended to include systems with unstructured uncertainties while eliminating the known dynamics assumption. The general trend for previous control strategies developed for uncertain dynamics in nonlinear systems is that the more unstructured the system uncertainty, the more control effort (i.e., high gain or high frequency feedback) is required to reject the uncertainty, and the resulting stability and performance of the system are diminished (e.g., uniformly ultimately bounded stability). The result in Chapter 4 is the first result that illustrates how the amalgamation of an adaptive model-based feedforward term with a high gain integral feedback term can be used to yield an asymptotic tracking result for systems that have mixed unstructured and structured uncertainty. Experimental results are provided that illustrate a reduced root mean squared tracking error.

CHAPTER 1
INTRODUCTION

The class of Euler-Lagrange systems considered in this thesis are described by the following nonlinear dynamic model:

$$M(q)\ddot{q} + V_m(q, \dot{q})\dot{q} + G(q) + f(\dot{q}) = \tau(t). \tag{1–1}$$

In (1–1), $M(q) \in \mathbb{R}^{n \times n}$ denotes the inertia matrix, $V_m(q, \dot{q}) \in \mathbb{R}^{n \times n}$ denotes the centripetal-Coriolis matrix, $G(q) \in \mathbb{R}^n$ denotes the gravity vector, $f(\dot{q}) \in \mathbb{R}^n$ denotes friction vector, $\tau(t) \in \mathbb{R}^n$ represents the torque input control vector, and $q(t)$, $\dot{q}(t)$, $\ddot{q}(t) \in \mathbb{R}^n$ denote the link position, velocity, and acceleration vectors, respectively. For high-performance engineering systems, model-based controllers (see Dixon et al. [16]) are typically used to accommodate for the system nonlinearities. In general, either accurate models of the inertial effects can be developed or numerous continuous adaptive and robust control methods can be applied to mitigate the effects of any potential mismatch in the inertial parameters. Unfortunately, developing accurate models for friction has been historically problematic. In fact, after centuries of theoretical and experimental investigation, a general model for friction has not been universally accepted, especially at low speeds where friction effects are exaggerated. In fact, Armstrong-Helouvry [1] examined the destabilizing effects of certain friction phenomena (i.e., the Stribeck effect) at low speeds. To further complicate the development of model-based controllers for high-performance systems, friction is often modeled as discontinuous; thus, requiring model-based controllers to be discontinuous to compensate for the effects.

Motivated by the desire to develop an accurate representation of friction in systems, various control researchers have developed different analytical models, estimation methods to identity friction effects, and adaptive and robust methods to compensate for or reject the friction effects. In general, the dominant friction components that have been modeled include: *static friction* (i.e., the torque that opposes the motion at zero velocity), *Coulomb friction* (i.e., the constant motion opposing torque at non-zero velocity), *viscous friction* (i.e., when full fluid lubrication exists between the contact surfaces), *asymmetries* (i.e., different friction behavior for different directions of motion), *Stribeck effect* (i.e., at very low speed, when partial fluid lubrication exists, contact between the surfaces decreases and thus friction decreases exponentially from stiction), and *position dependence* (oscillatory behavior of the friction torque due to small imperfections on the motor shaft and reductor centers, as well as the elastic deformation of ball bearings).

Classical friction models are derived from static maps between velocity and friction force. From a comprehensive survey of friction models in control literature (see Armstrong-Helouvry [1] and Armstrong-Helouvry et al. [2]), some researchers believe that dynamic friction effects are necessary to complete the friction model. Several dynamic friction models have been proposed (see Bliman and Sorine [5] and Canudas de Wit et al. [8]). These models combine the Dahl model (see Dahl [14]) with the arbitrary steady-state friction characteristics of the bristle-based LuGre model proposed by Canudas de Wit et al. [8]. A recent modification to the LuGre model is given in the Leuven model by Swevers et al. [52] that incorporates a hysteresis function with non-local memory unlike the Lu-Gre model. The Leuven model was later experimentally confirmed by Ferretti et al. [21]. However, a modification to the Leuven model is provided by Lampaert et al. [34] that replaces the stack mechanism used to implement the hysteresis by the more efficient Maxwell slip model. Another criticism to the LuGre model has been recently

raised by Dupont et al. [18], who underline a nonphysical drift phenomenon that arises when the applied force is characterized by small vibrations below the static friction limit. Recently single and multistate integral friction models have been developed by Ferretti and Magnani et al. [22] based on the integral solution of the Dahl model. However, these friction models are based on the assumption that the friction coefficient is constant with sliding speed and have a singularity at the onset of slip. Unfortunately, each of the aforementioned models are discontinuous (i.e., a signum function of the velocity is used to assign the direction of friction force such as the results by Dupont et al. [18], Ferretti et al.[22], Lampaert et al. [34], and Swevers et al. [52]), and many other models are only piecewise continuous (e.g., the LuGre model in [8]). As stated previously, the use of discontinuous and piecewise continuous friction models is problematic for the development of high-performance continuous controllers.

Chapter 2 and the preliminary efforts by Makkar et al. [42] and Makkar and Dixon et al. [43] provide a first step at creating a continuously differentiable friction model that captures a number of essential aspects of friction without involving discontinuous or piecewise continuous functions. The proposed model is generic enough that other subtleties such as frictional anisotropy with sliding direction can be addressed by mathematically distorting this model without compromising the continuous differentiability.

If the friction effects in a system can be accurately modeled, there is an improved potential to design controllers that can cancel the effects (e.g., model-based controllers); whereas, excessive steady-state tracking errors, oscillations, and limit cycles can result from controllers that do not accurately compensate for friction. Given the past difficulty in accurately modeling and compensating for friction effects, researchers have proposed a variety of (typically offline) friction estimation schemes with the objective of identifying the friction effects. For

example, an offline maximum likelihood, frequency-based approach (differential binary excitation) is proposed by Chen et al. [12] to estimate Coulomb friction effects. Another frequency-based offline friction identification approach was proposed by Kim and Ha [31]. Specifically, the approach by Kim and Ha [31] uses a kind of frequency-domain linear regression model derived from Fourier analysis of the periodic steady-state oscillations of the system. The approach by Kim and Ha [31] requires a periodic excitation input with sufficiently large amplitude and/or frequency content. A new offline friction identification tool is proposed by Kim et al. [32] where the static-friction models are not required to be linear parameterizable. However the offline optimization result by Kim et al. [32] is limited to single degree-of-freedom systems where the initial and final velocity are equal. Another frequency domain identification strategy developed to identify dynamic model parameters for presliding behavior is given by Hensen and Angelis et al. [26]. Additional identification methods include least-squares as developed by Canudas de Wit and Lichinsky [10] and Kalman filtering by Hensen et al. [27].

In addition to friction identification schemes, researchers have developed adaptive, robust, and learning controllers to achieve a control objective while accommodating for the friction effects, but not necessarily identifying friction. For example, given a desired trajectory that is periodic and not constant over some interval of time, the development by Cho et al. [13] provides a learning control approach to damp out periodic steady-state oscillations due to friction. As stated by Cho et al. [13], a periodic signal is applied to the system and when the system reaches a steady-state oscillation, the learning update law is applied. Liao et al. [37] proposed a discontinuous linearizing controller along with an adaptive estimator to achieve an exponentially stable tracking result that estimates the unknown Coulomb friction coefficient. However, Zhang and Guay [60] describe a technical error in the result presented by Liao et al. [37] that invalidates the

result. Additional development is provided by Zhang and Guay [60] that modifies the result by Liao et al. [37] to achieve asymptotic Coulomb friction coefficient estimation provided a persistence of excitation condition is satisfied. Tomei in [53] proposed a robust adaptive controller where only instantaneous friction is taken into account (dynamic friction effects are not included).

Motivated by the desire to include dynamic friction models in the control design, numerous researchers have embraced the LuGre friction model proposed by Canudas de Wit et al. [8]. For example, the result by Tomei [53] was extended in [54] to include the LuGre friction model proposed by Canudas de Wit et al. [8], resulting in an asymptotic tracking result for square integrable disturbances. Robust adaptive controllers were also proposed by Jain et al. [29] and Sivakumar and Khorrami [50] to account for the LuGre model. Canudas et al. investigated the development of observer-based approaches for the LuGre model in [8]. Canudas and Lichinsky in [9] proposed an adaptive friction compensation method, and Canudas and Kelly in [11] proposed a passivity-based friction compensation term to achieve global asymptotic tracking using the LuGre model. Barabanov and Ortega in [4] developed necessary and sufficient conditions for the passivity of the LuGre model. Three observer-based control schemes were proposed by Vedagarbda et al. [56] assuming exact model knowledge of the system dynamics. The results by Vedagarbda et al. [56] were later extended to include two adaptive observers to account for selected uncertainty in the model. The observer-based design in Vedagarbda et al. [56] was further extended by Feemester et al. [20]. Specifically, a partial-state feedback exact model knowledge controller was developed to achieve global exponential link position tracking of a robot manipulator by Feemster et al. [20]. Two adaptive, partial-state feedback global asymptotic controllers were also proposed in [20] that compensate for selected uncertainty in the system model. In addition, a new adaptive control technique was proposed by Feemster et al. [20] to

compensate for the nonlinear parameterizable Stribeck effect, where the average square integral of the position tracking errors were forced to an arbitrarily small value.

In Chapter 3 and in the preliminary results by Makkar et al. [40] and Makkar and Dixon et al. [41], a tracking controller is developed for a general Euler-Lagrange system that contains the new continuously differentiable friction model with uncertain nonlinear parameterizable terms that was developed in Chapter 2. The continuously differentiable property of the proposed model enabled the development of a new identification scheme based on a new integral feedback compensation term. A semi-global tracking result is achieved while identifying the friction on-line, assuming exact model knowledge of the remaining dynamics.

The control development in Chapter 3 is based on the assumption of exact model knowledge of the system dynamics except friction. The control of systems with uncertain nonlinear dynamics, however, is still a much researched area of focus. For systems with dynamic uncertainties that can be linear parameterized, a variety of adaptive (e.g., see Krstic [33], Sastry and Bodson [47], and Slotine et al. [51]) feedforward controllers can be utilized to achieve an asymptotic result. Some recent adaptive control results have also targeted the application of adaptive controllers for nonlinearly parameterized systems (see Lin and Qian [38]). Learning controllers have been developed for systems with periodic disturbances (see Antsaklis et al. [3]), and recent research has focused on the use of exosystems by Serrani et al. [49] to compensate for disturbances that are the solution of a linear time-invariant system with unknown coefficients. A variety of methods have also been proposed to compensate for systems with unstructured uncertainty including: various sliding mode controllers (e.g., see Slotine and Li [51], and Utkin [55]), robust control schemes (see Qu [46]), and neural network and fuzzy logic controllers (see Lewis et al. [36]). From a review of these approaches a general

trend that can be determined is that controllers developed for systems with more unstructured uncertainty will require more control effort (i.e., high gain or high frequency feedback) and yield reduced performance (e.g., uniformly ultimately bounded stability).

A significant outcome of the new control structure developed by Xian and Dawson et al. [57] is that asymptotic stability is obtained despite a fairly general uncertain disturbance. This technique was used by Cai et al. [7] to develop a tracking controller for nonlinear systems in the presence of additive disturbances and parametric uncertainties under the assumption that the disturbances are C^2 with bounded time derivatives. Xian et al. [58] utilized this strategy to propose a new output feedback discontinuous tracking controller for a general class of nonlinear mechanical (i.e., second-order) systems whose uncertain dynamics are first-order differentiable. Zhang et al. [59] combined the high gain feedback structure with a high gain observer at the sacrifice of yielding a semi-global uniformly ultimately bounded result. This particular high gain feedback method has also been used as an identification technique. For example, the method has been applied to identify friction (see Makkar et al. [40] and Makkar and Dixon et al. [41]), for range identification in perspective and paracatadioptric vision systems (e.g., see Dixon et al. [17], and Gupta et al. [25]), and for fault detection and identification (e.g., see McIntyre et al. [44]).

The result in Chapter 4 and the preliminary results in Patre et al. [45] is motivated by the desire to include some knowledge of the dynamics in the control design as a means to improve the performance and reduce the control effort while eliminating the assumption that the dynamics of the system is completely known. For systems that include some dynamics that can be segregated into structured (i.e., linear parameterizable) and unstructured uncertainty, this result illustrates how a new controller, error system, and stability analysis can be crafted to include

a model-based adaptive feedforward term in conjunction with the high gain integral feedback technique to yield an asymptotic tracking result. This chapter presents the first result that illustrates how the amalgamation of these compensation methods can be used to yield an asymptotic result. Experimental results are presented to reinforce these heuristic notions.

CHAPTER 2
MODELING OF NONLINEAR UNCERTAINTY-FRICTION

Friction force discontinuities have been debated for at least three centuries
dating back to the published works by Amonton in 1699 (e.g., see the classic text
by Bowden and Tabor [6]). Modern publications assume the sliding motion between
solids occurs at a large number of very small and discrete contacts. In contrast
to popular and simple models that assume a structural interaction across regular
and repeating surface features, the contact across engineering surfaces is known
to occur on the tops of asperities or surface protuberances, which, like fractals,
are distributed across all length scales. The number of contacts for engineering
systems is enormous, which led to the seminal work by Greenwood and Williamson
[24], who treated the distributions of these contacts using statistical distributions.
These functions were integrated to give a continuous expression for the relationship
between contact area and pressure. During sliding, and in particular at the
initiation of gross motion (i.e., pre-sliding), the dynamics of individual asperity
contacts breaking and forming is of great theoretical interest; however, due to
the large number of contacts in engineering systems, the dynamics are treated as
continuous following classical statistical methods.

This chapter provides a first step at creating a continuously differentiable
friction model that captures a number of essential aspects of friction without
involving discontinuous or piecewise continuous functions. In unlubricated or
boundary lubricated sliding, wear is inevitable. The proposed friction model
contains time-varying coefficients that can be developed (e.g., modeled by a
differential equation) to capture spatially and temporally varying effects due to
wear. This continuously differentiable model represents a foundation that captures

the major effects reported and discussed in friction modeling and experimentation. The proposed model is generic enough that other subtleties such as frictional anisotropy with sliding direction can be addressed by mathematically distorting this model without compromising the continuous differentiability.

This chapter is organized as follows. The friction model and the associated properties are provided in Section 2.1. The generality of the model is demonstrated through a numerical simulation in Section 2.2. Specifically, numerical simulations are provided for different friction model parameters to illustrate the different effects that the model captures. Section 2.3 describes that the developed model approximates the experimental results obtained in Makkar et al. [41].

2.1   Friction Model and Properties

The proposed model for the friction term $f(\dot{q})$ in (1–1):

$$f(\dot{q}) = \gamma_1(\tanh(\gamma_2\dot{q}) - \tanh(\gamma_3\dot{q})) + \gamma_4\tanh(\gamma_5\dot{q}) + \gamma_6\dot{q} \qquad (2\text{--}1)$$

where $\gamma_i \in \mathbb{R}\ \forall i = 1, 2, ...6$ denote unknown positive constants[1] . The friction model in (2–1) has the following properties.

- It is continuously differentiable and not linear parameterizable.

- It is symmetric about the origin.

- The static coefficient of friction can be approximated by the term $\gamma_1 + \gamma_4$.

- The term $\tanh(\gamma_2\dot{q}) - \tanh(\gamma_3\dot{q})$ captures the Stribeck effect where the friction coefficient decreases from the static coefficient of friction with increasing slip velocity near the origin.

- A viscous dissipation term is given by $\gamma_6\dot{q}$.

- The Coulombic friction is present in the absence of viscous dissipation and is modeled by the term $\gamma_4\tanh(\gamma_5\dot{q})$.

---

[1] These parameters could also be time-varying.

- The friction model is dissipative in the sense that a passive operator $\dot{q}(t) \rightarrow$ $f(\cdot)$ satisfies the following integral inequality [4]

$$\int_{t_0}^{t} \dot{q}(\tau) f(\dot{q}(\tau)) d\tau \geq -c^2$$

where c is a positive constant, provided $\dot{q}(t)$ is bounded.

Figures 2–1 and 2–2 illustrate the sum of the different effects and characteristics of the friction model. Figure 2–3 shows the flexibility of such a model.

2.2 Stick-Slip Simulation

The qualitative mechanisms of friction are well-understood. To illustrate how the friction model presented in (2–1) exhibits these effects, various numerical simulations are presented in this section. The system considered in Figure 2–4 is a simple mass-spring system, in which a unit mass M is attached to a spring with stiffness k resting on a plate moving with a velocity $\dot{x}_p(t)$ in the positive X direction, which causes the block to move with a velocity $\dot{x}_b(t)$ in the same direction. The modeled system can be compared to a mass attached to a fixed spring moving on a conveyor belt. The plate is moving with a velocity that slowly increases and saturates, given by the following relation:

$$\dot{x}_p = 1 - e^{-0.1t}.$$

The system described by Figure 2–4 is modelled as follows:

$$M\ddot{x}_b(t) + kx_b(t) - Mgf(\dot{x}_p(t) - \dot{x}_b(t)) = 0$$

where the term $\dot{x}_p(t) - \dot{x}_b(t)$ represents the slip velocity, (i.e., the difference between the plate velocity and block velocity at any instant of time). To demonstrate the flexibility of the model, model parameters were varied in order to capture the Stribeck effect, Coulombic friction effect and viscous dissipation. For example,
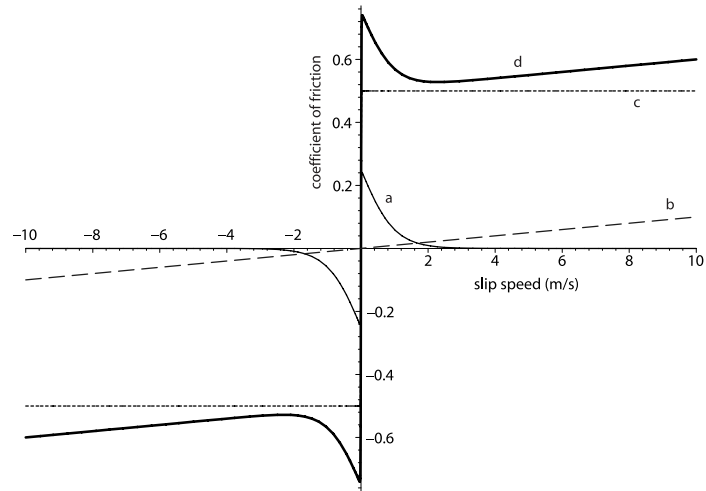
Figure 2–1: Friction model as a composition of different effects including: a) Stribeck effect, b) viscous dissipation, c) Coulomb effect, and d) the combined model.
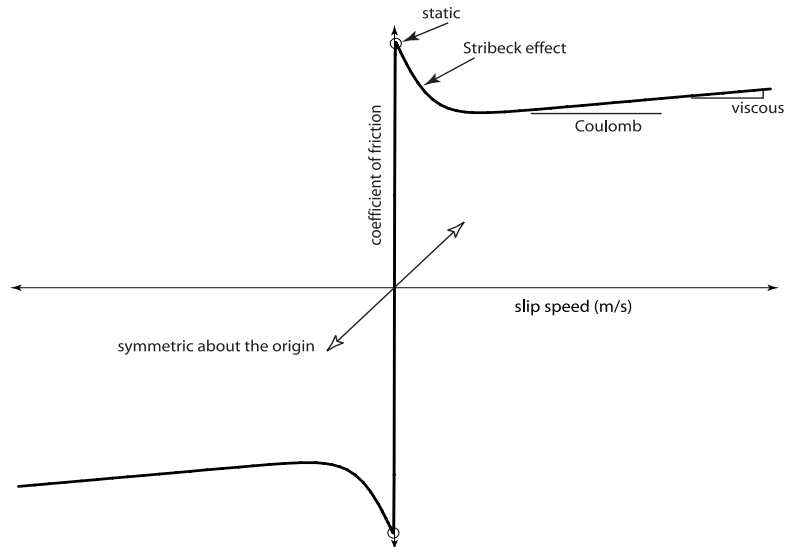
Figure 2–2: Characteristics of the friction model.
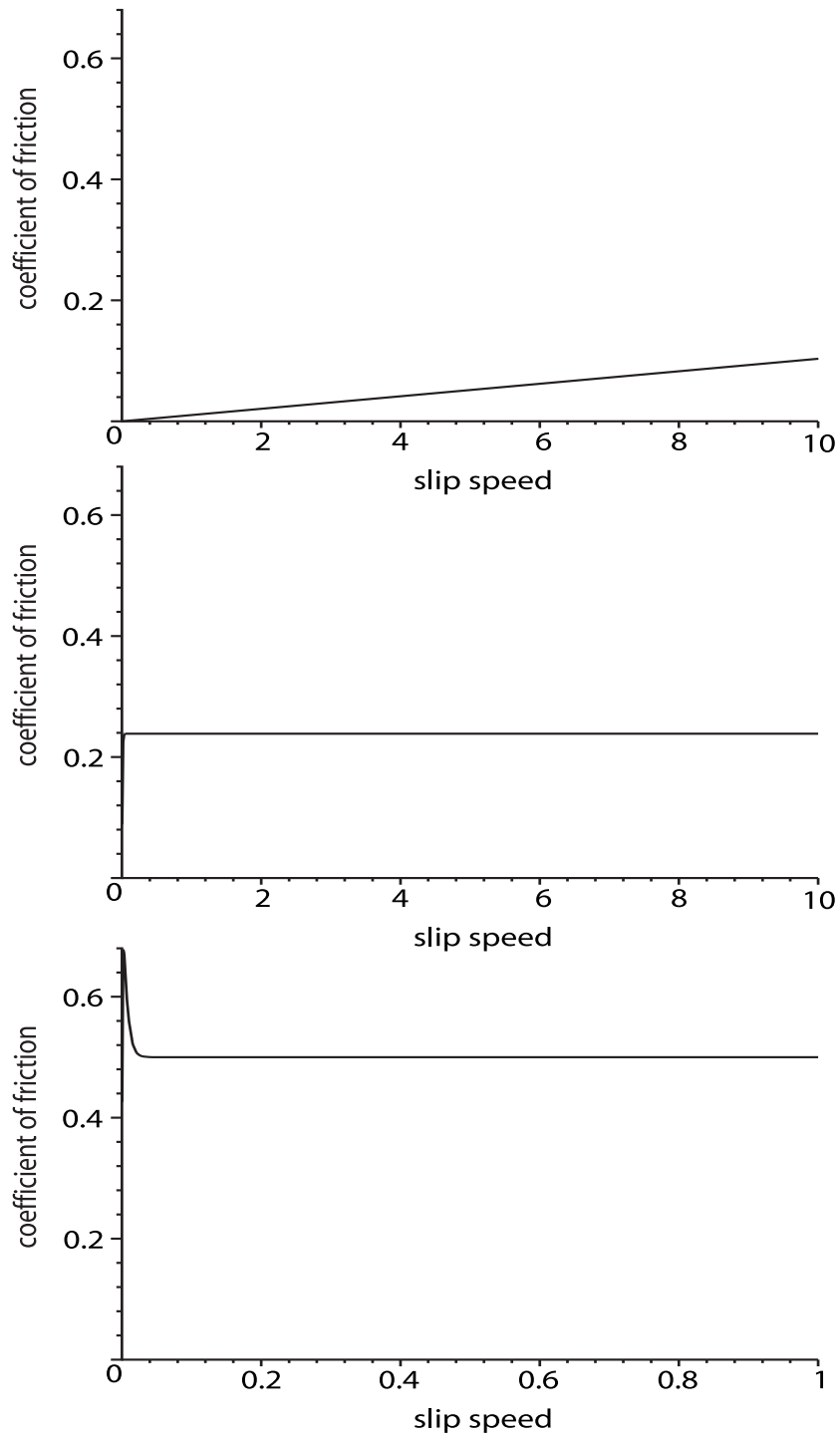
Figure 2–3: Modular ability of the model to selectively model different friction regimes: top plot-viscous regime (e.g., hydrodynamic lubrication), middle plot-Coulombic friction regime (e.g., solid lubricant coatings at moderate sliding speeds), and bottom plot-abrupt change from static to kinetic friction (e.g., non-lubricous polymers).
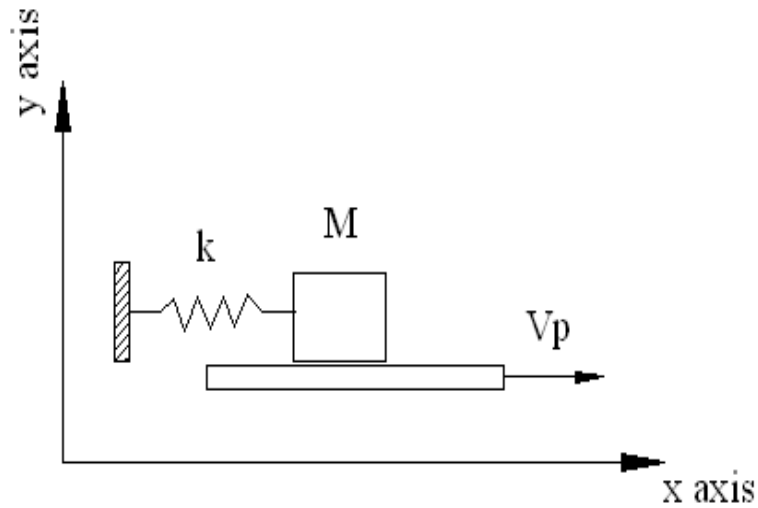
Figure 2–4: Mass-spring system for demonstrating stick-slip friction.

hydrodynamic lubrication in many operating regimes is viscous, lacking the other effects, which are easily set to zero in the model. Simple Coulombic friction models are often good for solid lubricant coatings at moderate sliding speeds. To capture this effect, the static and viscous terms can be set to zero. For some sticky or non-lubricous polymers, there exists an abrupt change from static to kinetic friction, which is captured by making the Stribeck decay very rapid.

A Coulombic friction regime is displayed in Figure 2–5 where the friction model parameters in (2–1) were set as follows: $\gamma_1 = 0$, $\gamma_2 = 0$, $\gamma_3 = 0$, $\gamma_4 = 0.1$, $\gamma_5 = 100$, $\gamma_6 = 0$. The Coulombic friction coefficient is a constant, opposing the motion of the block as seen in Figures 2–5 and 2–8. The block velocity, slip velocity, and the friction force as a function of time are depicted in Figures. 2–6 - 2–8. These figures indicate that the block velocity slowly rises, reaches a maximum and then begins to oscillate. The slip velocity also rises and then oscillates after reaching a maximum value. These figures indicate that the friction force causes the block to move along with the plate until the spring force overcomes the friction force; hence, the block begins to slip in an opposite direction of the plate velocity
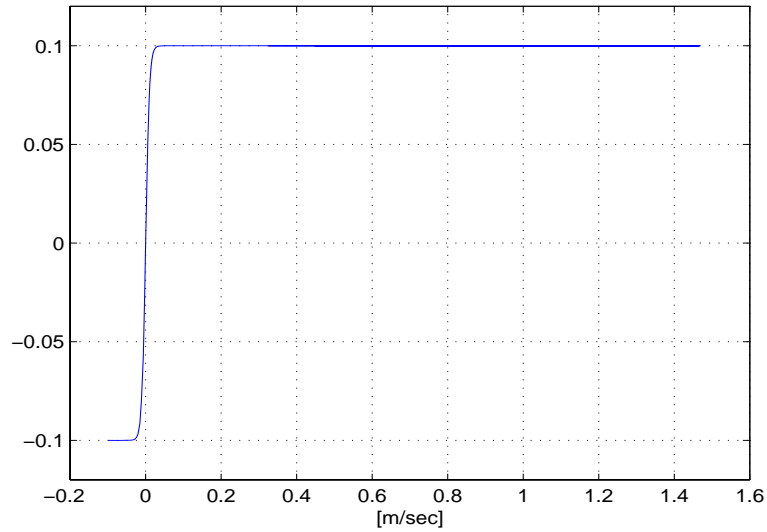
Figure 2–5: Friction coefficient vs slip velocity.

causing the spring to compress. As the spring releases energy back into the system, the block velocity exceeds the plate velocity. The magnitude of the constant friction coefficient results in a constant oscillation between the friction force and the spring force.

The viscous friction plot in Figure (2–9) is obtained by adjusting the parameters as follows: $\gamma_1 = 0$, $\gamma_2 = 0$, $\gamma_3 = 0$, $\gamma_4 = 0$, $\gamma_5 = 0$, $\gamma_6 = 0.01$. The block velocity, slip velocity and the friction force are given in Figures 2–10 - 2–12. The block velocity in Figure 2–10 slowly decreases as the viscous friction increases as displayed in Figure 2–9. The viscous coefficient of friction is an order of magnitude smaller in comparison to the Coulombic friction coefficient, as a result the friction force is not sufficient enough to sustain the oscillations of the block. The block eventually comes to rest and constantly slips on the moving plate.

The Stribeck effect in (2–13) is modeled using the following friction model parameter values: $\gamma_1 = 0.25$, $\gamma_2 = 100$, $\gamma_3 = 10$, $\gamma_4 = 0$, $\gamma_5 = 0$, $\gamma_6 = 0$. The block velocity, slip velocity and the friction force are plotted in Figures 2–14 - 2–16. As seen in Figure 2–13, the Stribeck effect is seen as the high breakaway force at
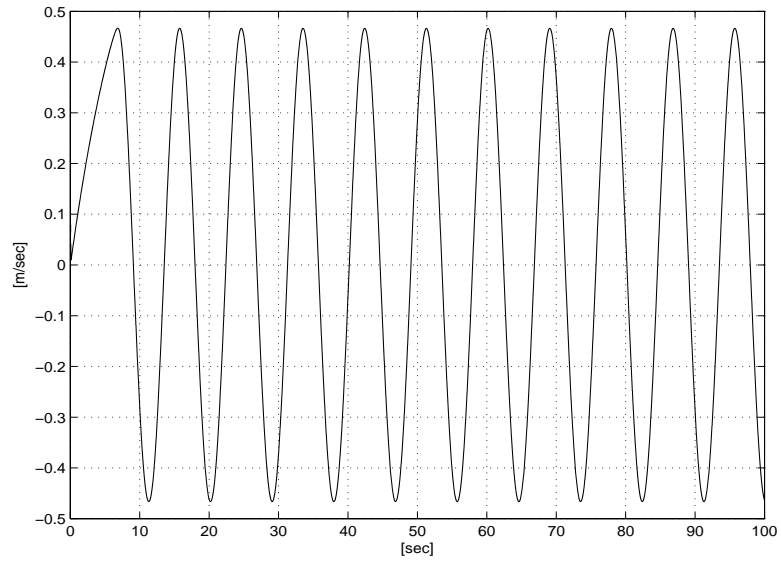
Figure 2–6: Block velocity vs time.
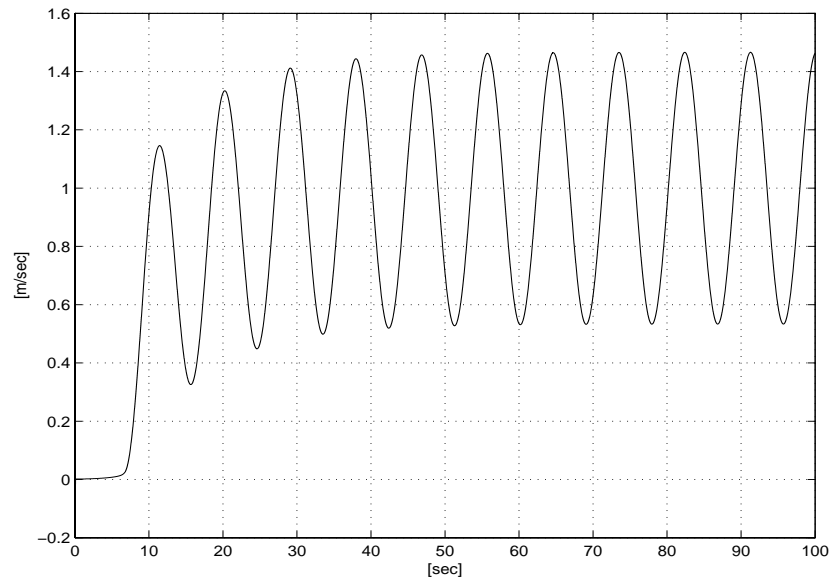
Figure 2–7: Slip velocity vs time.
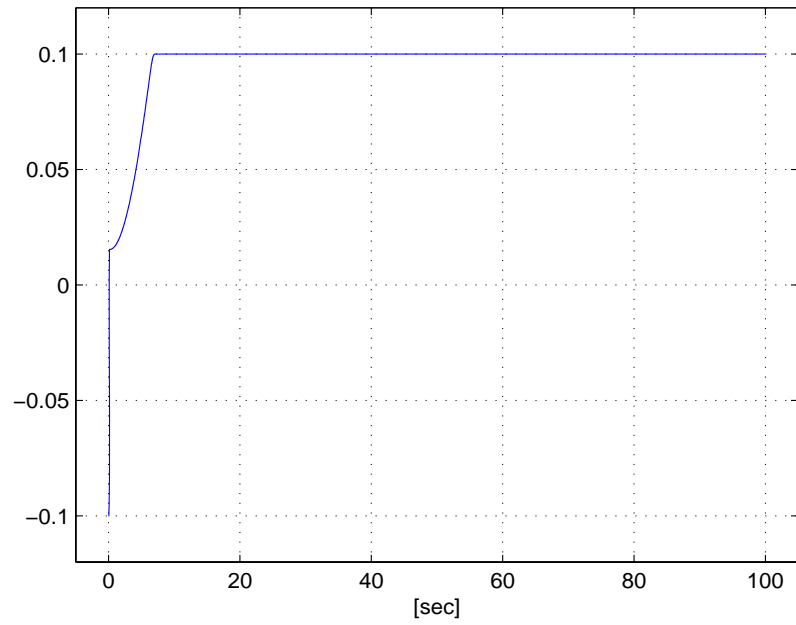
Figure 2–8: Friction coefficient vs time.
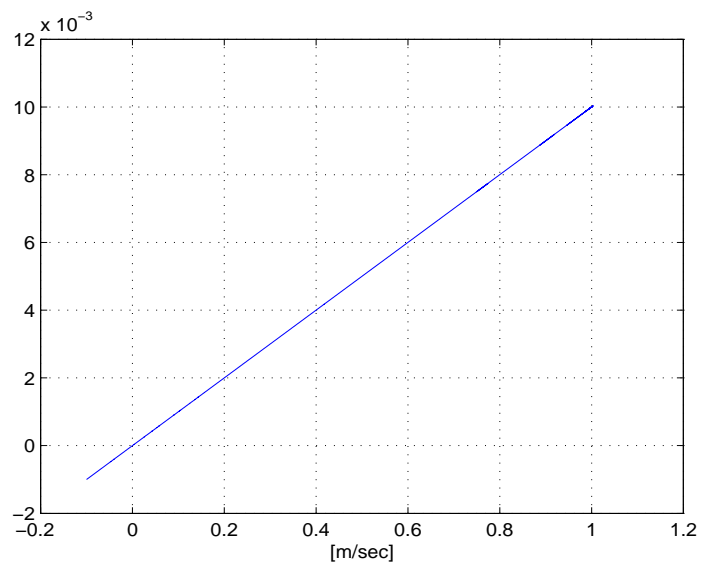
Figure 2–9: Friction coefficient vs slip velocity.
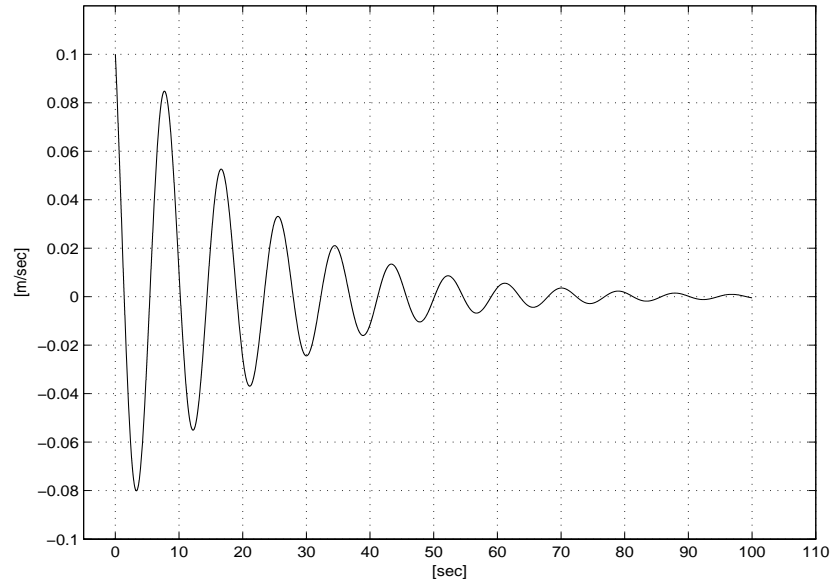
Figure 2–10: Block velocity vs time.
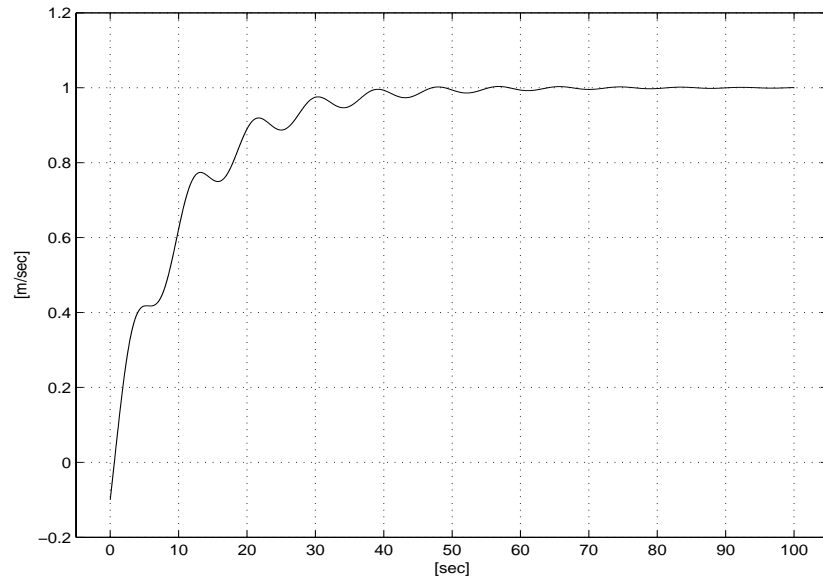
Figure 2–11: Slip velocity vs time.
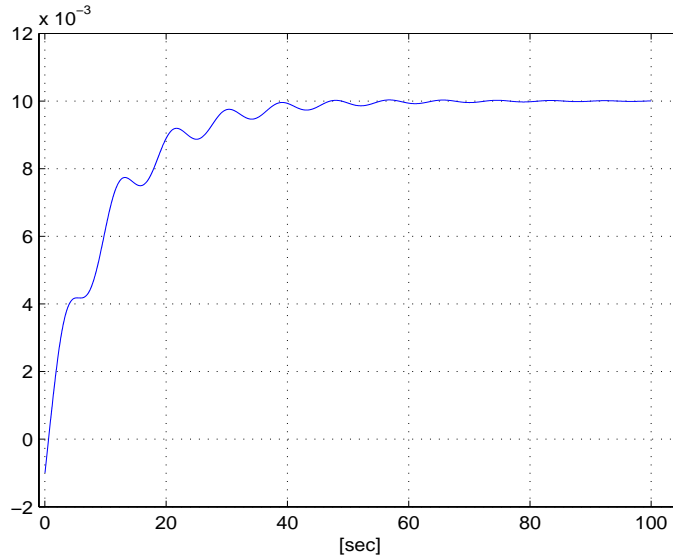
Figure 2–12: Friction coefficient vs time.

the beginning of the motion of the block, which then exponentially decreases. The block moves with the plate due to the initial friction force. Eventually enough energy is stored in the spring so that the spring force overcomes the breakaway friction. The friction force exponentially decays after the breakaway force is reached. After the block overcomes the breakaway force, the spring force becomes dominant and causes the block to reverse its direction and move towards the spring. Since there is no force opposing this motion, a large slip velocity is exhibited while the spring compresses and releases, pushing the block faster than the plate.

Figure 2–17 illustrates the sum of the different effects in the friction model in a stick-slip regime with the following friction model parameters $\gamma_1 = 0.25$, $\gamma_2 = 100$, $\gamma_3 = 10$, $\gamma_4 = 0.1$, $\gamma_5 = 100$, $\gamma_6 = 0.01$. Figures 2–18 - 2–20 show the velocity of the block, slip velocity and friction force as a function of time. The block velocity slowly increases and stores enough energy to reverse the direction of the block. This storage and release of energy causes the system to oscillate. Figure 2–20 shows the stick-slip phenomenon.
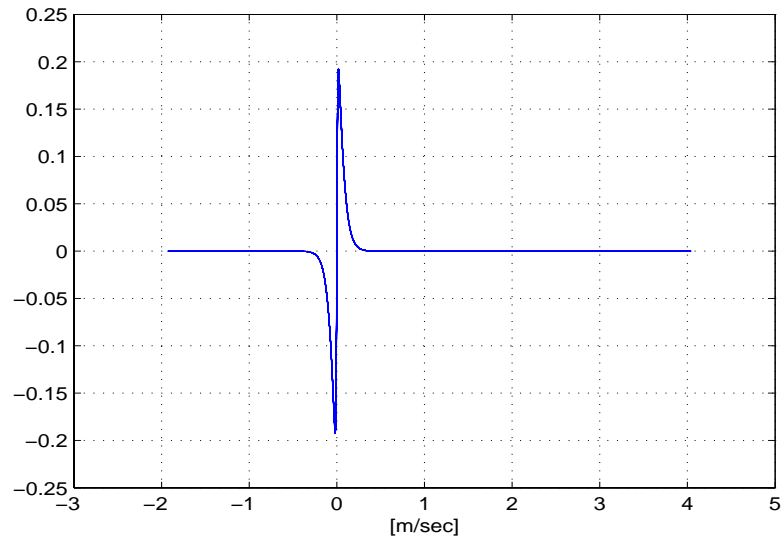
Figure 2–13: Friction coefficient vs slip velocity.
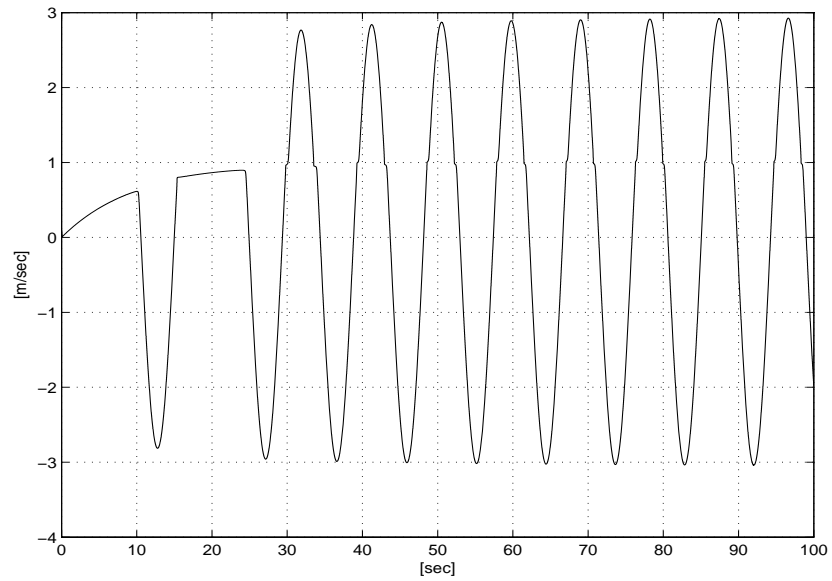
Figure 2–14: Block velocity vs time.
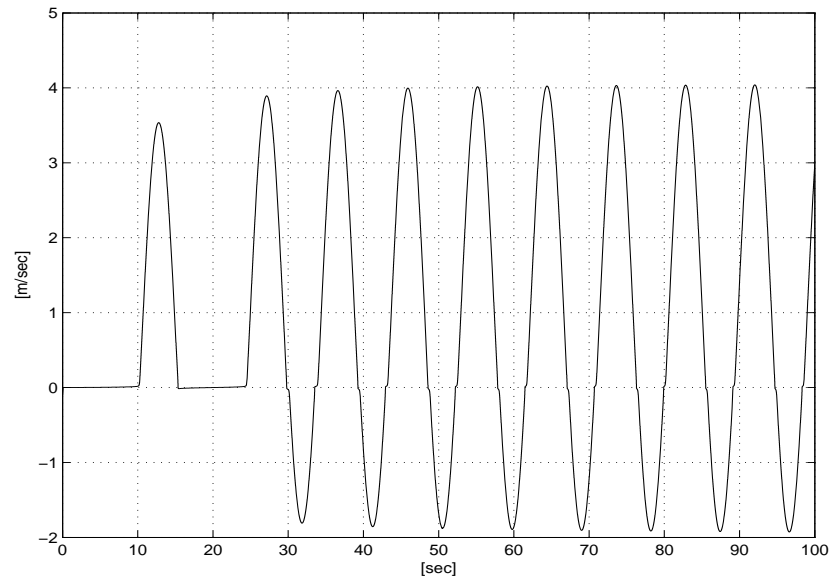
Figure 2–15: Slip velocity vs time.
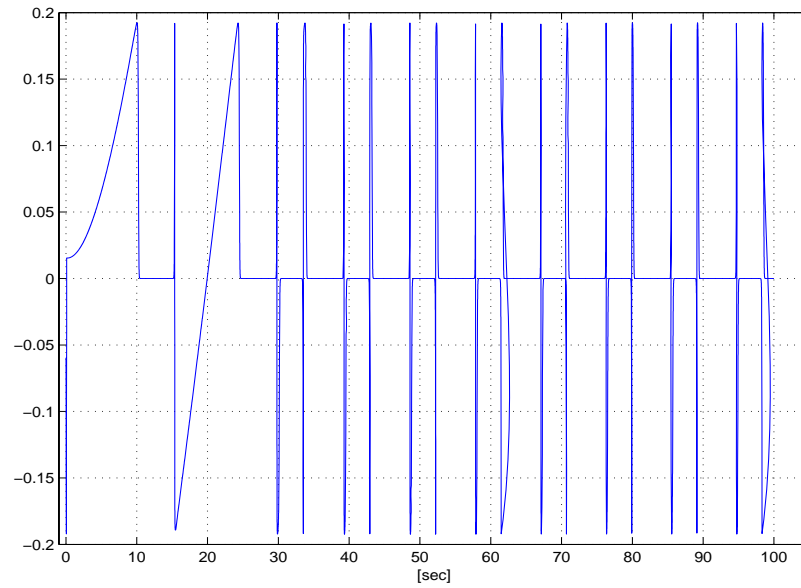
Figure 2–16: Friction coefficient vs time.
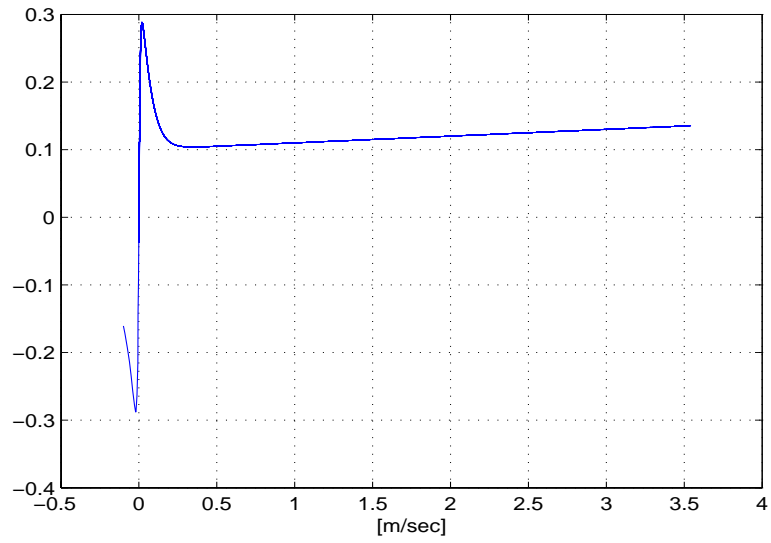
Figure 2–17: Friction coefficient vs slip velocity.
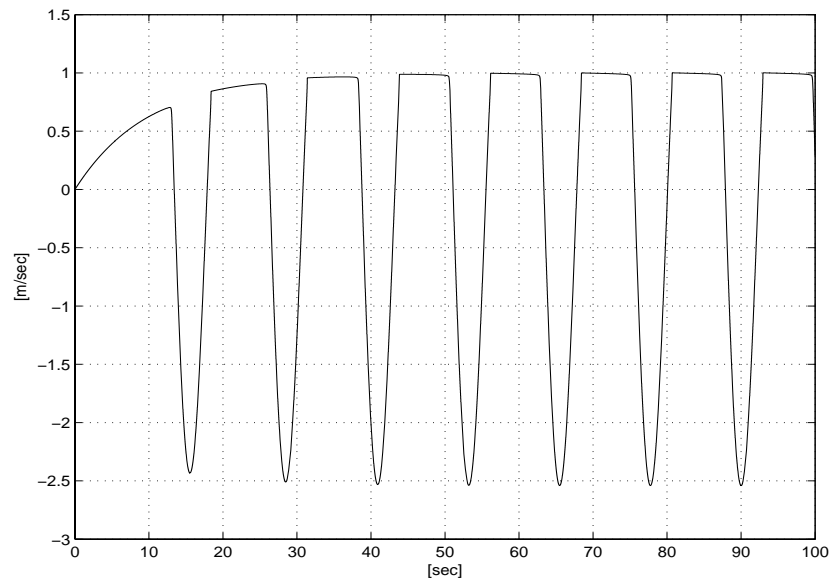
Figure 2–18: Block velocity vs time.
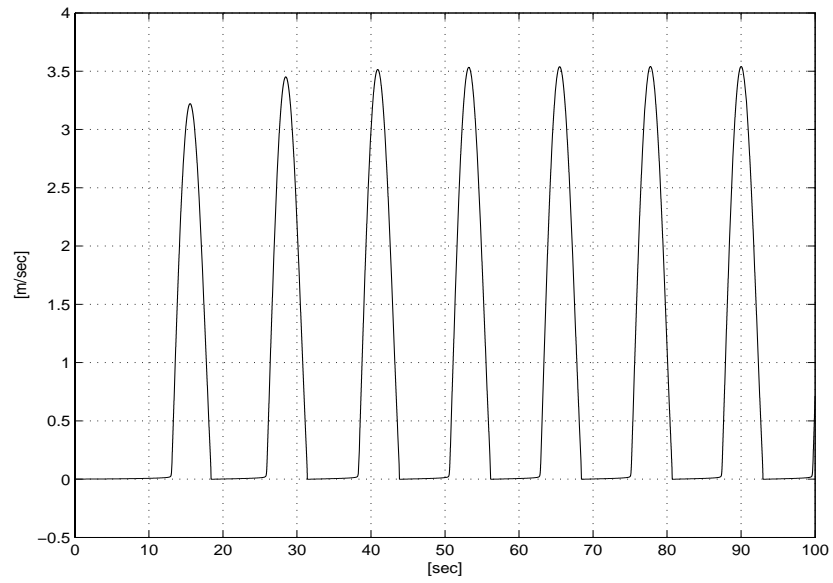
Figure 2–19: Slip velocity vs time.
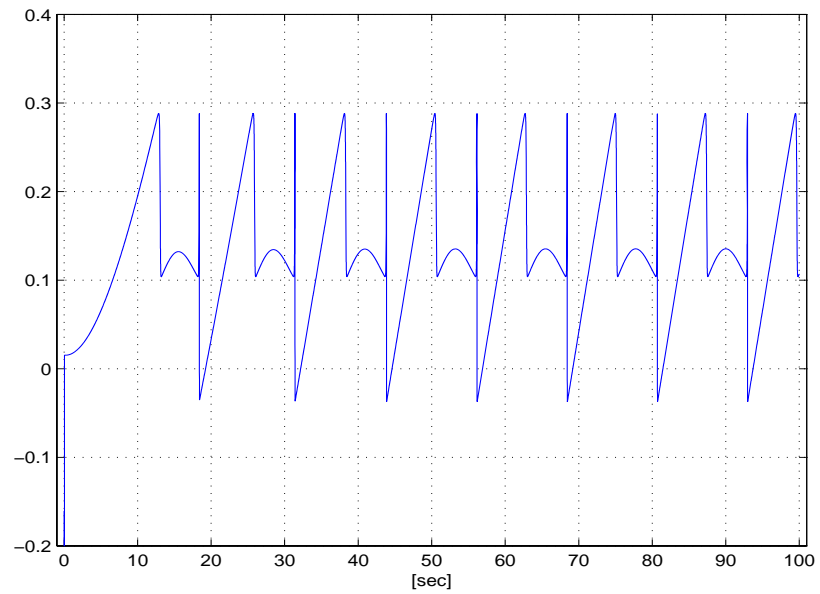
Figure 2–20: Friction coefficient vs time.

2.3 Experimental Results

The experimental testbed shown in Figure 2–21 consists of a circular disk made of Aluminium, mounted on a NSK direct-drive switched reluctance motor (240.0 Nm Model YS5240-GN001). The NSK motor is controlled through power electronics operating in torque control mode. The motor resolver provides rotor position measurements with a resolution of 153600 pulses/revolution at a resolver and feedback resolution of 10 bits. A Pentium 2.8 GHz PC operating under QNX hosts the control algorithm, which was implemented via Qmotor 3.0, a graphical user-interface, to facilitate real-time graphing, data logging, and adjust control gains without recompiling the program (for further information on Qmotor 3.0, the reader is referred to Loffler et al. [39]). Data acquisition and control implementation were performed at a frequency of 1.0 kHz using the ServoToGo I/O board. A 0.315 m X 0.108 m X 0.03175 m rectangular Nylon block was mounted on a pneumatic linear thruster to apply an external friction load to the rotating disk. A pneumatic regulator maintained a constant pressure of 15 pounds per square inch on the circular disk. This testbed was used to implement a tracking controller with adaptive friction identification developed by the authors in Makkar et al. [40].

The aim of this experiment was to match the experimentally identified friction torque using the adaptive term in Makkar et al. [40] and Makkar and Dixon et al. [41] with the friction torque calculated from the new proposed friction model in (2–1). The experimentally identified friction is depicted Figure 2–22.

The coefficients in (2–1) were varied to match the experimentally identified friction torque. The friction torque in (2–1) was calculated as a function of the rotor velocity with the coefficients chosen as

$$\gamma_1 = 34.8 \quad \gamma_2 = 650 \quad \gamma_3 = 1 \quad \gamma_4 = 26 \quad \gamma_5 = 200 \quad \gamma_6 = 19.5 \qquad (2\text{--}2)$$

Figure 2–21: Testbed for the experiment.

Figure 2–22 shows a plot of the experimentally determined friction torque, a plot of friction torque developed from (2–1) and a plot comparing the experimentally determined friction torque with the developed friction model overlaid.

The experimentally obtained friction torque in Figure 2–22 has viscous and static friction components and exhibits the Stribeck effect. These facts were taken into consideration while choosing the constants in (2–1). Values for γ_1 and γ_4 were chosen to account for the static friction, and γ_6 was chosen to capture the viscous friction component. As seen in Figure 2–22, the analytical model approximates the experimental data with the exception of some overshoot. The experimental origin of the directional frictional anisotropy is discussed in detail in Schmitz et al. [48] and is attributed to small misalignment between the loading axis and the motor axis.

2.4   Concluding Remarks

A new continuously differentiable friction model with nonlinear parameterizable terms is proposed. This model captures a number of essential aspects of friction without involving discontinuous or piecewise continuous functions and can
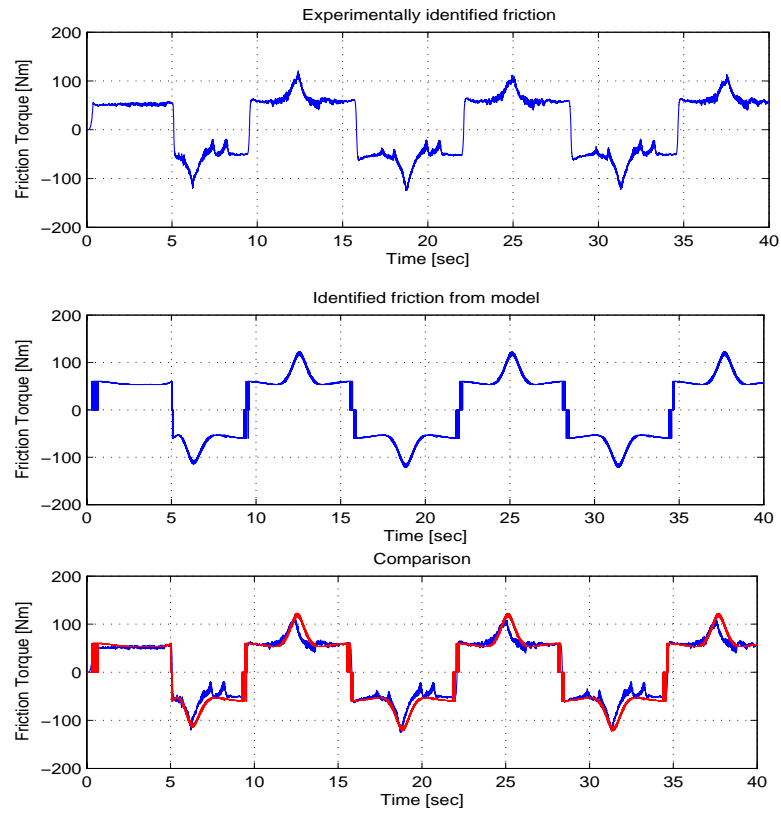
Figure 2–22: The proposed friction model very closely approximates the experimentally identified friction term obtained from the adaptive controller developed in Makkar et al. [41]. Top plot depicts the experimentally obtained friction torque, middle plot depitcs the friction plot obtained from the proposed model and the bottom plot depicts a comparison of the two with solid line indicating experimentally obtained friction torque and dashed line indicating friction torque obtained from the proposed friction model.

be modified to include additional effects. The continuously differentiable property of the proposed model provides a foundation to develop continuous controllers that can identify and compensate for nonlinear frictional effects. The development of one such controller is discussed in next chapter.

IDENTIFICATION AND COMPENSATION FOR FRICTION BY HIGH GAIN
FEEDBACK

Motivated by the desire to include dynamics friction models in the control
design, a new tracking controller is developed in this chapter that contains the new
continuously differentiable friction model with uncertain nonlinear parameterizable
terms that was developed in Chapter 2. Friction models are often based on the
assumption that the friction coefficient is constant with sliding speed and have a
singularity at the onset of slip. Such models typically include a signum function of
the velocity to assign the direction of friction force (e.g., see Lampaert et al. [34],
and Swevers et al. [52]), and many other models are only piecewise continuous
(e.g., the LuGre model in [8]). In Makkar et al. [42], Makkar and Dixon et al.
[43], and Chapter 2, a new friction model is proposed that captures a number of
essential aspects of friction without involving discontinuous or piecewise continuous
functions. The simple continuously differentiable model represents a foundation
that captures the major effects reported and discussed in friction modeling and
experimentation and the model is generic enough that other subtleties such as
frictional anisotropy with sliding direction can be addressed by mathematically
distorting this model without compromising the continuous differentiability.
Based on the fact that the developed model is continuously differentiable, a
new integral feedback compensation term originally proposed by Xian et al.
[57] is exploited to enable a semi-global tracking result while identifying the
friction on-line, assuming exact model knowledge of the remaining dynamics.
A Lyapunov-based stability analysis is provided to conclude the tracking and
friction identification results. Experimental results show two orders of magnitude

improvement in tracking control over a proportional derivative (PD) controller, and a one order of magnitude improvement over the model-based controller. Experimental results are also used to illustrate that the experimentally identified friction can be approximated by the model in Makkar et al. [42] and Makkar and Dixon et al. [43].

This chapter is organized as follows. The dynamic model and the associated properties are provided in Section 3.1. Section 3.2 describes the development of errorsystem followed by the stability analysis in Section 3.3. Section 3.4 describes the experimental set up and results that indicate improved performance obtained by implementing the proposed controller followed by discussion in Section 3.5 and conclusion in Section 3.6.

3.1 Dynamic Model and Properties

The class of nonlinear dynamic systems considered are assumed to be modeled by the general Euler-Lagrange formulation in (1–1) where the friction term $f(\dot{q})$ is assumed to have the form in (2–1) as in Makkar et al. [42] and Makkar et al. [43].

The subsequent development is based on the assumption that $q(t)$ and $\dot{q}(t)$ are measurable and that $M(q)$, $V_m(q,\dot{q})$, $G(q)$ are known. Moreover, the following properties and assumptions will be exploited in the subsequent development:

Property 3.1: The inertia matrix $M(q)$ is symmetric, positive definite, and satisfies the following inequality $\forall\, y(t) \in \mathbb{R}^n$:

$$m_1 \|y\|^2 \leq y^T M(q)y \leq \bar{m}(q) \|y\|^2 \tag{3–1}$$

where $m_1 \in \mathbb{R}$ is a known positive constant, $\bar{m}(q) \in \mathbb{R}$ is a known positive function, and $\|\cdot\|$ denotes the standard Euclidean norm.

Property 3.2: If $q(t) \in \mathcal{L}_\infty$, then $\dfrac{\partial M(q)}{\partial q}$, and $\dfrac{\partial^2 M(q)}{\partial q^2}$ exist and are bounded. Moreover, if $q(t)$, $\dot{q}(t) \in \mathcal{L}_\infty$ then $V_m(q,\dot{q})$ and $G(q)$ are bounded.

Property 3.3: Based on the structure of $f(\dot{q})$ given in (2–1), $f(\dot{q})$, $\dot{f}(\dot{q}, \ddot{q})$, and $\ddot{f}(\dot{q}, \ddot{q}, \dddot{q})$ exist and are bounded provided $q(t)$, $\dot{q}(t)$, $\ddot{q}(t)$, $\dddot{q}(t) \in \mathcal{L}_\infty$.

3.2   Error System Development

The control objective is to ensure that the system tracks a desired trajectory, denoted by $q_d(t)$, that is assumed to be designed such that $q_d(t)$, $\dot{q}_d(t)$, $\ddot{q}_d(t)$, $\dddot{q}_d(t) \in \mathbb{R}^n$ exist and are bounded. A position tracking error, denoted by $e_1(t) \in \mathbb{R}^n$, is defined as follows to quantify the control objective:

$$e_1 \triangleq q_d - q. \tag{3–2}$$

The following filtered tracking errors, denoted by $e_2(t)$, $r(t) \in \mathbb{R}^n$, are defined to facilitate the subsequent design and analysis:

$$e_2 \triangleq \dot{e}_1 + \alpha_1 e_1 \tag{3–3}$$

$$r \triangleq \dot{e}_2 + \alpha_2 e_2 \tag{3–4}$$

where α_1, $\alpha_2 \in \mathbb{R}$ denote positive constants. The filtered tracking error $r(t)$ is not measurable since the expression in (3–4) depends on $\dddot{q}(t)$.

After premultiplying (3–4) by $M(q)$, the following expression can be obtained:

$$M(q)r = M(q)\dddot{q}_d + V_m(q, \dot{q})\dot{q} + G(q) \tag{3–5}$$
$$+ f(\dot{q}) - \tau(t) + M(q)\alpha_1 \dot{e}_1 + M(q)\alpha_2 e_2$$

where (1–1), (3–2), and (3–3) were utilized. Based on the expression in (3–5) the control torque input is designed as follows:

$$\tau(t) = M(q)\dddot{q}_d + V_m(q, \dot{q})\dot{q} + G(q) + M(q)\alpha_1 \dot{e}_1 + M(q)\alpha_2 e_2 + \mu(t) \tag{3–6}$$

where $\mu(t) \in \mathbb{R}^n$ denotes a subsequently designed control term. By substituting (3–6) into (3–5), the following expression can be obtained:

$$M(q)r = f(\dot{q}) - \mu(t). \tag{3–7}$$

From (3–7), it is evident that if $r(t) \rightarrow 0$, then $\mu(t)$ will identify the friction dynamics; therefore, the objective is to design the control term $\mu(t)$ to ensure that $r(t) \rightarrow 0$. To facilitate the design of $\mu(t)$, we differentiate (3–7) as follows:

$$M(q)\dot{r} = \dot{f}(\dot{q}) - \dot{\mu}(t) - \dot{M}(q)r. \tag{3–8}$$

Based on (3–8) and the subsequent stability analysis, $\mu(t)$ is designed as follows:

$$\mu(t) = (k_s + 1)e_2(t) - (k_s + 1)e_2(t_0) \tag{3–9}$$
$$+ \int_{t_0}^{t} [(k_s + 1)\alpha_2 e_2(\tau) + \beta sgn(e_2(\tau))]d\tau$$

where $k_s \in \mathbb{R}$ and $\beta \in \mathbb{R}$ are positive constants. The time derivative of (3–9) is given as

$$\dot{\mu}(t) = (k_s + 1)r + \beta sgn(e_2). \tag{3–10}$$

The expression in (3–9) for $\mu(t)$ does not depend on the unmeasurable filtered tracking error term $r(t)$. However, the time derivative of $\mu(t)$ (which is not implemented) can be expressed as a function of $r(t)$. After substituting (3–10) into (3–8), the following closed-loop error system can be obtained:

$$M(q)\dot{r} = -\frac{1}{2}\dot{M}(q)r - (k_s + 1)r - e_2 - \beta sgn(e_2) + N(t) \tag{3–11}$$

where $N(t) \in \mathbb{R}^n$ denotes the following unmeasurable auxiliary term:

$$N(q, \dot{q}, t) \triangleq \dot{f}(\dot{q}) - \frac{1}{2}\dot{M}(q)r + e_2. \tag{3–12}$$

To facilitate the subsequent analysis, another unmeasurable auxiliary term $N_d(t) \in \mathbb{R}^n$ is defined as follows:

$$N_d(t) \triangleq \frac{\partial f(\dot{q}_d)}{\partial \dot{q}_d}\ddot{q}_d = \gamma_1\gamma_2\ddot{q}_d - \gamma_1\gamma_2\ddot{q}_d \|\tanh(\gamma_2\dot{q}_d)\|^2 - \gamma_1\gamma_3\ddot{q}_d \tag{3–13}$$
$$+ \gamma_1\gamma_3\ddot{q}_d \|\tanh(\gamma_3\dot{q}_d)\|^2 + \gamma_4\gamma_5\ddot{q}_d - \gamma_4\gamma_5\ddot{q}_d \|\tanh(\gamma_5\dot{q}_d)\|^2 + \gamma_6\ddot{q}_d.$$

The time derivative of (3–13) is given as follows:

$$\dot{N}_d(t) = \frac{\partial^2 f(\dot{q}_d)}{\partial \dot{q}_d^2}\ddot{q}_d^2 + \frac{\partial f(\dot{q}_d)}{\partial \dot{q}_d}\dddot{q}_d = \dddot{q}_d(\gamma_1\gamma_2 - \gamma_1\gamma_3 + \gamma_4\gamma_5 + \gamma_6) \quad (3\text{–}14)$$

$$-\gamma_1\gamma_2\dddot{q}_d\|\tanh(\gamma_2\dot{q}_d)\|^2 + \gamma_1\gamma_3\dddot{q}_d\|\tanh(\gamma_3\dot{q}_d)\|^2 - \gamma_4\gamma_5\dddot{q}_d\|\tanh(\gamma_5\dot{q}_d)\|^2$$

$$-2\gamma_1\gamma_2^2\|\ddot{q}_d\|^2\tanh(\gamma_2\dot{q}_d)[1 - \|\tanh(\gamma_2\dot{q}_d)\|^2] + 2\gamma_1\gamma_3^2\|\ddot{q}_d\|^2\tanh(\gamma_3\dot{q}_d)$$

$$[1 - \|\tanh(\gamma_3\dot{q}_d)\|^2] - 2\gamma_4\gamma_5^2\|\ddot{q}_d\|^2\tanh(\gamma_5\dot{q}_d)[1 - \|\tanh(\gamma_5\dot{q}_d)\|^2].$$

After adding and subtracting (3–13), the closed-loop error system in (3–11) can be expressed as follows:

$$M(q)\dot{r} = -\frac{1}{2}\dot{M}(q)r - (k_s + 1)r - e_2 - \beta sgn(e_2) + \tilde{N}(t) + N_d(t) \quad (3\text{–}15)$$

where the unmeasurable auxiliary term $\tilde{N}(t) \in \mathbb{R}^n$ is defined as

$$\tilde{N}(t) \triangleq N(t) - N_d(t). \quad (3\text{–}16)$$

Based on the expressions in (3–13) and (3–14), the following inequalities can be developed:

$$\|N_d(t)\| \leq \|\ddot{q}_d\| \cdot |\gamma_1\gamma_2 + \gamma_4\gamma_5 + \gamma_6 - \gamma_1\gamma_3| \leq \zeta_{N_d} \quad (3\text{–}17)$$

$$\left\|\dot{N}_d(t)\right\| \leq \|\dddot{q}_d\| \cdot |\gamma_1\gamma_2 + \gamma_4\gamma_5 + \gamma_6 - \gamma_1\gamma_3| + \|\ddot{q}_d\|^2(2\gamma_1\gamma_2^2 + 2\gamma_1\gamma_3^2 + 2\gamma_4\gamma_5^2) \quad (3\text{–}18)$$

$$\leq \zeta_{N_d 2}$$

where $\zeta_{N_d}, \zeta_{N_d 2} \in \mathbb{R}$ are known positive constants.

3.3   Stability Analysis

Theorem 3.1: The controller given in (3–6) and (3–9) ensures that the position tracking error is regulated in the sense that

$$e_1(t) \to 0 \qquad as \qquad t \to \infty$$

provided β is selected according to the following sufficient condition:

$$\beta > \zeta_{N_d} + \frac{1}{\alpha_2}\zeta_{N_d2} \tag{3–19}$$

where ζ_{N_d} and ζ_{N_d2} are introduced in (3–17) and (3–18), respectively, and k_s is selected sufficiently large. The control system represented by (3–6) and (3–9) also ensures that all system signals are bounded under closed-loop operation and that the friction in the system can be identified in the sense that

$$f(\dot{q}) - \mu(t) \to 0 \qquad as \qquad t \to \infty.$$

Proof: Let $\mathcal{D} \subset \mathbb{R}^{3n+1}$ be a domain containing $y(t) = 0$, where $y(t) \in \mathbb{R}^{3n+1}$ is defined as

$$y(t) \triangleq [z^T(t) \quad \sqrt{P(t)}]^T \tag{3–20}$$

where $z(t) \in \mathbb{R}^{3n}$ is defined as

$$z(t) \triangleq [e_1^T \quad e_2^T \quad r^T]^T, \tag{3–21}$$

and the auxiliary function $P(t) \in \mathbb{R}$ is defined as

$$P(t) \triangleq \beta \, ||e_2(t_0)|| - e_2(t_0)^T N_d(t_0) - \int_{t_0}^t L(\tau)d\tau \tag{3–22}$$

where $\beta \in \mathbb{R}$ is nonnegative by design. In (3–22), the auxiliary function $L(t) \in \mathbb{R}$ is defined as

$$L(t) \triangleq r^T(N_d(t) - \beta sgn(e_2)). \tag{3–23}$$

The derivative $\dot{P}(t) \in \mathbb{R}$ can be expressed as

$$\dot{P}(t) = -L(t) = -r^T(N_d(t) - \beta sgn(e_2)). \tag{3–24}$$

Provided the sufficient condition introduced in (3–19) is satisfied, the following inequality can be obtained as

$$\int_{t_0}^t L(\tau)d\tau \le \beta \, |e_2(t_0)| - e_2(t_0)^T N_d(t_0). \tag{3–25}$$

Hence, (3–25) can be used to conclude that $P(t) \geq 0$. Let $V(y,t) : \mathcal{D} \times [0, \infty) \to \mathbb{R}$ be a continuously differentiable positive definite function defined as

$$V(y,t) \triangleq e_1^T e_1 + \frac{1}{2} e_2^T e_2 + \frac{1}{2} r^T M(q) r + P \qquad (3\text{–}26)$$

that can be bounded as

$$W_1(y) \leq V(y,t) \leq W_2(y) \qquad (3\text{–}27)$$

provided the sufficient condition introduced in (3–19) is satisfied. In (3–27), the continuous positive definite functions $W_1(y)$, $W_2(y) \in \mathbb{R}$ are defined as

$$W_1(y) = \lambda_1 \|y\|^2 \qquad W_2(y) = \lambda_2(q) \|y\|^2 \qquad (3\text{–}28)$$

where λ_1, $\lambda_2(q) \in \mathbb{R}$ are defined as

$$\lambda_1 \triangleq \frac{1}{2} \min\{1, m_1\}$$

$$\lambda_2(q) \triangleq \max\{\frac{1}{2}\bar{m}(q), 1\}$$

where m_1, $\bar{m}(q)$ are introduced in (3–1). After taking the time derivative of (3–26), $\dot{V}(y,t)$ can be expressed as

$$\dot{V}(y,t) = r^T M(q)\dot{r} + \frac{1}{2} r^T \dot{M}(q) r + e_2^T \dot{e}_2 + 2e_1^T \dot{e}_1 + \dot{P}.$$

After utilizing (3–3), (3–4), (3–15), and (3–24), $\dot{V}(y,t)$ can simplified as follows:

$$\dot{V}(y,t) = r^T \tilde{N}(t) - (k_s + 1) \|r\|^2 - \alpha_2 \|e_2\|^2 - 2\alpha_1 \|e_1\|^2 + 2e_2^T e_1. \qquad (3\text{–}29)$$

Because $e_2^T(t)e_1(t)$ can be upper bounded as

$$e_2^T e_1 \leq \frac{1}{2} \|e_1\|^2 + \frac{1}{2} \|e_2\|^2,$$

$\dot{V}(y,t)$ can be upper bounded using the squares of the components of $z(t)$ as follows:

$$\dot{V}(y,t) \leq r^T \tilde{N}(t) - (k_s + 1) \|r\|^2 - \alpha_2 \|e_2\|^2 - 2\alpha_1 \|e_1\|^2 + \|e_1\|^2 + \|e_2\|^2.$$

By using the fact $||\tilde{N}(t)|| \leq \rho(||z||) \, ||z||$, the expression in (3–29) can be rewritten as follows:

$$\dot{V}(y,t) \leq -\lambda_3 \, ||z||^2 - \left(k_s \, ||r||^2 - \rho(||z||) \, ||r|| \, ||z)|| \right) \tag{3–30}$$

where $\lambda_3 \triangleq \min\{2\alpha_1 - 1, \alpha_2 - 1, 1\}$ and the bounding function $\rho(||z||) \in \mathbb{R}$ is a positive globally invertible nondecreasing function; hence, α_1, α_2 must be chosen according to the following conditions:

$$\alpha_1 > \frac{1}{2}, \qquad \alpha_2 > 1.$$

After completing the squares for the second and third term in (3–30), the following expression can be obtained:

$$\dot{V}(y,t) \leq -\lambda_3 \, ||z||^2 + \frac{\rho^2(z) \, ||z||^2}{4k_s}. \tag{3–31}$$

The following expression can then be obtained from (3–31):

$$\dot{V}(y,t) \leq -W(y) \tag{3–32}$$

where $W(y) = c \, ||z||^2$, for some positive constant $c \in \mathbb{R}$, is a continuous positive semi-definite function that is defined on the following domain:

$$D \triangleq \{y \in \mathbb{R}^{3n+1} \mid ||y|| \leq \rho^{-1}(2\sqrt{\lambda_3 k_s})\}.$$

The inequalities in (3–27) and (3–32) can be used to show that $V(y,t) \in \mathcal{L}_\infty$ in $\mathcal{D}$; hence, $e_1(t), e_2(t)$, and $r(t) \in \mathcal{L}_\infty$ in $\mathcal{D}$. Given that $e_1(t), e_2(t)$, and $r(t) \in \mathcal{L}_\infty$ in $\mathcal{D}$, standard linear analysis methods (e.g., Lemma 1.4 of [15]) can be used to prove that $\dot{e}_1(t), \dot{e}_2(t) \in \mathcal{L}_\infty$ in $\mathcal{D}$ from (3–3) and (3–4). Since $e_1(t), e_2(t), r(t) \in \mathcal{L}_\infty$ in $\mathcal{D}$, the assumption that $q_d(t), \dot{q}_d(t), \ddot{q}_d(t)$ exist and are bounded can be used along with (3–2)-(3–4) to conclude that $q(t), \dot{q}(t), \ddot{q}(t) \in \mathcal{L}_\infty$ in $\mathcal{D}$. Since $q(t), \dot{q}(t) \in \mathcal{L}_\infty$ in $\mathcal{D}$, Property 2 can be used to conclude that $M(q), V_m(q,\dot{q}), G(q)$, and $f(\dot{q}) \in \mathcal{L}_\infty$ in $\mathcal{D}$. From (3–6) and (3–9), we can show that $\mu(t), \tau(t) \in \mathcal{L}_\infty$ in $\mathcal{D}$. Given that

$r(t) \in \mathcal{L}_\infty$ in $\mathcal{D}$, (3–10) can be used to show that $\dot{\mu}(t) \in \mathcal{L}_\infty$ in $\mathcal{D}$. Property 2 and Property 3 can be used to show that $\dot{f}(q)$ and $\dot{M}(q) \in \mathcal{L}_\infty$ in $\mathcal{D}$; hence, (3–8) can be used to show that $\dot{r}(t) \in \mathcal{L}_\infty$ in $\mathcal{D}$. Given that $\dot{r}(t) \in \mathcal{L}_\infty$ in $\mathcal{D}$, then (3–2)-(3–4) can be used to conclude that $\dddot{q}(t) \in \mathcal{L}_\infty$ in $\mathcal{D}$. Since $\dot{e}_1(t)$, $\dot{e}_2(t)$, $\dot{r}(t) \in \mathcal{L}_\infty$ in $\mathcal{D}$, the definitions for $W(y)$ and $z(t)$ can be used to prove that $W(y)$ is uniformly continuous in $\mathcal{D}$.

Let $\mathcal{S} \subset \mathcal{D}$ denote a set defined as follows:

$$\mathcal{S} \triangleq \left\{ y(t) \subset \mathcal{D} \mid W_2(y(t)) < \lambda_1 \left(\rho^{-1}(2\sqrt{\lambda_3 k_s}) \right)^2 \right\}. \tag{3–33}$$

The region of attraction in (3–33) can be made arbitrarily large to include any initial conditions by increasing the control gain k_s (i.e., a semi-global type of stability result) as in Xian et al. [57]. Theorem 8.4 of [30] can now be invoked to state that

$$c \, \|z(t)\|^2 \to 0 \qquad as \qquad t \to \infty \qquad \forall y(t_0) \in \mathcal{S}. \tag{3–34}$$

Based on the definition of $z(t)$, (3–34) can be used to show that

$$r(t) \to 0 \qquad as \qquad t \to \infty \qquad \forall y(t_0) \in \mathcal{S}. \tag{3–35}$$

Hence, from (3–3) and (3–4), standard linear analysis methods (e.g., Lemma 1.6 of [15]) can be used to prove that

$$e_1(t) \to 0 \qquad as \qquad t \to \infty \qquad \forall y(t_0) \in \mathcal{S}.$$

The result in (3–35) can also be used to conclude from (3–7) that

$$\mu(t) - f(\dot{q}(t)) \to 0 \qquad as \qquad t \to \infty \qquad \forall y(t_0) \in \mathcal{S}.$$

3.4 Experimental Results

The experimental testbed used for implementing the controller is described in Chapter 2. The dynamics for the testbed are given as follows:

$$\tau(t) = \underbrace{\left[I_m + 0.5ma^2\right][\ddot{q}]}_{M(q)\ddot{q}} + f(\dot{q}) \qquad (3\text{--}36)$$

where I_m(rotor moment of inertia) $= 0.255$ kg-m^2, m (mass of the circular disk) $= 3.175$ kg, a (radius of the disk) $= 0.25527$ m, and the friction torque $f(\dot{q}) \in \mathbb{R}$ is defined in (2–1). The control torque input $\tau(t)$ given in (3–6) is simplified (i.e., the centripetal-Coriolis matrix and gravity terms were omitted) as follows for the simple testbed:

$$\tau(t) = M(q)\ddot{q}_d + M(q)\alpha_1\dot{e}_1 + M(q)\alpha_2 e_2 + \mu(t) \qquad (3\text{--}37)$$

where $\mu(t)$ is the adaptive friction identification term defined in (3–9). The desired disk trajectory (see Figure 3–1) was selected similar to the one used in Feemster et al. [20] as follows (in degrees):

$$q_d(t) = 11.25 \tan^{-1}(3.0\sin(0.5t))(1 - \exp(-0.01t^3)). \qquad (3\text{--}38)$$

This soft-sinusoidal trajectory was proposed in [20] to emphasize a low-speed transition from forward to reverse directions. For all experiments, the rotor velocity signal is obtained by applying a standard backwards difference algorithm to the position signal. All states were initialized to zero. In addition, the integral structure of the adaptive term in (3–37) was computed on-line via a standard trapezoidal algorithm.
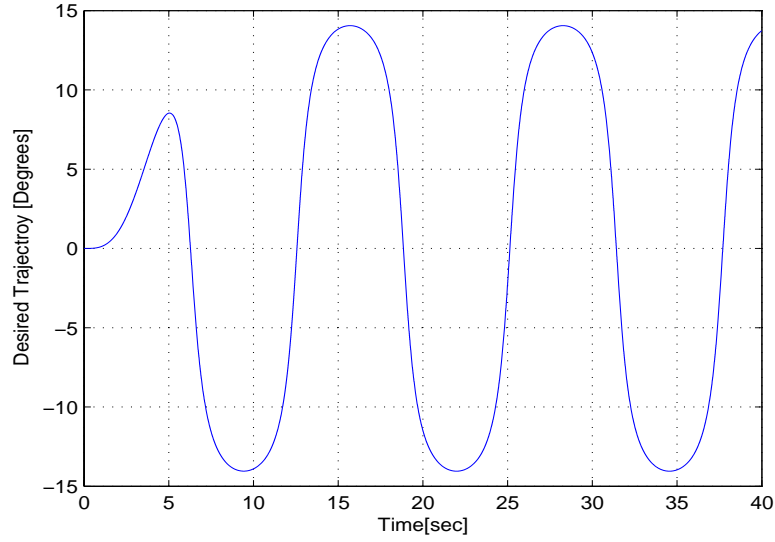
Figure 3–1: Desired disk trajectory.

3.4.1 Experiment 1

In the first experiment, no external load from the thruster was applied to the circular disk. In addition to the controller given in (3–36) and (3–37), a PD controller and a model-based controller were also implemented for comparison. The PD controller was implemented as:

$$\tau(t) = k_d \dot{e}_1 + k_p e_1 \tag{3–39}$$

where $k_d \in \mathbb{R}$ is the derivative gain and $k_p \in \mathbb{R}$ is the proportional gain. The model-based controller was implemented with standard friction feedforward terms as:

$$\tau(t) = M(q)\ddot{q}_d + M(q)\alpha_1 \dot{e}_1 + M(q)\alpha_2 e_2 + k_c sgn(\dot{q}) + k_v \dot{q} + k_s q \tag{3–40}$$

where $k_c \in \mathbb{R}$ is the Coulomb friction coefficient, $k_v \in \mathbb{R}$ is the viscous friction coefficient, and $k_s \in \mathbb{R}$ is the static friction coefficient.

The gains for each controller that yielded the best steady-state performance were determined as follows for the PD controller, model-based controller, and proposed controller, respectively:

- PD controller

$$k_d = 2600 \quad k_p = 2600 \tag{3-41}$$

- Model-based controller

$$\alpha_1 = 315 \quad \alpha_2 = 315 \quad k_c = 0.0828 \tag{3-42}$$

$$k_v = 0.0736 \quad k_s = 0.104$$

Proposed controller

$$k_s = 10 \quad \beta = 5 \quad \alpha_1 = 100 \quad \alpha_2 = 600. \tag{3-43}$$

The coefficient k_c, k_v, and k_s in (3–40) were calculated from the friction identification plot in Fig. 3–10. The coefficient k_s is calculated from the peak friction torque at the onset of a cycle, k_c is calculated from the flat portion of the curve after the initial peak, and k_v is calculated from the high peak after the flat portion of the curve.

The position tracking error from each controller is plotted in Figures 3–2-3–4 respectively. A comparison of the position tracking error from each controller is seen in Figure 3–5. Figure 3–6 depicts an enlarged view of the comparison of position tracking errors from the model-based controller and the proposed controller. The torque input by each controller is depicted in Figures 3–7-3–9 respectively. The friction identification term in (3–9) from the proposed controller obtained from the experiment is given in Figure 3–10.

The signum function for the control scheme in (3–9) was defined as

$$sgn(e_2(t)) = \begin{cases} 1 & e_2 > 0 \\ -1 & e_2 < 0 \\ 0 & e_2 = 0 \end{cases}.$$
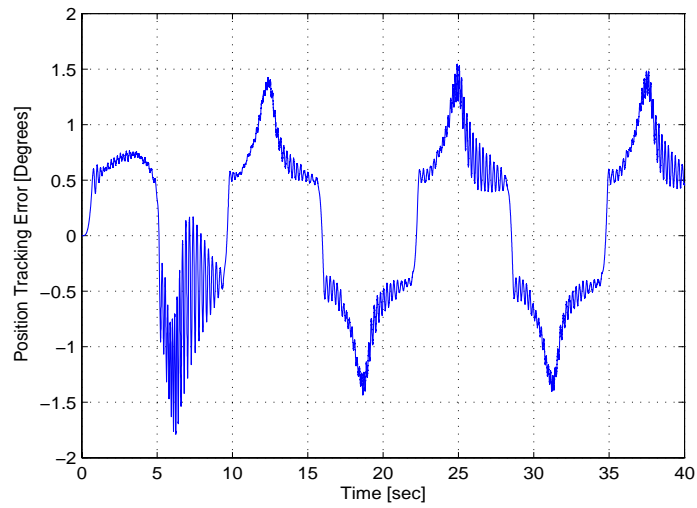
Figure 3–2: Position tracking error from the PD controller.
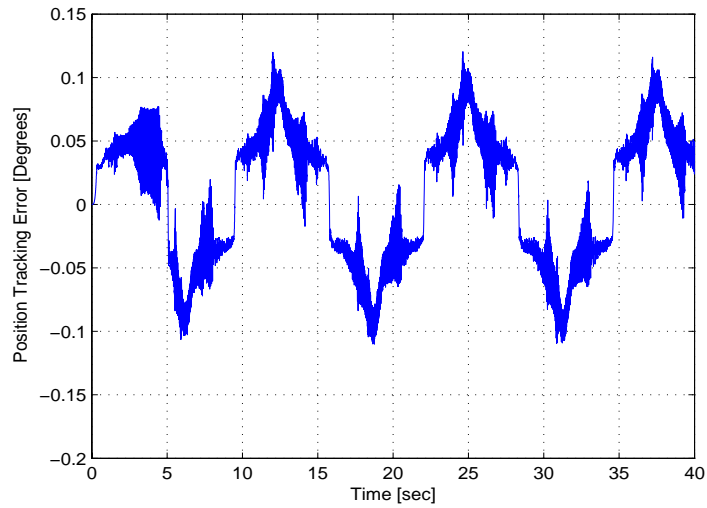
Figure 3–3: Position tracking error from the model-based controller with friction feedforward terms as described in (3–40).
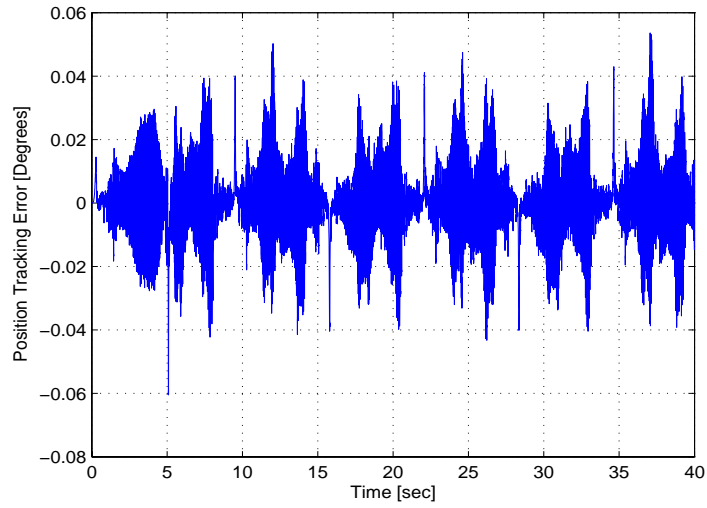
Figure 3–4: Position tracking error from the proposed controller.
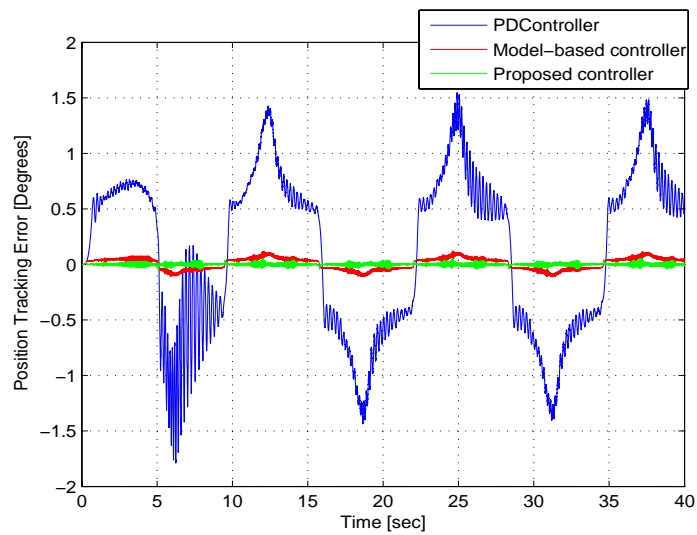
Figure 3–5: Comparison of position tracking errors from the three control schemes.
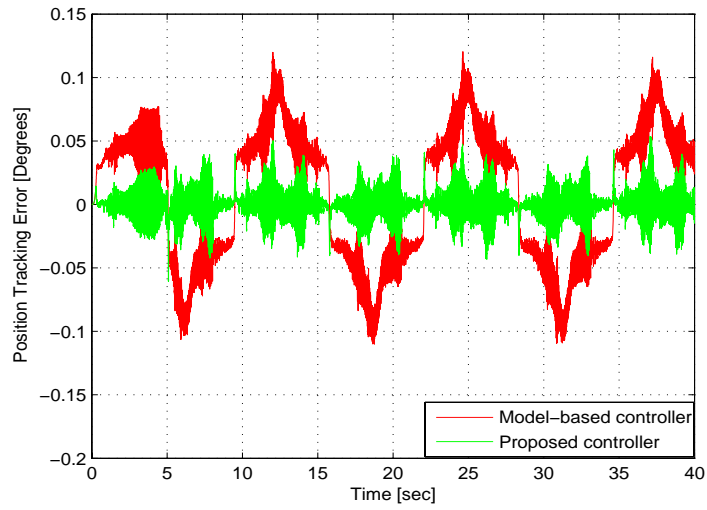
Figure 3–6: Comparison of position tracking errors from the model-based controller and the proposed controller.
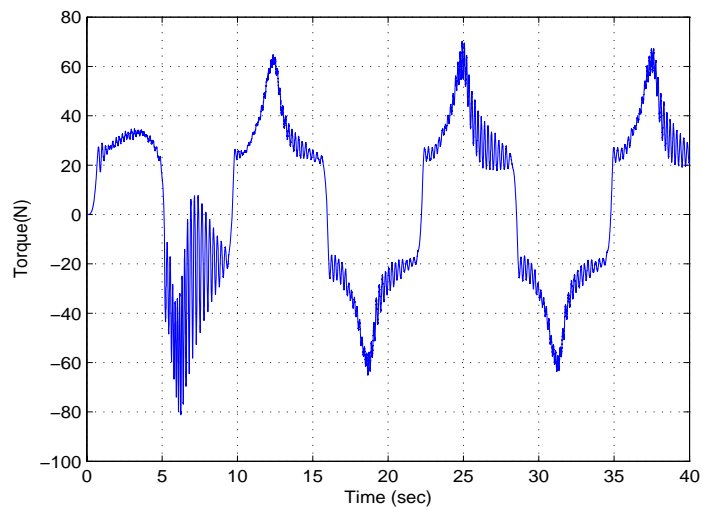
Figure 3–7: Torque input by the PD controller.
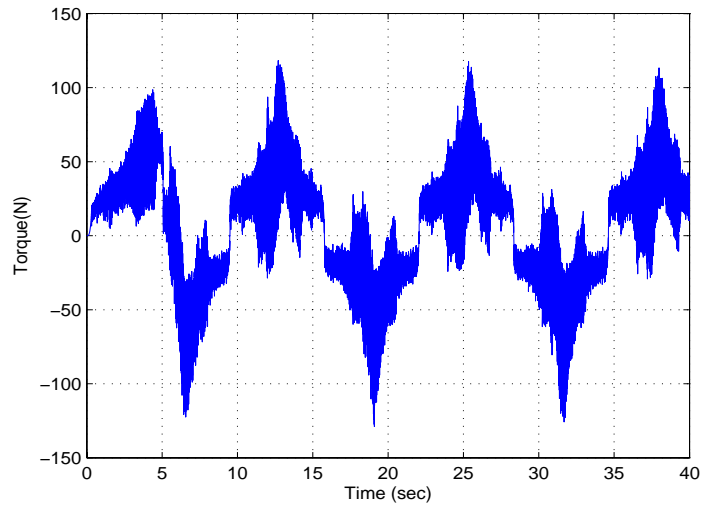
Figure 3–8: Torque input by the model-based controller with friction feedforward terms as described in (3–40).
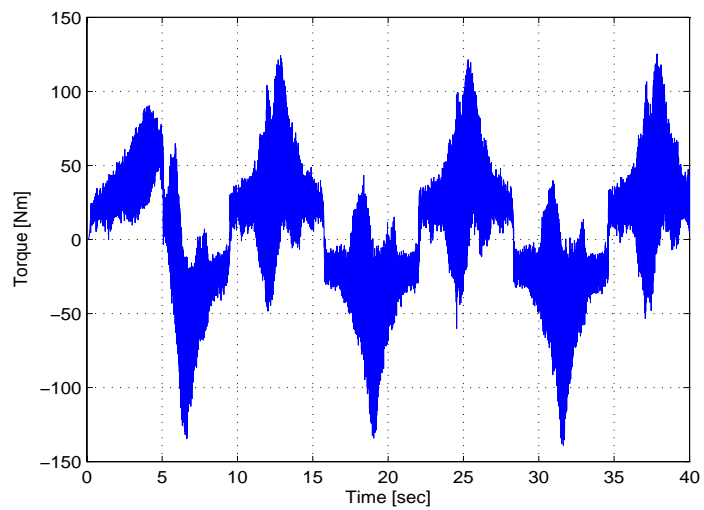
Figure 3–9: Torque input by the proposed controller.
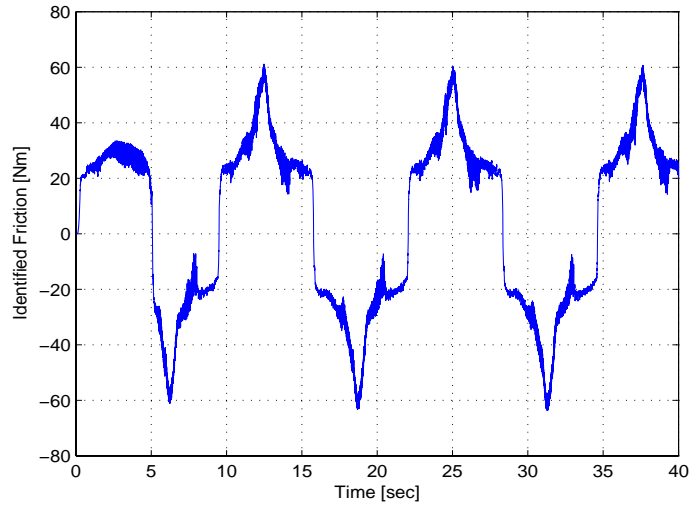
Figure 3–10: Identified friction from the adaptive term in the proposed controller.

3.4.2   Experiment 2

In the second experiment, an external friction load was induced on the system. An external moment load of 12.774 Nm was applied to the circular disk using the linear thruster (see Figure 2–21). The desired disk trajectory of (3–38) was again utilized. The control schemes of (3–37),(3–39), and (3–40) were implemented with the following gain values:

- PD controller

$$k_d = 2600 \quad k_p = 2600$$

- Model-based controller

$$\alpha_1 = 350 \quad \alpha_2 = 350 \quad k_c = 0.0828$$

$$k_v = 0.0736 \quad k_s = 0.104$$

- Proposed controller

$$k_s = 8.9 \quad \beta = 5.005 \quad \alpha_1 = 98 \quad \alpha_2 = 780. \tag{3–44}$$

The corresponding position tracking error from each controller is shown in Figures 3–11-3–13, respectively. A comparison of the position tracking error from each controller is seen in Figure 3–14. Figure 3–15 depicts an enlarged view of the comparison of position tracking errors from the model-based controller and the proposed controller. The control torque input by each controller is shown in Figures 3–16-3–18, respectively. The friction identification term in (3–9) from the proposed controller obtained from the experiment is given in Figure 3–19.
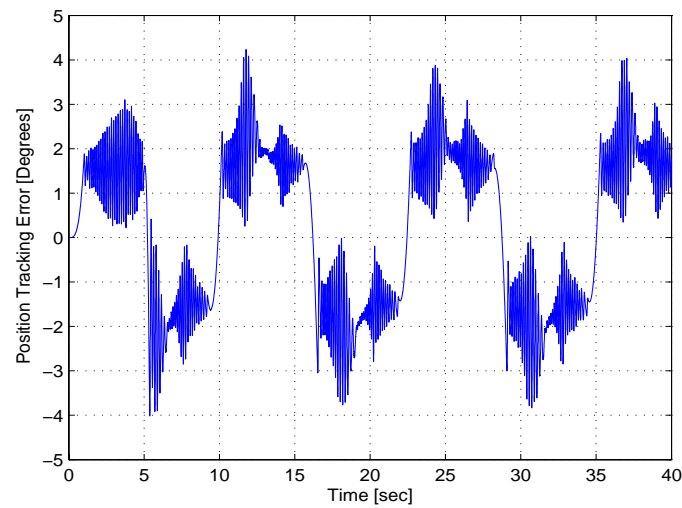
Figure 3–11: Position tracking error from the PD controller.

3.4.3 Experiment 3

In the third experiment, lubrication was used to examine changes in the system performance. The circular disk was lubricated with motor oil and the control scheme in (3–37) was implemented with same control gains as in Experiment 2 to minimize the position tracking error. The resulting position tracking error is shown in Figure 3–20, the control torque input is shown in Figure 3–21, and the friction identification term in (3–9) from the proposed controller obtained from the experiment is given in Figure 3–22.
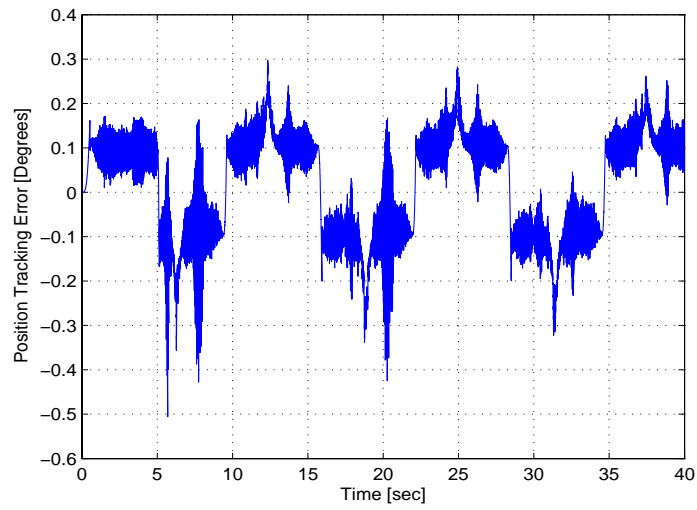
Figure 3–12: Position tracking error from the model-based controller with friction feedforward terms as described in (3–40).
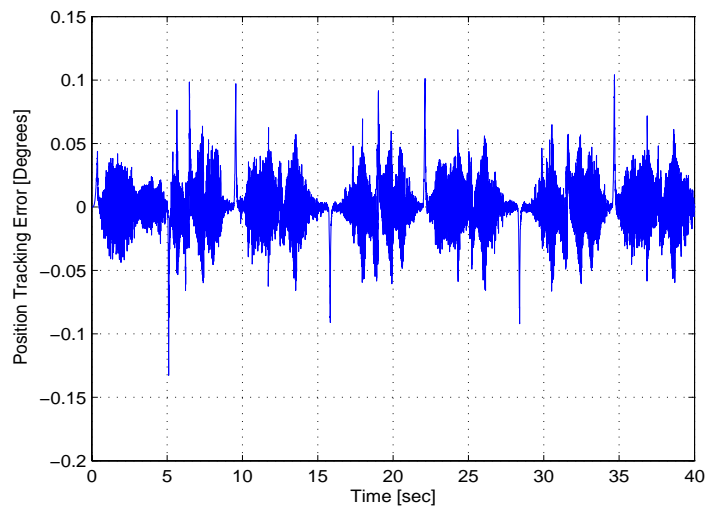
Figure 3–13: Position traking error from the proposed controller.
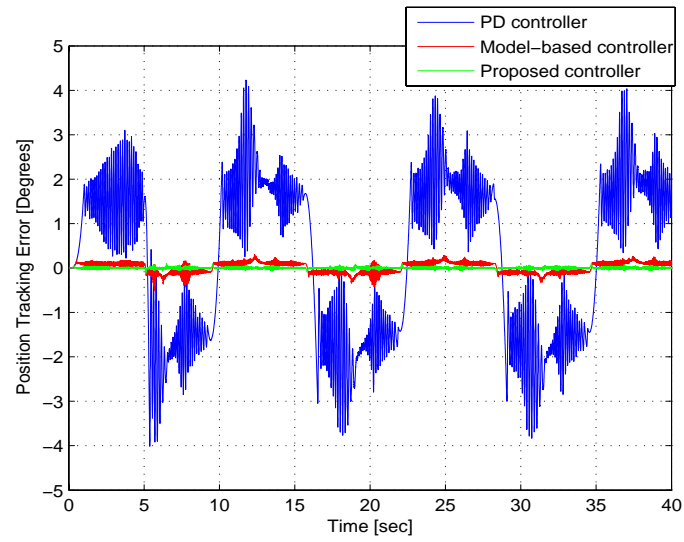
Figure 3–14: Comparison of position tracking errors from the three control schemes.
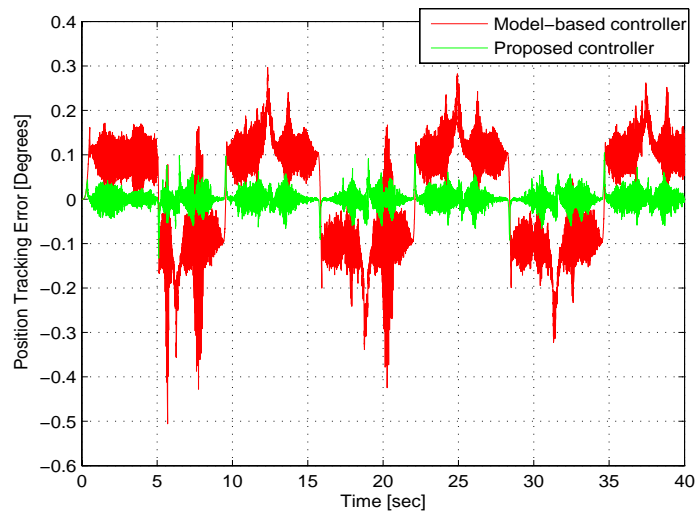
Figure 3–15: Comparison of position tracking errors from the model-based controller and the proposed controller.
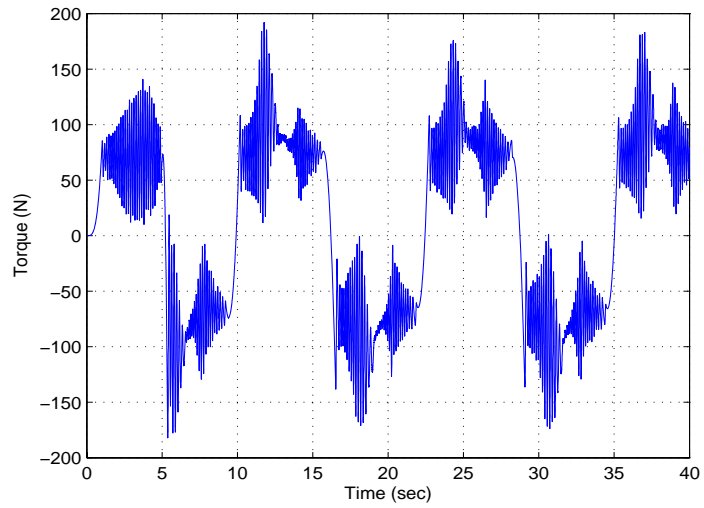
Figure 3–16: Torque input by the PD controller.
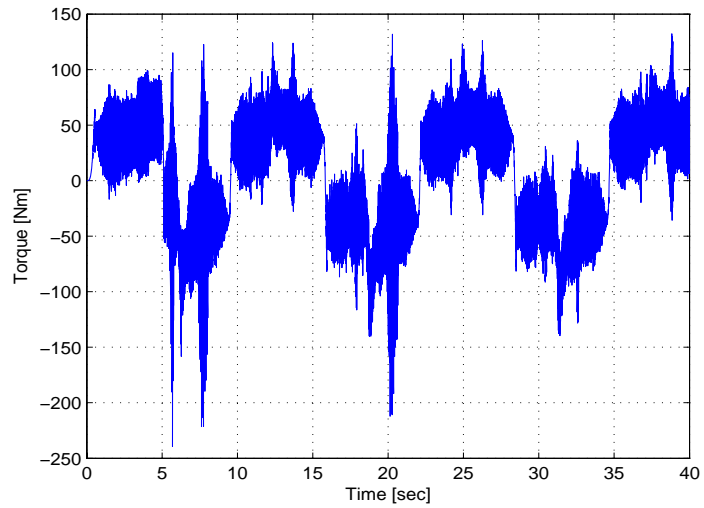
Figure 3–17: Torque input by the model-based controller with friction feedforward terms as described in (3–40).
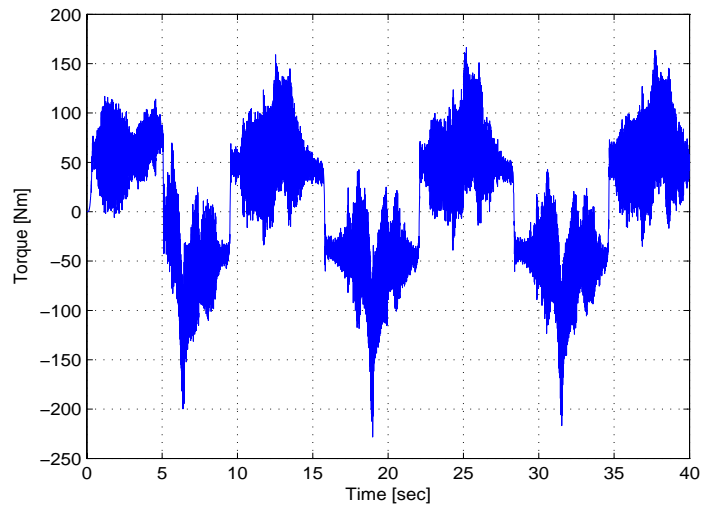
Figure 3–18: Torque input by the proposed controller.
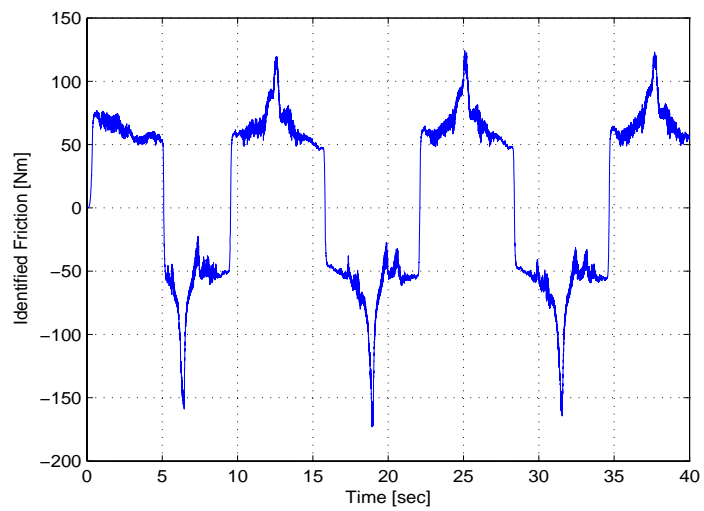
Figure 3–19: Identified friction from the adaptive term in the proposed controller.
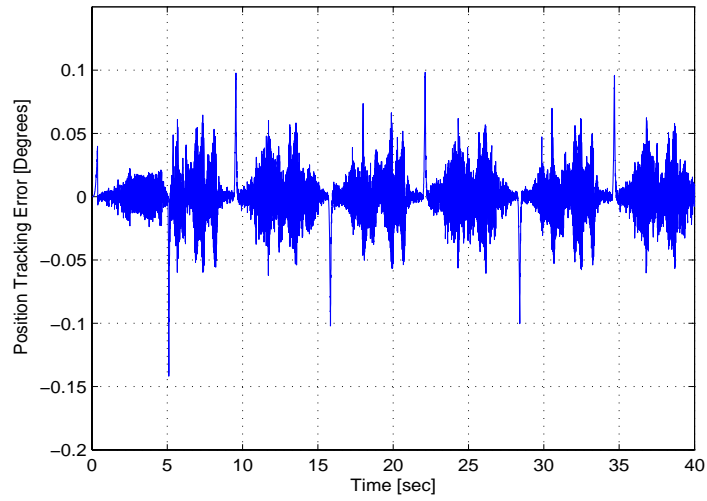
Figure 3–20: Position tracking error with the proposed controller when the circular disk was lubricated.
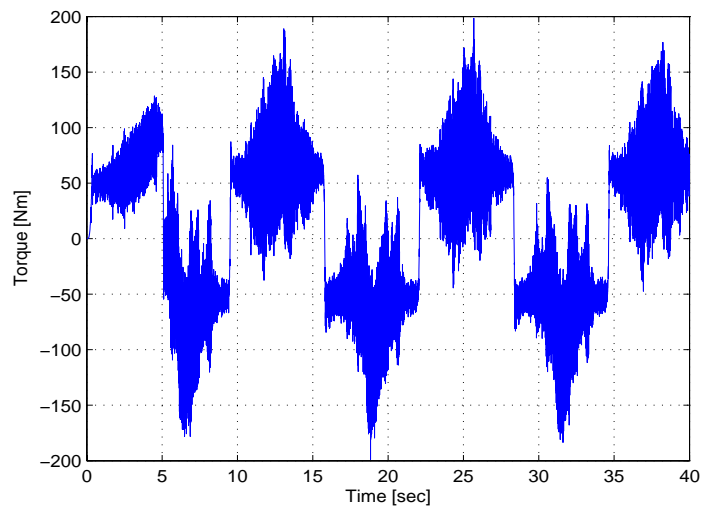
Figure 3–21: Torque input by the proposed controller when the circular disk was lubricated.
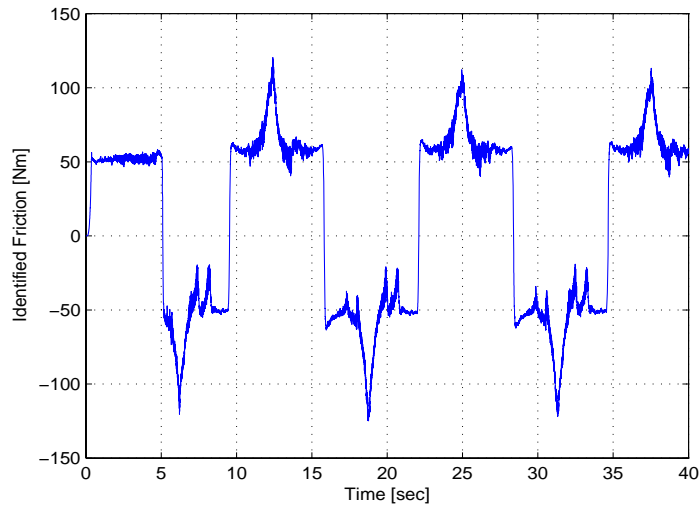
Figure 3–22: Identified friction from the adaptive term in the proposed controller when the circular disk was lubricated.

3.4.4   Experiment 4

In the fourth experiment, the net external friction induced on the system as a result of external load applied to the circular disk by the linear thruster was identified. The friction in the testbed under no-load conditions was identified as in Experiment 1 using the control gains of Experiment 2. This identified friction term was subtracted from the identified friction terms obtained from Experiment 2 and Experiment 3 respectively. The friction between the circular disk and Nylon block when the disk was not lubricated can be seen in Figure 3–23, and the friction when the disk was lubricated can be seen in Figure 3–24.

3.4.5   Experiment 5

In the fifth experiment, the experimentally identified friction torque using the adaptive term in (3–9) was compared with the friction torque model in (2–1). The friction identified in Figure 3–22 was compared with the model parameters in (2–1) that were adjusted to match the experimental data. The rotor velocity signal was obtained by applying a standard backwards difference algorithm to the position signal, and the friction torque in (2–1) was calculated as a function of this rotor
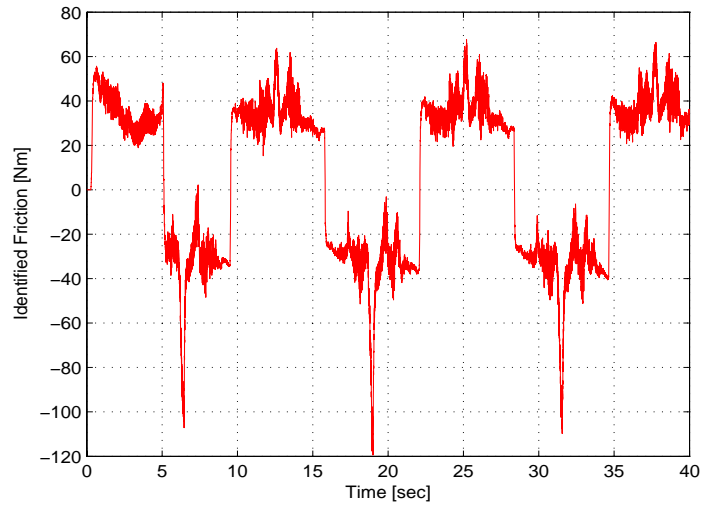
Figure 3–23: Net external friction induced with no lubrication. The net friction was calculated by subracting the identified friction term in Experiment 1 from the identified friction term in Experiment 2.
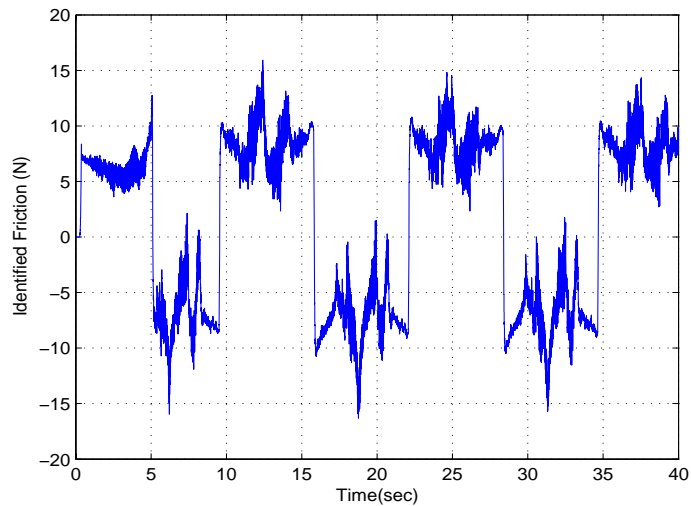
Figure 3–24: Net external friction induced with lubrication. The net friction was calculated by subracting the identified friction term in Experiment 1 from the identified friction term in Experiment 3.

velocity with the constants chosen as

$$\gamma_1 = 34.8 \quad \gamma_2 = 650 \quad \gamma_3 = 1$$

$$\gamma_4 = 26 \quad \gamma_5 = 200 \quad \gamma_6 = 19.5.$$

The matching of the friction torque with the experimental data is plotted in Figure 3–25.
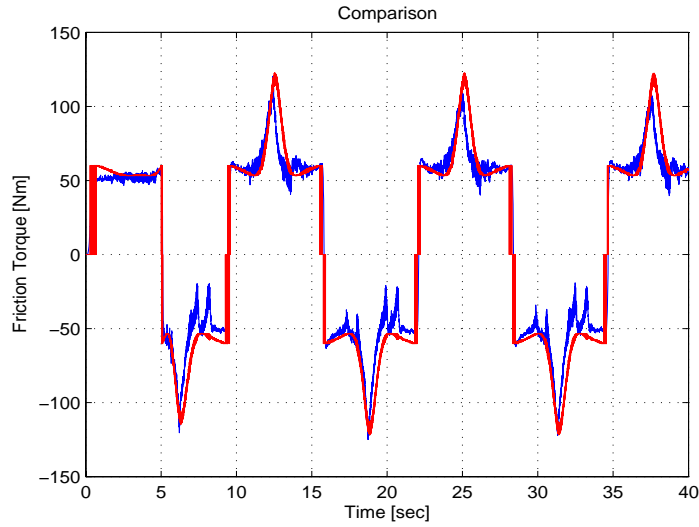
Figure 3–25: The friction torque calculated from the model in (2–1) approximates the experimentally identified friction torque in (3–9).

3.5   Discussion

In Experiment 1, it was observed that the position tracking error obtained from the PD controller in (3–39) deviated around 0.7337 degrees (as seen in Figure 3–2) compared to 0.0506 degrees (as in Figure 3–3) in the model-based controller in (3–40). This error was further reduced to about 0.0116 degrees when the proposed controller in (3–37) was implemented (as seen in Figure 3–4). A detailed comparison of the position tracking errors (in degrees) and control torque (in Nm) can be seen in Table I.

Similar difference in the order of the magnitude of position tracking errors was also observed in Experiment 2, when an external friction was applied to the

Table 3–1: Comparison of tracking results when no external load was applied to the circular disk.

	PD controller	Model-based controller	Proposed controller
Standard deviation in error	0.7337	0.0506	0.0116
Root mean square value	0.7442	0.0512	0.0116
Standard deviation in torque	33.2926	36.7456	37.5658
Root mean square value	33.7704	37.2826	32.1060

Table 3–2: Comparison of tracking results when an external load was applied to the circular disk.

	PD controller	Model-based controller	Proposed controller
Standard deviation in error	1.8225	0.1203	0.0186
Root mean square value	1.8373	0.1212	0.0186
Standard deviation in torque	82.7043	103.0262	72.9409
Root mean square value	83.3753	103.8698	73.9593

circular disk. The position tracking error when the PD controller in (3–39) was implemented deviated about 1.8225 degrees (see Figure 3–11), whereas in the model-based controller in (3–40) deviated about 0.1203 degrees as seen in Figure 3–12. Under the same load conditions, when the proposed controller in (3–37) was implemented, the position tracking error deviated around 0.0186 degrees (see Figure 3–13). A detailed comparison of the magnitudes of the position tracking errors (in degrees) and control torque (in Nm) can be seen in Table II.

Experiments 1-3 illustrate an approximate factor of 60 improvement over a PD controller, and a factor of approximately 3 over a typical exact model knowledge controller with static and viscous friction feedforward terms (see Figure 3–5, Figure 3–14, Figure 3–6, and 3–15). The significant improvement in the tracking error is also observed from Table I and Table II, where the rms value of error from the proposed controller is about two orders of magnitude better than the PD controller and about one order of magnitude better than the model-based controller. This

improvement in performance from the proposed controller was obtained while using similar or lower input torque as can be seen in Table I and Table II.

This improvement is based on the fact that the proposed controller contains a feedforward term that identifies the friction as a general time-varying disturbance. To develop the friction identification term, the friction model is required to be continuously differentiable. Experiments 1-5 illustrate the identified friction torque, and Experiment 5 specifically illustrates that a continuously differentiable friction model proposed in Makkar et al. [42] and Makkar and Dixon et al. [43] closely matches the identified friction. Mismatches between the identified friction and the friction model can be attributed to a number of effects such as wear, nonuniformity of the material, etc. However, the structure of the friction identification term enables these anisotropic effects to be captured.

It is interesting to compare the identified friction component from each of the experiments. The difference between Experiment 1 and 2 is that an external friction load is applied in Experiment 2. By comparing the identified friction component in Figure 3–10 and Figure 3–19, as expected, a factor of 2-3 increase in the static friction component is observed in Figure 3–19 with some increase in the viscous friction effects. The difference between Experiment 2 and 3 is that the contact surface is lubricated in Experiment 3. By comparing the identified friction component in Figure 3–19 and Figure 3–22, the static friction component is unchanged and a slight reduction in the viscous friction is observed. This is because the viscous friction of the motor assembly is the dominant viscous effect, as is illustrated by the results from Experiment 4.

In Experiment 5, the parameters of the nonlinear parameterizable friction model in (2–1) were varied to match the experimentally obtained friction torque in Figure 3–22. Figure 3–25 shows that the proposed friction model in (2–1) very closely approximates the experimental friction torque. However, since friction is

Figure 3–26: Wearing of the Nylon block where it rubbed against the circular disk.

anisotropic in nature, the magnitude of friction in experimental data is not symmetrical about the horizontal axis whereas the friction model in (2–1) approximates it as symmetric. Hence, future work can focus on mathematically distorting the model proposed in (2–1) by addition of more terms to make it asymmetric or making the unknown coefficients time-varying in order to capture more friction effects such as wear. Wear is evident on the Nylon block as indicated by groves (see Figure 3–26 and Figure 3–27) in the surface.

3.6 Concluding Remarks

A semi-global asymptotic tracking controller is developed based on the proposed continuously differentiable friction model that contains uncertain nonlinear parameterizable terms. To achieve the tracking result, an integral feedback compensation term is used to identify the system friction effects. A Lyapunov-based stability analysis is provided to conclude the tracking and friction identification results. Experimental results show two orders of magnitude improvement in tracking control over a proportional derivative (PD) controller, and a one order of magnitude improvement over the model-based controller. This controller assumes exact
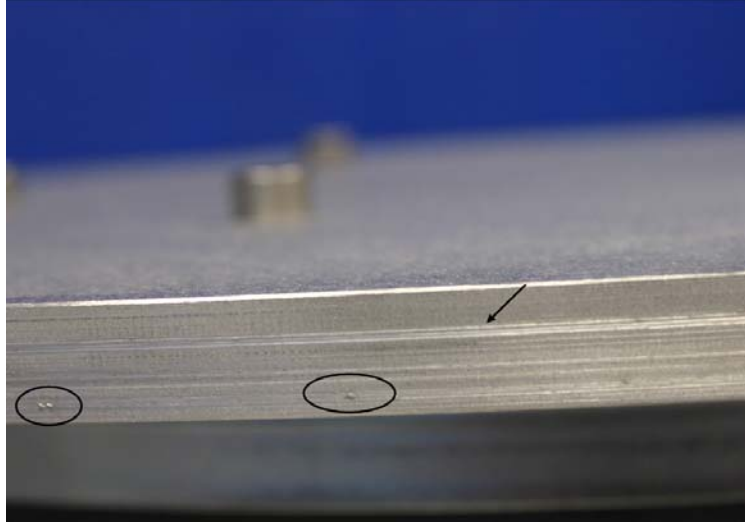
Figure 3–27: Wear on the circular disk.

model knowledge of the system dynamics except friction. The control development in the next chapter is motivated to eliminate this assumption and design a controller that can segregate the structured and unstructured uncertainties in the dynamics while achieving asymptotic tracking.

CHAPTER 4
TRACKING CONTROL IN THE PRESENCE OF FRICTION BY HIGH GAIN
FEEDBACK AND A MODEL-BASED FEEDFORWARD COMPONENT-AN
EXTENSION

The result in this chapter is motivated by the desire to include some knowledge of the dynamics in the control design as a means to improve the performance and reduce the control effort while eliminating the assumption that the dynamics of the system is completely known. Specifically, for systems that include some dynamics that can be segregated into structured (i.e., linear parameterizable) and unstructured uncertainty, this result illustrates how a new controller, error system, and stability analysis can be crafted to include a model-based adaptive feedforward term in conjunction with the high gain integral feedback technique to yield an asymptotic tracking result.

This chapter presents the first result that illustrates how the amalgamation of these compensation methods can be used to yield an asymptotic result. Heuristically, the addition of the model-based adaptive feedforward term should reduce the overall control effort because some of the disturbance has been isolated and compensated for by a non-high gain feedforward element. Moreover, the addition of the adaptive feedforward term injects some knowledge of the dynamics in the control structure, which could lead to improved performance.

Preliminary experimental results are presented to reinforce these heuristic notions. Specifically, the presented controller was implemented on a simple one-link robot testbed and demonstrated reduced tracking error. For this testbed, the only dynamics that were included in the feedforward term included the inertia of the linkage system. This chapter is organized as follows. The dynamic

model and the associated properties are provided in Section 4.1. Section 4.2 describes the development of errorsystem followed by the stability analysis in Section 4.3. Section 4.4 describes the experimental set up and results that indicate improved performance obtained by implementing the proposed controller followed by discussion in Section 4.5 and conclusion in Section 4.6.

4.1 Dynamic Model and Properties

The class of nonlinear dynamic systems considered are described in Chapter 1 and Chapter 2 by the general Euler-Lagrange formulation in (1–1) where the term $f(\dot{q}) \in \mathbb{R}^n$ denotes a general nonlinear disturbance (e.g., friction as in Makkar et al. [42] and Makkar and Dixon et al. [43], unmodeled effects).

The subsequent development is based on the assumption that $q(t)$ and $\dot{q}(t)$ are measurable and that $M(q)$, $V_m(q, \dot{q})$ and $G(q)$ are unknown. Moreover, the following properties and assumptions will be exploited in the subsequent development:

Property 4.1: The inertia matrix $M(q)$ as in (3–1) is symmetric, positive definite, and satisfies the following inequality $\forall\, y(t) \in \mathbb{R}^n$:

$$m_1 \|y\|^2 \le y^T M(q) y \le \bar{m}(q) \|y\|^2 \tag{4–1}$$

where $m_1 \in \mathbb{R}$ is a known positive constant, $\bar{m}(q) \in \mathbb{R}$ is a known positive function, and $\|\cdot\|$ denotes the standard Euclidean norm.

Property 4.2: If $q(t)$, $\dot{q}(t) \in \mathcal{L}_\infty$, then $V_m(q, \dot{q})$, $f(\dot{q})$ and $G(q)$ are bounded. Moreover, if $q(t)$, $\dot{q}(t) \in \mathcal{L}_\infty$, then $\dfrac{\partial M(q)}{\partial q}$, $\dfrac{\partial^2 M(q)}{\partial q^2}$, $\dfrac{\partial V_m(q, \dot{q})}{\partial q}$, $\dfrac{\partial^2 V_m(q, \dot{q})}{\partial q^2}$, $\dfrac{\partial V_m(q, \dot{q})}{\partial \dot{q}}$, $\dfrac{\partial^2 V_m(q, \dot{q})}{\partial \dot{q}^2}$, $\dfrac{\partial f(\dot{q})}{\partial \dot{q}}$, $\dfrac{\partial^2 f(\dot{q})}{\partial \dot{q}^2}$, $\dfrac{\partial G(q)}{\partial q}$, and $\dfrac{\partial^2 G(q)}{\partial q^2}$ exist and are bounded.

Property 4.3: There exist positive scalar constant ζ_{c1} such that

$$\|V_m(q, \dot{q})\| \le \zeta_{c1} \|\dot{q}\|, \quad \forall q, \dot{q} \in \mathbb{R}^n. \tag{4–2}$$

Property 4.4: The dynamic equation in (1–1) can be linear parameterized as

$$Y_d\left(q_d, \dot{q}_d, \ddot{q}_d\right) \theta \triangleq M(q_d)\ddot{q}_d + V_m(q_d, \dot{q}_d)\dot{q}_d + G(q_d) \tag{4–3}$$

where $\theta \in \mathbb{R}^p$ contains the constant unknown system parameters, and the desired regression matrix $Y_d\left(q_d, \dot{q}_d, \ddot{q}_d\right) \in \mathbb{R}^{n \times p}$ contains known functions of the desired link position, velocity, and acceleration, $q_d\left(t\right), \dot{q}_d\left(t\right), \ddot{q}_d\left(t\right) \in \mathbb{R}^n$, respectively. The desired trajectory is assumed to be designed such that $q_d(t)$, $\dot{q}_d(t)$, $\ddot{q}_d(t)$, $\dddot{q}_d(t)$, $\ddddot{q}_d(t) \in \mathbb{R}^n$ exist and are bounded.

4.2 Error System Development

The control objective is to ensure that the system tracks a desired time-varying trajectory despite structured and unstructured uncertainties in the dynamic model. To quantify this objective, a position tracking error as in (3–2), denoted by $e_1(t) \in \mathbb{R}^n$, is defined as

$$e_1 = q_d - q. \tag{4–4}$$

To facilitate the subsequent analysis, filtered tracking errors as in (3–3 and 3–4), denoted by $e_2(t)$, $r(t) \in \mathbb{R}^n$, are also defined as

$$e_2 = \dot{e}_1 + \alpha_1 e_1 \tag{4–5}$$

$$r = \dot{e}_2 + \alpha_2 e_2 \tag{4–6}$$

where α_1, $\alpha_2 \in \mathbb{R}$ denote positive constants. The filtered tracking error $r(t)$ is not measurable since the expression in (4–6) depends on $\ddot{q}(t)$.

The open-loop tracking error system can be developed by premultiplying (4–6) by $M(q)$ and utilizing the expressions in (1–1), (4–3), (4–4), and (4–5) to obtain the following expression:

$$M(q)r = Y_d\theta + W - \tau(t) \tag{4–7}$$

where $Y_d(t)\theta \in \mathbb{R}^n$ is defined in (4–3), and the auxiliary signal $W(e_1, e_2, t) \in \mathbb{R}^n$ is

defined as

$$W = M(q)\left(\ddot{q}_d + \alpha_1\dot{e}_1 + \alpha_2 e_2\right) + V_m(q,\dot{q})\dot{q} + G(q) + f(\dot{q}) - Y_d\theta. \qquad (4\text{--}8)$$

Based on the expression in (4–7), the control torque input is designed as follows:

$$\tau = Y_d\hat{\theta} + \mu. \qquad (4\text{--}9)$$

In (4–9), $\mu(t) \in \mathbb{R}^n$ denotes a high-gain feedback control term defined as

$$\mu(t) = (k_s + 1)e_2(t) - (k_s + 1)e_2(t_0) \qquad (4\text{--}10)$$
$$+ \int_{t_0}^{t}[(k_s + 1)\alpha_2 e_2(\sigma) + \beta sgn(e_2(\sigma))]d\sigma$$

where $k_s, \beta \in \mathbb{R}$ are positive constant control gains as in (3–9), and $\hat{\theta}(t) \in \mathbb{R}^p$ denotes a parameter estimate vector generated on-line according to the following update law:

$$\dot{\hat{\theta}} = \Gamma\dot{Y}_d^T r \qquad (4\text{--}11)$$

with $\Gamma \in \mathbb{R}^{p\times p}$ being a known, constant, diagonal, positive-definite, adaptation gain matrix. Since $\dot{Y}_d(t)$ is only a function of the known time varying trajectory, (4–11) can be integrated by parts as follows:

$$\hat{\theta}(t) = \hat{\theta}(t_0) + \Gamma\dot{Y}_d^T e_2(\sigma)\Big|_{t_0}^{t} - \Gamma\int_{t_0}^{t}\left\{\ddot{Y}_d^T e_2(\sigma) - \alpha_2\dot{Y}_d^T e_2(\sigma)\right\}d\sigma \qquad (4\text{--}12)$$

so that the parameter estimate vector $\hat{\theta}(t)$ implemented in (4–9) does not depend on the unmeasurable signal $r(t)$.

Remark 4.1: *The control design in (4–9) is similar to the results in Xian et al. [57]. However, previous designs based on [57] could only compensate for uncertainty in the system through the high gain feedback term $\mu(t)$. Through the new error system development and stability analysis methods presented in the current result, an adaptive feedforward term can also be used to compensate for system uncertainty. This flexibility presents a significant advantage because it*

allows more system dynamics to be incorporated in the control design. Specifically, if some of the system uncertainty can be segregated into a linear parameterizable form, then the model-based adaptive feedforward term can be injected to compensate for the uncertainty instead of just relying on the non-model based high gain feedback term. Heuristically, this contribution should improve the tracking performance and reduce the control effort. Preliminary experimental results on a simple one-link robot manipulator provide some validation of this heuristic idea.

The closed-loop tracking error system can be developed by substituting (4–9) into (4–7) as

$$M(q)r = Y_d\tilde{\theta} + W - \mu(t) \tag{4–13}$$

where $\tilde{\theta}(t) \in \mathbb{R}^p$ represents the parameter estimation error vector defined as

$$\tilde{\theta} = \theta - \hat{\theta}. \tag{4–14}$$

To facilitate the subsequent stability analysis (and to illustrate some insight into the structure of the design for $\mu(t)$), the time derivative of (4–13) is determined as

$$M(q)\dot{r} = -\dot{M}(q)r + \dot{Y}_d\tilde{\theta} - Y_d\dot{\hat{\theta}} + \dot{W} - \dot{\mu}(t). \tag{4–15}$$

The time derivative of (4–10) is given as

$$\dot{\mu}(t) = (k_s + 1)r + \beta sgn(e_2). \tag{4–16}$$

After substituting (4–11) and (4–16) into (4–15), the following closed-loop error system can be obtained:

$$M(q)\dot{r} = -\frac{1}{2}\dot{M}(q)r + \dot{Y}_d\tilde{\theta} + N - \dot{\mu}(t) - e_2 \tag{4–17}$$

where $N(e_1, e_2, r, t) \in \mathbb{R}^n$ denotes the following unmeasurable auxiliary term:

$$N = -Y_d\Gamma\dot{Y}_d^T r + \dot{W} + e_2 - \frac{1}{2}\dot{M}(q)r. \tag{4–18}$$

After substituting for the time derivative of $W(e_1, e_2, t)$, auxiliary term in (4–18) can be expressed as

$$N = -Y_d \Gamma \dot{Y}_d^T r + \frac{\partial M(q)}{\partial q} \dot{q} \left[\alpha_1 e_2 - \alpha_1^2 e_1 + \alpha_2 e_2 \right] + M(q) \alpha_1 r - \alpha_2 e_2 \qquad (4\text{–}19)$$

$$- \alpha_1 (e_2 - \alpha_1 e_1) + \alpha_2 (r - \alpha_2 e_2) + \frac{\partial M(q)}{\partial q} \dot{q} \ddot{q}_d + M(q) \dddot{q}_d + \frac{\partial V_m(q, \dot{q})}{\partial q} \dot{q}^2$$

$$+ \frac{\partial V_m(q, \dot{q})}{\partial \dot{q}} \dot{q} \ddot{q} + V_m(q, \dot{q}) \ddot{q} + \frac{\partial G(q)}{\partial q} \dot{q} + \frac{\partial f(\dot{q})}{\partial \dot{q}} \ddot{q} - \dot{Y}_d \theta + e_2 - \frac{1}{2} \frac{\partial M(q)}{\partial q} \dot{q} r.$$

To further facilitate the subsequent analysis, another unmeasurable auxiliary term $N_d(q_d, \dot{q}_d, \ddot{q}_d, t) \in \mathbb{R}^n$ is defined as

$$N_d = \frac{\partial f(\dot{q}_d)}{\partial \dot{q}_d} \ddot{q}_d + \frac{\partial M(q_d)}{\partial q_d} \dot{q}_d \ddot{q}_d + M(q_d) \dddot{q}_d + \frac{\partial V_m(q_d, \dot{q}_d)}{\partial q_d} \dot{q}_d^2 \qquad (4\text{–}20)$$

$$+ \frac{\partial V_m(q_d, \dot{q}_d)}{\partial \dot{q}_d} \dot{q}_d \ddot{q}_d + V_m(q_d, \dot{q}_d) \ddot{q}_d + \frac{\partial G(q_d)}{\partial q_d} \dot{q}_d - \dot{Y}_d \theta.$$

After adding and subtracting (4–20), the closed-loop error system in (4–17) can be expressed as

$$M(q)\dot{r} = -\frac{1}{2} \dot{M}(q) r + \dot{Y}_d \tilde{\theta} - \dot{\mu}(t) - e_2 + \tilde{N}(t) + N_d(t) \qquad (4\text{–}21)$$

where the unmeasurable auxiliary term $\tilde{N}(e_1, e_2, r, t) \in \mathbb{R}^n$ is defined as

$$\tilde{N}(t) = N(t) - N_d(t). \qquad (4\text{–}22)$$

In a similar manner as in Xian et al. [57], the Mean Value Theorem can be used to develop the following upper bound

$$\left\| \tilde{N}(t) \right\| \le \rho \left(\|z\| \right) \|z\| \qquad (4\text{–}23)$$

where $z(t) \in \mathbb{R}^{3n}$ is defined as

$$z(t) \triangleq [e_1^T \quad e_2^T \quad r^T]^T. \qquad (4\text{–}24)$$

The following inequalities can be developed based on the expression in (4–20) and its time derivative:

$$\|N_d(t)\| \le \zeta_{N_d} \qquad \left\| \dot{N}_d(t) \right\| \le \zeta_{N_d 2} \qquad (4\text{–}25)$$

where ζ_{N_d}, $\zeta_{N_d2} \in \mathbb{R}$ are known positive constants.

4.3 Stability Analysis

Theorem 4.1: The controller given in (4–9), (4–10), and (4–12) ensures that all system signals are bounded under closed-loop operation and that the position tracking error is regulated in the sense that

$$e_1(t) \to 0 \qquad as \qquad t \to \infty$$

provided the control gain k_s introduced in (4–10) is selected sufficiently large, and β is selected according to the following sufficient condition:

$$\beta > \zeta_{N_d} + \frac{1}{\alpha_2}\zeta_{N_d2} \tag{4–26}$$

where ζ_{N_d} and ζ_{N_d2} are introduced in (4–25).

Proof: Let $\mathcal{D} \subset \mathbb{R}^{3n+p+1}$ be a domain containing $y(t) = 0$, where $y(t) \in \mathbb{R}^{3n+p+1}$ is defined as

$$y(t) = [z^T(t) \quad \tilde{\theta}^T(t) \quad \sqrt{P(t)}]^T \tag{4–27}$$

and the auxiliary function $P(t) \in \mathbb{R}$ is defined as

$$P(t) = \beta \, ||e_2(t_0)|| - e_2(t_0)^T N_d(t_0) - \int_{t_0}^{t} L(\tau)d\tau. \tag{4–28}$$

In (4–28), the auxiliary function $L(t) \in \mathbb{R}$ is defined as

$$L(t) = r^T(N_d(t) - \beta sgn(e_2)). \tag{4–29}$$

The derivative $\dot{P}(t) \in \mathbb{R}$ can be expressed as

$$\dot{P}(t) = -L(t) = -r^T(N_d(t) - \beta sgn(e_2)). \tag{4–30}$$

Provided the sufficient condition introduced in (4–26) is satisfied, the following inequality can be obtained (see Xian et al. [57])

$$\int_{t_0}^{t} L(\tau)d\tau \leq \beta \, ||e_2(t_0)|| - e_2(t_0)^T N_d(t_0). \tag{4–31}$$

Hence, (4–31) can be used to conclude that $P(t) \geq 0$.

Let $V(y,t) : \mathcal{D} \times [0, \infty) \to \mathbb{R}$ be a continuously differentiable positive definite function defined as

$$V(y,t) = e_1^T e_1 + \frac{1}{2} e_2^T e_2 + \frac{1}{2} r^T M(q) r + P + \frac{1}{2} \tilde{\theta}^T \Gamma^{-1} \tilde{\theta} \qquad (4\text{–}32)$$

which satisfies the following inequalities:

$$U_1(y) \leq V(y,t) \leq U_2(y) \qquad (4\text{–}33)$$

provided the sufficient condition introduced in (4–26) is satisfied. In (4–33), the continuous positive definite functions $U_1(y)$, $U_2(y) \in \mathbb{R}$ are defined as

$$U_1(y) = \eta_1 \|y\|^2 \qquad U_2(y) = \eta_2(q) \|y\|^2 \qquad (4\text{–}34)$$

where η_1, $\eta_2(q) \in \mathbb{R}$ are defined as

$$\eta_1 \triangleq \frac{1}{2} \min\{1, m_1, \lambda_{\min}\{\Gamma^{-1}\}\},$$

$$\eta_2(q) \triangleq \max\{\frac{1}{2}\bar{m}(q), \frac{1}{2}\lambda_{\max}\{\Gamma^{-1}\}, 1\}$$

where m_1, $\bar{m}(q)$ are introduced in (4–1) and $\lambda_{\min}\{\cdot\}$, $\lambda_{\max}\{\cdot\}$ denote the minimum and maximum eigenvalue of the argument respectively. After taking the time derivative of (4–32), $\dot{V}(y,t)$ can be expressed as

$$\dot{V}(y,t) = r^T M(q)\dot{r} + \frac{1}{2} r^T \dot{M}(q) r + e_2^T \dot{e}_2 + 2 e_1^T \dot{e}_1 + \dot{P} - \tilde{\theta}^T \Gamma^{-1} \dot{\hat{\theta}}.$$

After utilizing (4–5), (4–6), (4–11), (4–16), (4–21), and (4–30), $\dot{V}(y,t)$ can be simplified as follows:

$$\dot{V}(y,t) = r^T \tilde{N}(t) - (k_s + 1)\|r\|^2 - \alpha_2 \|e_2\|^2 - 2\alpha_1 \|e_1\|^2 + 2 e_2^T e_1. \qquad (4\text{–}35)$$

Because $e_2^T(t)e_1(t)$ can be upper bounded as

$$e_2^T e_1 \leq \frac{1}{2} \|e_1\|^2 + \frac{1}{2} \|e_2\|^2,$$

$\dot{V}(y,t)$ can be upper bounded using the squares of the components of $z(t)$ as follows:

$$\dot{V}(y,t) \leq r^T \tilde{N}(t) - (k_s + 1) \|r\|^2 - \alpha_2 \|e_2\|^2 - 2\alpha_1 \|e_1\|^2 + \|e_1\|^2 + \|e_2\|^2 \,.$$

By using (4–23), the expression in (4–35) can be rewritten as follows:

$$\dot{V}(y,t) \leq -\lambda_3 \|z\|^2 - \left(k_s \|r\|^2 - \rho(\|z\|) \|r\| \|z\|\right) \tag{4–36}$$

where $\lambda_3 \triangleq \min\{2\alpha_1 - 1, \alpha_2 - 1, 1\}$, and the bounding function $\rho(\|z\|) \in \mathbb{R}$ is a positive globally invertible nondecreasing function; hence, α_1, α_2 must be chosen according to the following conditions:

$$\alpha_1 > \frac{1}{2}, \qquad \alpha_2 > 1.$$

After completing the squares for the second and third term in (4–36), the following expression can be obtained:

$$\dot{V}(y,t) \leq -\lambda_3 \|z\|^2 + \frac{\rho^2(z) \|z\|^2}{4k_s}. \tag{4–37}$$

The following expression can then be obtained from (4–37)

$$\dot{V}(y,t) \leq -U(y) \tag{4–38}$$

where $U(y) = c\|z\|^2$, for some positive constant $c \in \mathbb{R}$, is a continuous positive semi-definite function that is defined on the following domain:

$$D \triangleq \{y \in \mathbb{R}^{3n+p+1} \mid \|y\| \leq \rho^{-1}(2\sqrt{\lambda_3 k_s})\}.$$

The inequalities in (4–33) and (4–38) can be used to show that $V(y,t) \in \mathcal{L}_\infty$ in $\mathcal{D}$; hence, $e_1(t)$, $e_2(t)$, $r(t)$, and $\tilde{\theta}(t) \in \mathcal{L}_\infty$ in $\mathcal{D}$. Given that $e_1(t)$, $e_2(t)$, and $r(t) \in \mathcal{L}_\infty$ in $\mathcal{D}$, standard linear analysis methods can be used to prove that $\dot{e}_1(t)$, $\dot{e}_2(t) \in \mathcal{L}_\infty$ in $\mathcal{D}$ from (4–5) and (4–6). Since $\theta \in \mathbb{R}^p$ contains the constant unknown

system parameters and $\tilde{\theta}(t) \in \mathcal{L}_\infty$ in $\mathcal{D}$, (4–14) can be used to prove that $\hat{\theta}(t) \in \mathcal{L}_\infty$ in $\mathcal{D}$. Since $e_1(t)$, $e_2(t)$, $r(t) \in \mathcal{L}_\infty$ in $\mathcal{D}$, the assumption that $q_d(t)$, $\dot{q}_d(t)$, $\ddot{q}_d(t)$ exist and are bounded can be used along with (4–4)-(4–6) to conclude that $q(t)$, $\dot{q}(t)$, $\ddot{q}(t) \in \mathcal{L}_\infty$ in $\mathcal{D}$. The assumption that $q_d(t)$, $\dot{q}_d(t)$, $\ddot{q}_d(t)$ $\dddot{q}_d(t)$, $\ddddot{q}_d(t)$ exist and are bounded along with Property 4 can be used to show that $Y_d(q_d, \dot{q}_d, \ddot{q}_d)$, $\dot{Y}_d(q_d, \dot{q}_d, \ddot{q}_d)$, and $\ddot{Y}_d(q_d, \dot{q}_d, \ddot{q}_d) \in \mathcal{L}_\infty$ in $\mathcal{D}$. Since $q(t)$, $\dot{q}(t) \in \mathcal{L}_\infty$ in $\mathcal{D}$, Property 2 can be used to conclude that $M(q)$, $V_m(q, \dot{q})$, $G(q)$, and $f(\dot{q}) \in \mathcal{L}_\infty$ in $\mathcal{D}$. From (4–9) and (4–10), we can show that $\mu(t)$, $\tau(t) \in \mathcal{L}_\infty$ in $\mathcal{D}$. Given that $r(t) \in \mathcal{L}_\infty$ in $\mathcal{D}$, (4–16) can be used to show that $\dot{\mu}(t) \in \mathcal{L}_\infty$ in $\mathcal{D}$. Since $\dot{q}(t)$, $\ddot{q}(t) \in \mathcal{L}_\infty$ in $\mathcal{D}$, Property 2 can be used to show that $\dot{V}_m(q, \dot{q})$, $\dot{G}(q)$, $\dot{f}(q)$ and $\dot{M}(q) \in \mathcal{L}_\infty$ in $\mathcal{D}$; hence, (4–15) can be used to show that $\dot{r}(t) \in \mathcal{L}_\infty$ in $\mathcal{D}$. Since $\dot{e}_1(t)$, $\dot{e}_2(t)$, $\dot{r}(t) \in \mathcal{L}_\infty$ in $\mathcal{D}$, the definitions for $U(y)$ and $z(t)$ can be used to prove that $U(y)$ is uniformly continuous in $\mathcal{D}$.

Let $\mathcal{S} \subset \mathcal{D}$ denote a set defined as follows:

$$\mathcal{S} \triangleq \left\{ y(t) \subset \mathcal{D} \mid U_2(y(t)) < \eta_1 \left(\rho^{-1}(2\sqrt{\lambda_3 k_s}) \right)^2 \right\}. \tag{4–39}$$

The region of attraction in (4–39) can be made arbitrarily large to include any initial conditions by increasing the control gain k_s (i.e., a semi-global type of stability result) as in Xian et al. [57]. Theorem 8.4 of [30] can now be invoked to state that

$$c \, \|z(t)\|^2 \to 0 \qquad as \qquad t \to \infty \qquad \forall y(t_0) \in \mathcal{S}. \tag{4–40}$$

Based on the definition of $z(t)$, (4–40) can be used to show that

$$r(t) \to 0 \qquad as \qquad t \to \infty \qquad \forall y(t_0) \in \mathcal{S}. \tag{4–41}$$

Hence, from (4–5) and (4–6), standard linear analysis methods can be used to prove that

$$e_1(t) \to 0 \qquad as \qquad t \to \infty \qquad \forall y(t_0) \in \mathcal{S}.$$
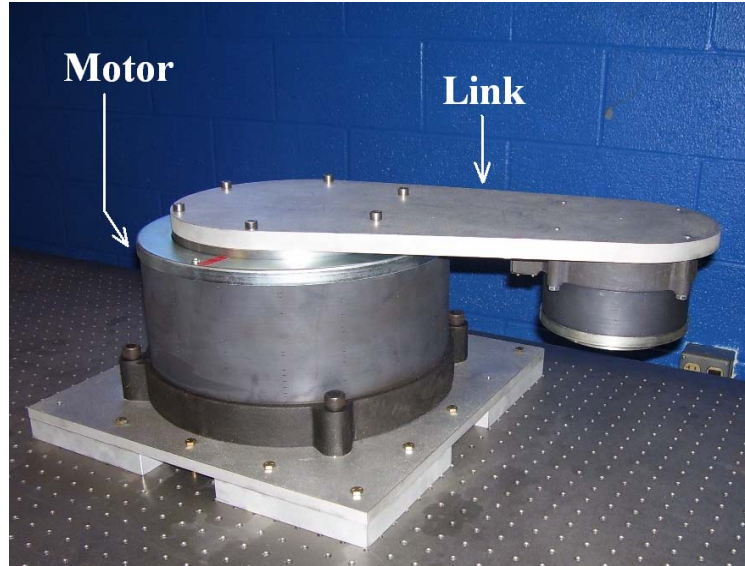
Figure 4–1: The experimental testbed consists of a 1-link robot mounted on a NSK direct-drive switched reluctance motor.

4.4   Experimental Results

The testbed depicted in Figure 4–1 was used to implement the developed controller. The testbed consists of a one-link robotic arm of unknown inertia mounted on a NSK direct-drive switched reluctance motor (240.0 Nm Model YS5240-GN001). The NSK motor is controlled through power electronics operating in torque control mode. The motor resolver provides rotor position measurements with a resolution of 614400 pulses/revolution at a resolver and feedback resolution of 12 bits. A Pentium 2.8 GHz PC operating under QNX hosts the control algorithm, which was implemented via Qmotor 3.0, a graphical user-interface, to facilitate real-time graphing, data logging, and adjustment of control gains without recompiling the program (for further information on Qmotor 3.0, the reader is referred to Loffler et al. [39]). Data acquisition and control implementation were performed at a frequency of 1.0 kHz using the ServoToGo I/O board.

The dynamics for the testbed are given as follows:

$$\tau(t) = J\ddot{q} + f(\dot{q}) \tag{4–42}$$

where $J \in \mathbb{R}$ denotes the inertia of the link assembly and $f(\dot{q}) \in \mathbb{R}$ represents the friction torque. The control torque input $\tau(t)$ given in (4–9) is simplified (i.e., the centripetal-Coriolis matrix and gravity terms were omitted) for the simple testbed as:

$$\tau(t) = \hat{J}\ddot{q}_d + \mu(t) \tag{4–43}$$

where $\hat{J}(t)$ denotes the adaptive estimate for the inertia of the link assembly, and $\mu(t)$ is the adaptive control term defined in (4–10). The adaptive estimate $\hat{J}(t)$ is updated according to the following update law:

$$\hat{J}(t) = \hat{J}(t_0) + \int_{t_0}^{t} \Gamma \ddot{q}_d r \tag{4–44}$$

where $\Gamma \in \mathbb{R}$ is a constant positive adaptive gain and $\hat{J}(t_0) = 0.179$ kg-m^2 is an initial guess for the inertia of the link assembly. The desired link trajectory (see Figure 4–2) was selected as follows (in degrees):

$$q_d(t) = 50.0\sin(1.5t))(1 - \exp(-0.01t^3)). \tag{4–45}$$

For all experiments, the rotor velocity signal is obtained by applying a standard backwards difference algorithm to the position signal. All states were initialized to zero. In addition, the integral structure of the adaptive term in (4–43) and (4–44) was computed on-line via a standard trapezoidal algorithm. The signum function for the control scheme in (4–10) was defined as:

$$sgn(e_2(t)) = \begin{cases} 1 & e_2 > 0 \\ -1 & e_2 < 0 \\ 0 & e_2 = 0 \end{cases}.$$
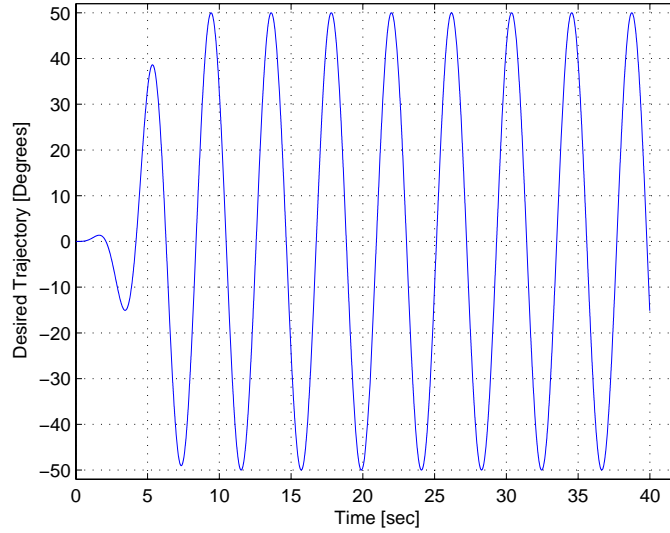
Figure 4–2: Desired trajectory used for the experiment.

4.4.1 Experiment 1

In the first experiment, the controller in (4–9) was implemented without updating the adaptation term (i.e., $\Gamma = 0$). Thus the control torque input given in (4–43) takes the following form:

$$\tau(t) = \hat{J}(t_0)\ddot{q}_d + \mu(t)$$

The gains for the controller that yielded the best steady-state performance were determined as follows:

$$k_s = 180 \quad \beta = 20 \quad \alpha_1 = 40 \quad \alpha_2 = 15. \qquad (4\text{–}46)$$

The position tracking error obtained from the controller is plotted in Figure 4–3. The torque input by the controller is depicted in Figure 4–4.

4.4.2 Experiment 2

In the second experiment, the update law defined in (4–44) was used to update the adaptive term defined in (4–43). The following control gains were used to implement the controller in (4–43):
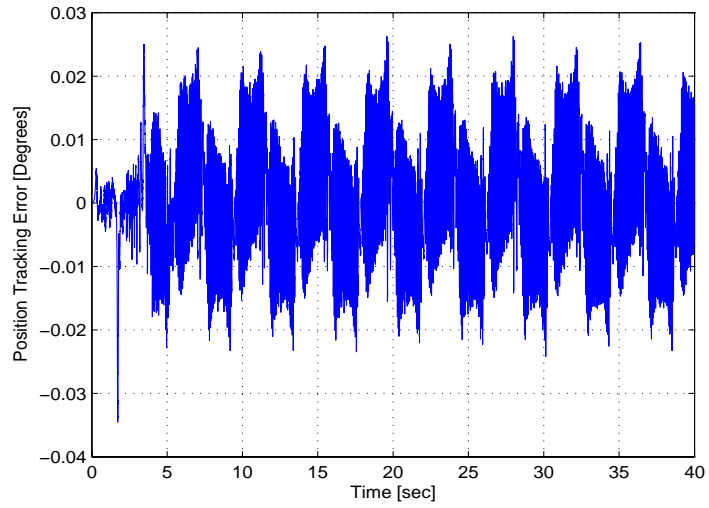
Figure 4–3: Position tracking error when the adaptive gain is zero.
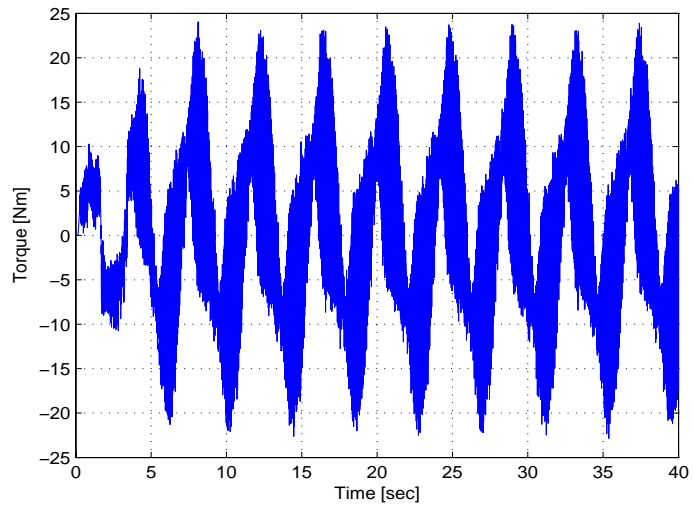
Figure 4–4: Torque input when the adaptive gain is zero.
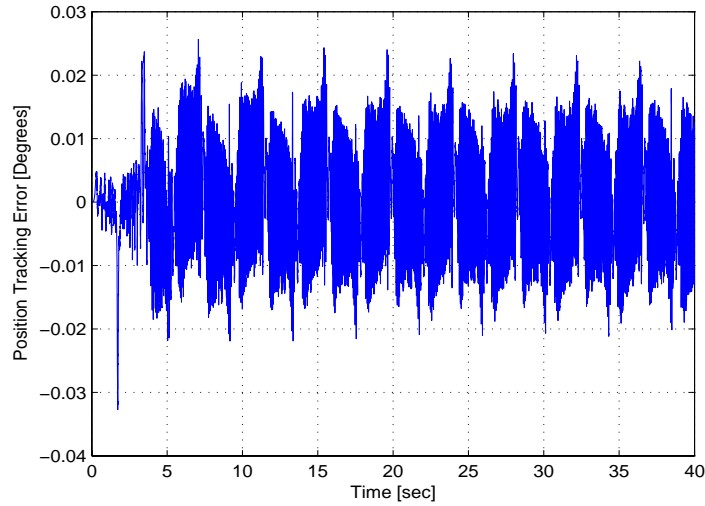
Figure 4–5: Position tracking error for the control structure that includes the adaptive update law.

$$k_s = 180 \quad \beta = 20 \quad \alpha_1 = 40 \quad \alpha_2 = 15 \quad \Gamma = 5.$$

The initial guess for the inertia of the link assembly was set to the same value as in the first experiment. The position tracking error obtained from the controller is plotted in Figure 4–5. The torque input by the controller is depicted in Figure 4–6. The inertia estimate is depicted in Figure 4–7.

4.5 Discussion

The position tracking errors for the two cases (without adaptation and with adaptation) are plotted in Figures 4–3 and 4–5. The results indicate that the RMS value of the position tracking error when the adaptive feedforward term is used, is about 5.62% less than the case when no adaptation term is used. This improvement in performance by the proposed controller was obtained while using similar input torque as can be seen in Figure 4–4 and Figure 4–6.

In these preliminary results, the adaptive feedforward term was limited to one parameter. A multi-link robotic testbed is currently being used to develop a more complete set of experimental results that would allow additional dynamic terms to
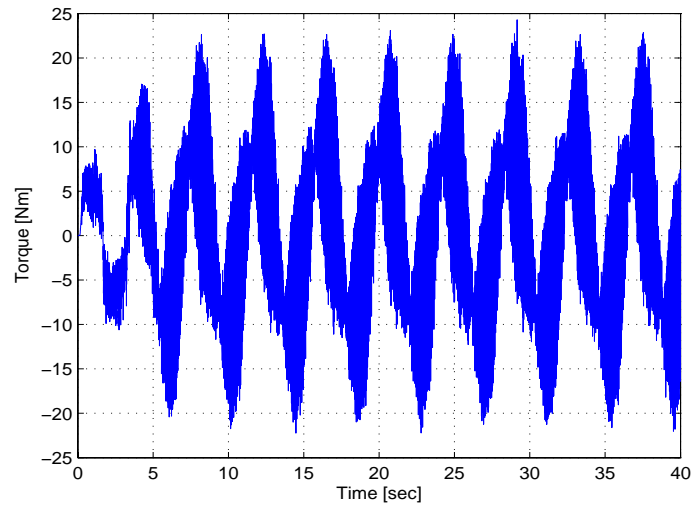
Figure 4–6: Torque input for the control structure that includes the adaptive update law.
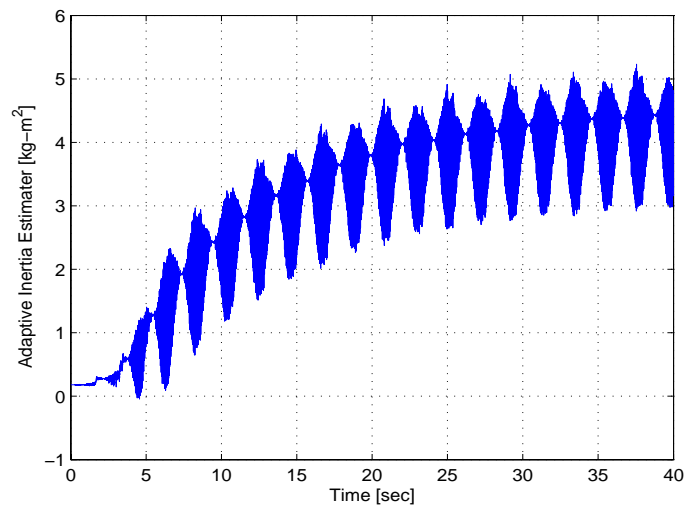
Figure 4–7: Parameter estimate for the mass of the link assembly.

be used in the adaptive feedforward term. It is expected that with more dynamics in the adaptive feedforward term that the control effort and tracking error will decrease even further in comparison with a controller that only contains a high gain feedback term.

4.6   Concluding Remarks

A new class of asymptotic controllers is developed that contains an adaptive feedforward term to account for linear parameterizable uncertainty and a high gain feedback term which accounts for unstructured disturbances. The motivation for injecting the adaptive feedforward term is that improved tracking performance and reduce control effort would result from including more knowledge of the system dynamics in the control structure. This idea was verified by our preliminary experimental results that indicate reduced RMS tracking errors when only an additional inertia estimate is used in the feedforward controller.

CHAPTER 5
CONCLUSION AND RECOMMENDATIONS

Motivated by the fact that discontinuous and piecewise continuous friction models are problematic for the development of high-performance continuous controllers, a new model for friction is proposed. The simple continuously differentiable model was shown to exhibit viscous, Coulombic, static, and Stribeck effects, and is inherently passive. A numerical simulation demonstrated the modularity of the model for use in different friction regimes. The model was also proven to closely approximate experimental data. A significant advantage of the proposed model is that the model supports the development of differentiable model-based controllers.

Based on the developed model, semi-global asymptotic tracking is proven in the presence of a proposed continuously differentiable friction model that contains uncertain nonlinear parameterizable terms. To achieve the tracking result, an integral feedback compensation term is used to identify the system friction effects. A Lyapunov-based stability analysis is provided to conclude the tracking and friction identification results. Experimental results show two orders of magnitude improvement in tracking control over a proportional derivative (PD) controller, and a one order of magnitude improvement over the model-based controller.

An extension of the developed tracking controller is presented in Chapter 4 where a new class of asymptotic controllers is developed that contains an adaptive feedforward term to account for linear parameterizable uncertainty and a high gain feedback term (as in Chapter 3) which accounts for unstructured disturbances. In comparison with previous results that used a similar high gain feedback control structure, new control development, error systems and stability analysis arguments were required to include the additional adaptive feedforward term. The motivation

for including the adaptive feedforward term is that improved tracking performance and reduce control effort would result from including more knowledge of the system dynamics in the control structure. This idea was verified by preliminary experimental results that indicate reduced RMS tracking errors when only an additional inertia estimate is used in the feedforward controller.

Future efforts can focus on expanding/adjusting the developed friction model to exhibit additional effects. Effects of wear, temperature, humidity, etc on the performance of the developed model to accurately predict friction can also be studied to make the model more robust. The developed model can also be modified to develop a more generic dynamic model for friction instead of a static map between velocity and friction.

The identification scheme developed in Chapter 3 can be used to identify nonlinear uncertainties and develop controllers to cancel their effects. For example, the developed scheme can be used to identify nonlinear disturbances during high-speed machining, in aircraft applications, etc.

Further, more controllers can be developed based on the idea of segregating the structured and unstructured uncertainties to further improve system performance. For example, neural networks and fuzzy logic can be explored to account for the structured uncertainties along with the integral feedback compensation strategy developed in Chapter 3 to account for unstructured uncertainties to achieve asymptotic stability results.

IDENTIFICATION AND COMPENSATION FOR FRICTION BY HIGH GAIN
FEEDBACK

Lemma: The term $f(\dot{q}) \in \mathbb{R}^n$ can be defined as in (2–1) as follows:

$$f(\dot{q}) = \gamma_1(\tanh(\gamma_2\dot{q}) - \tanh(\gamma_3\dot{q})) + \gamma_4\tanh(\gamma_5\dot{q}) + \gamma_6\dot{q}. \qquad \text{(A–1)}$$

The first and second time derivatives of $f(\dot{q})$ (i.e., $\dot{f}(\dot{q}, \ddot{q})$ and $\ddot{f}(\dot{q}, \ddot{q}, \dddot{q})$) exist and are bounded, provided $q(t)$, $\dot{q}(t)$, $\ddot{q}(t)$, $\dddot{q}(t) \in \mathcal{L}_\infty$.

Proof: After taking the time derivative of (A–1) the following expression can be obtained:

$$\dot{f}(\dot{q}, \ddot{q}) = \ddot{q}\left(\gamma_1\gamma_2 + \gamma_4\gamma_5 - \gamma_1\gamma_3 + \gamma_6\right) - \gamma_1\gamma_2\ddot{q}\left\|\tanh(\gamma_2\dot{q})\right\|^2 \qquad \text{(A–2)}$$
$$+ \gamma_1\gamma_3\ddot{q}\left\|\tanh(\gamma_3\dot{q})\right\|^2 - \gamma_4\gamma_5\ddot{q}\left\|\tanh(\gamma_5\dot{q})\right\|^2$$

where the following property was utilized:

$$\frac{d}{dt}\tanh(u(t)) = (1 - \tanh^2(u(t)))\frac{du(t)}{dt}.$$

The time derivative of (A–2) can be rewritten as follows:

$$\ddot{f}(\dot{q}, \ddot{q}, \dddot{q}) = \dddot{q}\left(\gamma_1\gamma_2 + \gamma_4\gamma_5 - \gamma_1\gamma_3 + \gamma_6\right) - \gamma_1\gamma_2\dddot{q}\left\|\tanh(\gamma_2\dot{q})\right\|^2 \qquad \text{(A–3)}$$
$$+ \gamma_1\gamma_3\dddot{q}\left\|\tanh(\gamma_3\dot{q})\right\|^2 - \gamma_4\gamma_5\dddot{q}\left\|\tanh(\gamma_5\dot{q})\right\|^2 - 2\gamma_1\gamma_2^2\ddot{q}^T\ddot{q}\tanh(\gamma_2\dot{q})$$
$$(1 - \left\|\tanh(\gamma_2\dot{q})\right\|^2) + 2\gamma_1\gamma_3^2\ddot{q}^T\ddot{q}\tanh(\gamma_3\dot{q})(1 - \left\|\tanh(\gamma_3\dot{q})\right\|^2)$$
$$- 2\gamma_4\gamma_5^2\ddot{q}^T\ddot{q}\tanh(\gamma_5\dot{q})(1 - \left\|\tanh(\gamma_5\dot{q})\right\|^2).$$

Assuming as in Property 3.3 that $\dot{q}(t)$, $\ddot{q}(t)$, and $\dddot{q}(t) \in \mathcal{L}_\infty$ in $\mathcal{D}$, it is straightforward from (A–1), (A–2), and (A–3) that $f(\dot{q})$, $\dot{f}(\dot{q}, \ddot{q})$, and $\ddot{f}(\dot{q}, \ddot{q}, \dddot{q}) \in \mathbb{R}^n$ exist and are bounded.

Lemma: The auxiliary error $\tilde{N}(t)$ defined in (3–16) as

$$\tilde{N}(t) = N(t) - N_d(t)$$

can be upper bounded as follows:

$$\tilde{N}(t) \leq \rho(\|z\|)\, \|z\|$$

where $\rho(\|z\|)$ is some positive globally invertible nondecreasing function.

Proof: Let $N(t) \in \mathbb{R}^n$ be defined as follows:

$$
\begin{aligned}
N(q, \dot{q}, \ddot{q}, e_1, e_2, r) &\triangleq \frac{\partial f(\dot{q})}{\partial \dot{q}} \ddot{q} - \frac{1}{2}\dot{M}(q)r + e_2 \\
&= \frac{\partial f(\dot{q})}{\partial \dot{q}} \ddot{q} - \frac{1}{2}\frac{\partial M(q)}{\partial q}\dot{q}r + e_2.
\end{aligned}
$$

The unmeasurable $\ddot{q}(t)$ can be expressed in terms of known and measurable values e_1, e_2, and r as

$$\ddot{q} = \ddot{q}_d - r - \alpha_1^2 e_1 + (\alpha_1 + \alpha_2)e_2.$$

Expanding the definition of $N(t)$, we have

$$
\begin{aligned}
N(q, \dot{q}, \ddot{q}_d, e_1, e_2, r) &\triangleq -\frac{1}{2}\frac{\partial M(q)}{\partial q}\dot{q}r + e_2 \\
&+ \frac{\partial f(\dot{q})}{\partial \dot{q}}(\ddot{q}_d - r - \alpha_1^2 e_1 + (\alpha_1 + \alpha_2)e_2).
\end{aligned}
$$

Recall the definition of $N_d(t)$:

$$
\begin{aligned}
N_d(t) &\triangleq N(q_d, \dot{q}_d, \ddot{q}_d, 0, 0, 0) \\
&= \frac{\partial f(\dot{q}_d)}{\partial \dot{q}_d}\ddot{q}_d.
\end{aligned}
$$

The auxiliary error $\tilde{N}(t)$ can then be written as the sum of errors pertaining to each of its arguments as follows:

$$\tilde{N}(t) = N(q, \dot{q}, \ddot{q}_d, e_1, e_2, r) - N(q_d, \dot{q}_d, \ddot{q}_d, 0, 0, 0)$$

$$= N(q, \dot{q}_d, \ddot{q}_d, 0, 0, 0) - N(q_d, \dot{q}_d, \ddot{q}_d, 0, 0, 0)$$

$$+ N(q, \dot{q}, \ddot{q}_d, 0, 0, 0) - N(q, \dot{q}_d, \ddot{q}_d, 0, 0, 0)$$

$$+ N(q, \dot{q}, \ddot{q}_d, 0, 0, 0) - N(q, \dot{q}, \ddot{q}_d, 0, 0, 0)$$

$$+ N(q, \dot{q}, \ddot{q}_d, e_1, 0, 0) - N(q, \dot{q}, \ddot{q}_d, 0, 0, 0)$$

$$+ N(q, \dot{q}, \ddot{q}_d, e_1, e_2, 0) - N(q, \dot{q}, \ddot{q}_d, e_1, 0, 0)$$

$$+ N(q, \dot{q}, \ddot{q}_d, e_1, e_2, r) - N(q, \dot{q}, \ddot{q}_d, e_1, e_2, 0).$$

Applying the Mean Value Theorem to further describe $\tilde{N}(t)$,

$$\tilde{N}(t) = \frac{\partial N(\sigma_1, \dot{q}_d, \ddot{q}_d, 0, 0, 0)}{\partial \sigma_1} |_{\sigma_1 = v_1} (q - q_d) \tag{A--4}$$

$$+ \frac{\partial N(q, \sigma_2, \ddot{q}_d, 0, 0, 0)}{\partial \sigma_2} |_{\sigma_2 = v_2} (\dot{q} - \dot{q}_d)$$

$$+ \frac{\partial N(q, \dot{q}, \sigma_3, 0, 0, 0)}{\partial \sigma_3} |_{\sigma_3 = v_3} (\ddot{q}_d - \ddot{q}_d)$$

$$+ \frac{\partial N(q, \dot{q}, \ddot{q}_d, \sigma_4, 0, 0)}{\partial \sigma_4} |_{\sigma_4 = v_4} (e_1 - 0)$$

$$+ \frac{\partial N(q, \dot{q}, \ddot{q}_d, e_1, \sigma_5, 0)}{\partial \sigma_5} |_{\sigma_5 = v_5} (e_2 - 0)$$

$$+ \frac{\partial N(q, \dot{q}, \ddot{q}_d, e_1, e_2, \sigma_6)}{\partial \sigma_6} |_{\sigma_6 = v_6} (r - 0)$$

where

$$v_1 \in (q_d, q)$$

$$v_2 \in (\dot{q}_d, \dot{q})$$

$$v_3 = \ddot{q}_d$$

$$v_4 \in (0, e_1)$$

$$v_5 \in (0, e_2)$$

$$v_6 \in (0, r).$$

From equation (A--4), $\tilde{N}(t)$ can be upper bounded as follows:

$$\|\tilde{N}(t)\| \leq \left\| \frac{\partial N(\sigma_1, \dot{q}_d, \ddot{q}_d, 0, 0, 0)}{\partial \sigma_1} |_{\sigma_1 = v_1} \right\| \|e_1\| \tag{A-5}$$

$$+ \left\| \frac{\partial N(q, \sigma_2, \ddot{q}_d, 0, 0, 0)}{\partial \sigma_2} |_{\sigma_2 = v_2} \right\| \|e_2 - \alpha_1 e_1\|$$

$$+ \left\| \frac{\partial N(q, \dot{q}, \ddot{q}_d, \sigma_4, 0, 0)}{\partial \sigma_4} |_{\sigma_4 = v_4} \right\| \|e_1\|$$

$$+ \left\| \frac{\partial N(q, \dot{q}, \ddot{q}_d, e_1, \sigma_5, 0)}{\partial \sigma_5} |_{\sigma_5 = v_5} \right\| \|e_2\|$$

$$+ \left\| \frac{\partial N(q, \dot{q}, \ddot{q}_d, e_1, e_2, \sigma_6)}{\partial \sigma_6} |_{\sigma_6 = v_6} \right\| \|r\| .$$

The partial derivatives of N as expressed in (A–5) can be expressed as follows:

$$\frac{\partial N(\sigma_1, \dot{q}_d, \ddot{q}_d, 0, 0, 0)}{\partial \sigma_1} = 0 \tag{A-6}$$

$$\frac{\partial N(q, \sigma_2, \ddot{q}_d, 0, 0, 0)}{\partial \sigma_2} = \frac{\partial^2 f(\dot{q})}{\partial \dot{q}^2} \ddot{q}_d$$

$$\frac{\partial N(q, \dot{q}, \ddot{q}_d, \sigma_4, 0, 0)}{\partial \sigma_4} = \frac{\partial f(\dot{q})}{\partial \dot{q}} (-\alpha_1^2)$$

$$\frac{\partial N(q, \dot{q}, \ddot{q}_d, e_1, \sigma_5, 0)}{\partial \sigma_5} = 1 + (\alpha_1 + \alpha_2) \frac{\partial f(\dot{q})}{\partial \dot{q}}$$

$$\frac{\partial N(q, \dot{q}, \ddot{q}_d, e_1, e_2, \sigma_6)}{\partial \sigma_6} = -\frac{1}{2} \frac{\partial M(q)}{\partial q} \dot{q} - \frac{\partial f(\dot{q})}{\partial \dot{q}} .$$

By noting that

$$v_2 = \dot{q} - c_2(\dot{q} - \dot{q}_d) \tag{A-7}$$

$$v_4 = e_1 - c_4(e_1 - 0) = e_1(1 - c_4)$$

$$= (q_d - q)(1 - c_4) \tag{A-8}$$

$$v_5 = e_2 - c_5(e_2 - 0) = e_2(1 - c_5)$$

$$= (\dot{e}_1 + \alpha_1 e_1)(1 - c_5) \tag{A-9}$$

$$= (\dot{q}_d - \dot{q} + \alpha_1(q_d - q))(1 - c_5)$$

$$v_6 = r - c_6(r - 0) = r(1 - c_6) = r(1 - c_6)$$

$$= (\ddot{q}_d - \ddot{q} + \alpha_1(\dot{q}_d - \dot{q}) + \alpha_2(\dot{q}_d - \dot{q} + \alpha_1(q_d - q)))(1 - c_6)$$

where $c_i \in (0, 1) \in \mathbb{R}$, $i = 2, 4, 5, 6$ are unknown constants, we can use Property 3.2

and Property 3.3 to upper bound (A–6) as follows:

$$\left\| \frac{\partial N(q, \sigma_2, \ddot{q}_d, 0, 0, 0)}{\partial \sigma_2} \Big|_{\sigma_2 = v_2} \right\| \leq \rho_2(\dot{q})$$

$$\left\| \frac{\partial N(q, \dot{q}, \ddot{q}_d, \sigma_4, 0, 0)}{\partial \sigma_4} \Big|_{\sigma_4 = v_4} \right\| \leq \rho_4(q, \dot{q})$$

$$\left\| \frac{\partial N(q, \dot{q}, \ddot{q}_d, e_1, \sigma_5, 0)}{\partial \sigma_5} \Big|_{\sigma_5 = v_5} \right\| \leq \rho_5(q, \dot{q})$$

$$\left\| \frac{\partial N(q, \dot{q}, \ddot{q}_d, e_1, e_2, \sigma_6)}{\partial \sigma_6} \Big|_{\sigma_6 = v_6} \right\| \leq \rho_6(q, \dot{q}, r)$$

where $\rho_2, \rho_4, \rho_5, \rho_6 \in \mathbb{R}$ are some positive functions nondecreasing in $q(t)$ and $\dot{q}(t)$, and where their arguments come from the variables of (A–6) and (A–7). Because equations (3–2) and (3–3) give us the following expressions for q and $\dot{q}$

$$q = q_d - e_1$$

$$\dot{q} = \dot{q}_d - e_2 + \alpha_1 e_1$$

it is seen that the upper bounds can be rewritten in terms of e_1, e_2, and r:

$$\left\| \frac{\partial N(q, \sigma_2, \ddot{q}_d, 0, 0, 0)}{\partial \sigma_2} \Big|_{\sigma_2 = v_2} \right\| \leq \rho_2(e_1, e_2)$$

$$\left\| \frac{\partial N(q, \dot{q}, \ddot{q}_d, \sigma_4, 0, 0)}{\partial \sigma_4} \Big|_{\sigma_4 = v_4} \right\| \leq \rho_4(e_1, e_2)$$

$$\left\| \frac{\partial N(q, \dot{q}, \ddot{q}_d, e_1, \sigma_5, 0)}{\partial \sigma_5} \Big|_{\sigma_5 = v_5} \right\| \leq \rho_5(e_1, e_2)$$

$$\left\| \frac{\partial N(q, \dot{q}, \ddot{q}_d, e_1, e_2, \sigma_6)}{\partial \sigma_6} \Big|_{\sigma_6 = v_6} \right\| \leq \rho_6(e_1, e_2, r).$$

The bound on $\tilde{N}(t)$ can be further simplified:

$$\left\| \tilde{N}(t) \right\| \leq \rho_2(e_1, e_2) \left\| e_2 - \alpha_1 e_1 \right\| + \rho_4(e_1, e_2) \left\| e_1 \right\|$$

$$+ \rho_5(e_1, e_2) \left\| e_2 \right\| + \rho_6(e_1, e_2, r) \left\| r \right\|$$

Using the upper bound

$$\left\| e_2 - \alpha_1 e_1 \right\| \leq \left\| e_2 \right\| + \alpha_1 \left\| e_1 \right\|$$

$\tilde{N}(t)$ can be further upper bounded as follows:

$$\left\|\tilde{N}(t)\right\| \le (\alpha_1 \rho_2(e_1, e_2) + \rho_4(e_1, e_2)) \|e_1\| + (\rho_2(e_1, e_2)$$
$$+ \rho_5(e_1, e_2)) \|e_2\| + \rho_6(e_1, e_2, r) \|r\|.$$

Using the definition of $z(t) \in \mathbb{R}^{3n}$ in (3–21), $\tilde{N}(t)$ can be expressed in terms of $z(t)$ as follows:

$$\left\|\tilde{N}(t)\right\| \le (\alpha_1 \rho_2(e_1, e_2) + \rho_4(e_1, e_2)) \|z(t)\| + (\rho_2(e_1, e_2)$$
$$+ \rho_5(e_1, e_2)) \|z(t)\| + \rho_6(e_1, e_2, r) \|z(t)\|$$
$$\le (\alpha_1 \rho_2(e_1, e_2) + \rho_4(e_1, e_2) + \rho_2(e_1, e_2) + \rho_5(e_1, e_2)$$
$$+ \rho_6(e_1, e_2, r)) \|z\|$$
$$\le \rho(\|z\|) \|z\|$$

where $\rho(\|z\|)$ is some positive globally invertible nondecreasing function (see Xian et al. [57]).

Lemma: Define the auxiliary function $L(t) \in \mathbb{R}$ as

$$L(t) \triangleq r^T (N_d(t) - \beta sgn(e_2)). \tag{A–10}$$

Then, if β satisfies

$$\beta > \zeta_{N_d} + \frac{1}{\alpha_2} \zeta_{N_d 2} \tag{A–11}$$

then

$$\int_{t_0}^{t} L(\tau) d\tau \le \zeta_b \tag{A–12}$$

where ζ_b is the following positive constant:

$$\zeta_b = \beta \|e_2(t_0)\| - e_2(t_0)^T N_d(t_0).$$

Proof: Integrating both sides of (A–10),

$$\int_{t_0}^{t} L(\tau)d\tau = \int_{t_0}^{t} r(\tau)^T (N_d(\tau) - \beta sgn(e_2(\tau)))d\tau. \tag{A–13}$$

Substituting (3–4) into (A–13),

$$\int_{t_0}^{t} L(\tau)d\tau = \int_{t_0}^{t} (\frac{\partial e_2(\tau)}{\partial \tau}^T N_d(\tau) + \alpha_2 e_2(\tau)^T N_d(\tau) \tag{A–14}$$

$$- \frac{\partial e_2(\tau)}{\partial \tau}^T \beta sgn(e_2(\tau)) - \alpha_2 \beta e_2(\tau)^T sgn(e_2(\tau)))d\tau$$

$$= \int_{t_0}^{t} \alpha_2 e_2(\tau)^T (N_d(\tau) - \beta sgn(e_2(\tau)))d\tau$$

$$+ \int_{t_0}^{t} \frac{\partial e_2(\tau)}{\partial \tau}^T N_d(\tau)d\tau - \int_{t_0}^{t} \frac{\partial e_2(\tau)}{\partial \tau}^T \beta sgn(e_2(\tau))d\tau.$$

After integrating the second integral in (A–14) using integration by parts,

$$\int_{t_0}^{t} L(\tau)d\tau = \int_{t_0}^{t} \alpha_2 e_2(\tau)^T (N_d(\tau) - \beta sgn(e_2(\tau)))d\tau \tag{A–15}$$

$$+ e_2(\tau)^T N_d(\tau) \mid_{t_0}^{t} - \int_{t_0}^{t} e_2(\tau)^T \frac{\partial N_d(\tau)}{d\tau} d\tau - \int_{t_0}^{t} \frac{\partial e_2(\tau)}{\partial \tau}^T \beta sgn(e_2(\tau))d\tau$$

$$= \int_{t_0}^{t} \alpha_2 e_2(\tau)^T (N_d(\tau) - \frac{1}{\alpha_2}(\frac{\partial N_d(\tau)}{\partial \tau}) - \beta sgn(e_2(\tau)))d\tau$$

$$+ e_2(t)^T N_d(t) - e_2(t_0)^T N_d(t_0) - \beta \|e_2(t)\| + \beta \|e_2(t_0)\|$$

$$\leq \int_{t_0}^{t} \alpha_2 \|e_2(\tau)\| (\|N_d(\tau)\| + \frac{1}{\alpha_2} \left\| \frac{\partial N_d(\tau)}{\partial \tau} \right\| - \beta)d\tau$$

$$+ \|e_2(t)\| (\|N_d(t)\| - \beta) + \beta \|e_2(t_0)\| - e_2(t_0)^T N_d(t_0).$$

Thus, it is clear from (A–15) that if β satisfies (A–11), then (A–12) holds [57].

APPENDIX B
TRACKING CONTROL IN THE PRESENCE OF FRICTION BY HIGH GAIN FEEDBACK AND A MODEL-BASED FEEDFORWARD COMPONENT-AN EXTENSION

Lemma: The auxiliary error $\tilde{N}(t)$ defined in (4–22) as

$$\tilde{N}(t) = N(t) - N_d(t)$$

can be upper bounded as follows:

$$\left\| \tilde{N}(t) \right\| \le \rho \left(\|z\| \right) \|z\|$$

where $\rho \left(\|z\| \right)$ is some positive globally invertible nondecreasing function.

Proof: $N(t) \in \mathbb{R}^n$ in (4–19) can be expressed as follows:

$$N\left(q, \dot{q}, \ddot{q}_d, \dddot{q}_d, e_1, e_2, r\right) = -Y_d \Gamma \dot{Y}_d^T r + \frac{\partial M(q)}{\partial q} \dot{q} \left\{ \begin{array}{c} \alpha_1 \left(e_2 - \alpha_1 e_1\right) \\ \\ +\alpha_2 e_2 \end{array} \right\}$$

$$+ M(q)\alpha_1 [\{r - \alpha_2 e_2 - \alpha_1 \left(e_2 - \alpha_1 e_1\right)\} + \alpha_2 \left(r - \alpha_2 e_2\right)]$$

$$+ \frac{\partial M(q)}{\partial q} \dot{q} \ddot{q}_d + M(q) \dddot{q}_d + \frac{\partial V_m(q, \dot{q})}{\partial q} \dot{q}^2 + \frac{\partial V_m(q, \dot{q})}{\partial \dot{q}} \dot{q}(\ddot{q}_d$$

$$- r + \alpha_2 e_2 + \alpha_1 e_2 - \alpha_1^2 e_1) + V_m(q, \dot{q})(\ddot{q}_d - r + \alpha_2 e_2$$

$$+ \alpha_1 e_2 - \alpha_1^2 e_1) + \frac{\partial G(q)}{\partial q} \dot{q} + \frac{\partial f(\dot{q})}{\partial \dot{q}} (\ddot{q}_d - r + \alpha_2 e_2$$

$$+ \alpha_1 e_2 - \alpha_1^2 e_1) - \dot{Y}_d \theta + e_2 - \frac{1}{2} \frac{\partial M(q)}{\partial q} \dot{q} r$$

where the following are used:

$$\dot{q} = \dot{q}_d - (e_2 - a_1 e_1), \tag{B–1}$$

$$\ddot{q} = \ddot{q}_d - r + \alpha_2 e_2 + \alpha_1 e_2 - \alpha_1^2 e_1.$$

Recall the definition of $N_d(t)$:

$$N_d(t) \triangleq N(q_d, \dot{q}_d, \ddot{q}_d, 0, 0, 0)$$

$$= \frac{\partial f(\dot{q}_d)}{\partial \dot{q}_d}\ddot{q}_d + \frac{\partial M(q_d)}{\partial q_d}\dot{q}_d\ddot{q}_d + M(q_d)\dddot{q}_d + \frac{\partial V_m(q_d, \dot{q}_d)}{\partial q_d}\dot{q}_d^2$$

$$+ \frac{\partial V_m(q_d, \dot{q}_d)}{\partial \dot{q}_d}\dot{q}_d\ddot{q}_d + V_m(q_d, \dot{q}_d)\ddot{q}_d + \frac{\partial G(q_d)}{\partial q_d}\dot{q}_d - \dot{Y}_d\theta.$$

The auxiliary error $\tilde{N}(t)$ can be written as the sum of errors pertaining to each of its arguments as follows:

$$\tilde{N}(t) = N\left(q, \dot{q}, \ddot{q}_d, \dddot{q}_d, e_1, e_2, r\right) - N\left(q_d, \dot{q}_d, \ddot{q}_d, \dddot{q}_d, 0, 0, 0\right)$$

$$= N\left(q, \dot{q}_d, \ddot{q}_d, \dddot{q}_d, 0, 0, 0\right) - N\left(q_d, \dot{q}_d, \ddot{q}_d, \dddot{q}_d, 0, 0, 0\right)$$

$$+ N\left(q, \dot{q}, \ddot{q}_d, \dddot{q}_d, 0, 0, 0\right) - N\left(q, \dot{q}_d, \ddot{q}_d, \dddot{q}_d, 0, 0, 0\right)$$

$$+ N\left(q, \dot{q}, \ddot{q}_d, \dddot{q}_d, 0, 0, 0\right) - N\left(q, \dot{q}, \ddot{q}_d, \dddot{q}_d, 0, 0, 0\right)$$

$$+ N\left(q, \dot{q}, \ddot{q}_d, \dddot{q}_d, 0, 0, 0\right) - N\left(q, \dot{q}, \ddot{q}_d, \dddot{q}_d, 0, 0, 0\right)$$

$$+ N\left(q, \dot{q}, \ddot{q}_d, \dddot{q}_d, e_1, 0, 0\right) - N\left(q, \dot{q}, \ddot{q}_d, \dddot{q}_d, 0, 0, 0\right)$$

$$+ N\left(q, \dot{q}, \ddot{q}_d, \dddot{q}_d, e_1, e_2, 0\right) - N\left(q, \dot{q}, \ddot{q}_d, \dddot{q}_d, e_1, 0, 0\right)$$

$$+ N\left(q, \dot{q}, \ddot{q}_d, \dddot{q}_d, e_1, e_2, r\right) - N\left(q, \dot{q}, \ddot{q}_d, \dddot{q}_d, e_1, e_2, 0\right).$$

Applying the Mean Value Theorem to further describe $\tilde{N}(t)$,

$$\tilde{N}(t) = \frac{\partial N(\sigma_1, \dot{q}_d, \ddot{q}_d, \dddot{q}_d, 0, 0, 0)}{\partial \sigma_1}\Big|_{\sigma_1 = v_1} (q - q_d) \qquad \text{(B--2)}$$

$$+ \frac{\partial N(q, \sigma_2, \ddot{q}_d, \dddot{q}_d, 0, 0, 0)}{\partial \sigma_2}\Big|_{\sigma_2 = v_2} (\dot{q} - \dot{q}_d)$$

$$+ \frac{\partial N(q, \dot{q}, \sigma_3, \dddot{q}_d, 0, 0, 0)}{\partial \sigma_3}\Big|_{\sigma_3 = v_3} (\ddot{q}_d - \ddot{q}_d)$$

$$+ \frac{\partial N(q, \dot{q}, \ddot{q}_d, \sigma_4, 0, 0, 0)}{\partial \sigma_4}\Big|_{\sigma_4 = v_4} (\dddot{q}_d - \dddot{q}_d)$$

$$+ \frac{\partial N(q, \dot{q}, \ddot{q}_d, \dddot{q}_d, \sigma_5, 0, 0)}{\partial \sigma_5}\Big|_{\sigma_5 = v_5} (e_1 - 0)$$

$$+ \frac{\partial N(q, \dot{q}, \ddot{q}_d, \dddot{q}_d, e_1, \sigma_6, 0)}{\partial \sigma_6}\Big|_{\sigma_6 = v_6} (e_2 - 0)$$

$$+ \frac{\partial N(q, \dot{q}, \ddot{q}_d, \dddot{q}_d, e_1, e_2, \sigma_7)}{\partial \sigma_7}\Big|_{\sigma_7 = v_7} (r - 0)$$

where

$$v_1 \in (q_d, q)$$

$$v_2 \in (\dot{q}_d, \dot{q})$$

$$v_3 \in (\ddot{q}_d, \ddot{q}_d)$$

$$v_4 \in (\dddot{q}_d, \dddot{q}_d)$$

$$v_5 \in (0, e_1)$$

$$v_6 \in (0, e_2)$$

$$v_7 \in (0, r).$$

From equation (B–2), $\tilde{N}(t)$ can be upper bounded as follows:

$$\left\| \tilde{N}(t) \right\| \leq \left\| \frac{\partial N(\sigma_1, \dot{q}_d, \ddot{q}_d, \dddot{q}_d, 0, 0, 0)}{\partial \sigma_1} \Big|_{\sigma_1 = v_1} \right\| \|e_1\| \tag{B–3}$$

$$+ \left\| \frac{\partial N(q, \sigma_2, \ddot{q}_d, \dddot{q}_d, 0, 0, 0)}{\partial \sigma_2} \Big|_{\sigma_2 = v_2} \right\| \|e_2 - a_1 e_1\|$$

$$+ \left\| \frac{\partial N(q, \dot{q}, \ddot{q}_d, \dddot{q}_d, \sigma_5, 0, 0)}{\partial \sigma_5} \Big|_{\sigma_5 = v_5} \right\| \|e_1\|$$

$$+ \left\| \frac{\partial N(q, \dot{q}, \ddot{q}_d, \dddot{q}_d, e_1, \sigma_6, 0)}{\partial \sigma_6} \Big|_{\sigma_6 = v_6} \right\| \|e_2\|$$

$$+ \left\| \frac{\partial N(q, \dot{q}, \ddot{q}_d, \dddot{q}_d, e_1, e_2, \sigma_7)}{\partial \sigma_7} \Big|_{\sigma_7 = v_7} \right\| \|r\|.$$

The partial derivatives of N as expressed in (B–3) can be expressed as follows:

$$\frac{\partial N(\sigma_1, \dot{q}_d, \ddot{q}_d, \dddot{q}_d, 0, 0, 0)}{\partial \sigma_1} = \frac{\partial^2 M(\sigma_1)}{\partial \sigma_1^2} \dot{q}_d \ddot{q}_d + \frac{\partial M(\sigma_1)}{\partial \sigma_1} \dddot{q}_d \tag{B–4}$$

$$+ \frac{\partial^2 V_m(\sigma_1, \dot{q}_d)}{\partial \sigma_1^2} \dot{q}_d^2 + \frac{\partial^2 V_m(\sigma_1, \dot{q}_d)}{\partial \sigma_1 \partial \dot{q}_d} \dot{q}_d \ddot{q}_d$$

$$+ \frac{\partial V_m(\sigma_1, \dot{q}_d)}{\partial \sigma_1} \ddot{q}_d + \frac{\partial^2 G(\sigma_1)}{\partial \sigma_1^2} \dot{q}_d - \frac{\partial \dot{Y}_d \theta}{\partial \sigma_1},$$

$$\frac{\partial N(q, \sigma_2, \ddot{q}_d, \dddot{q}_d, 0, 0, 0)}{\partial \sigma_2} = \frac{\partial M(q)}{\partial q}\ddot{q}_d + \frac{\partial^2 V_m(q, \sigma_2)}{\partial \sigma_2 \partial q}\sigma_2^2 + 2\frac{\partial V_m(q, \sigma_2)}{\partial q}\sigma_2$$

$$+ \frac{\partial^2 V_m(q, \sigma_2)}{\partial \sigma_2^2}\sigma_2\ddot{q}_d + \frac{\partial V_m(q, \sigma_2)}{\partial \sigma_2}\ddot{q}_d + \frac{\partial G(q)}{\partial q}$$

$$+ \frac{\partial^2 f(\sigma_2)}{\partial \sigma_2^2}\ddot{q}_d - \frac{\partial \dot{Y}_d \theta}{\partial \sigma_2},$$

$$\frac{\partial N(q, \dot{q}, \ddot{q}_d, \dddot{q}_d, \sigma_5, 0, 0)}{\partial \sigma_5} = -\alpha_1^2(\frac{\partial M(q)}{\partial q}\dot{q} + \frac{\partial V_m(q, \dot{q})}{\partial \dot{q}}\dot{q} + V_m(q, \ddot{q}_d)$$

$$+ \frac{\partial f(\dot{q})}{\partial \dot{q}}) + \alpha_1^3 M(q) - \frac{\partial \dot{Y}_d \theta}{\partial \sigma_5},$$

$$\frac{\partial N(q, \dot{q}, \ddot{q}_d, \dddot{q}_d, e_1, \sigma_6, 0)}{\partial \sigma_6} = \frac{\partial M(q)}{\partial q}\dot{q}(\alpha_1 + \alpha_2) - M(q)\left(\alpha_1\alpha_2 + \alpha_1^2 + \alpha_2^2\right)$$

$$- \frac{\partial \dot{Y}_d \theta}{\partial \sigma_6} + 1 + (\alpha_1 + \alpha_2)\left(\frac{\partial f(\dot{q})}{\partial \dot{q}} + V_m(q, \dot{q})\right)$$

$$+ \frac{\partial V_m(q, \dot{q})}{\partial \dot{q}}\dot{q}),$$

$$\frac{\partial N(q, \dot{q}, \ddot{q}_d, \dddot{q}_d, e_1, e_2, \sigma_7)}{\partial \sigma_7} = \frac{\partial Y_d \Gamma \dot{Y}_d^T}{\partial \sigma_7}\sigma_7 - Y_d \Gamma \dot{Y}_d^T + M(q)(\alpha_1 + \alpha_2) - \frac{\partial f(\dot{q})}{\partial \dot{q}}$$

$$- \frac{\partial V_m(q, \dot{q})}{\partial \dot{q}}\dot{q} - V_m(q, \dot{q}) - \frac{\partial \dot{Y}_d \theta}{\partial \sigma_7} - \frac{1}{2}\frac{\partial M(q)}{\partial q}\dot{q}.$$

By noting that

$$v_1 = q - c_1(q - q_d)$$

$$v_2 = \dot{q} - c_2(\dot{q} - \dot{q}_d)$$

$$v_5 = e_1(1 - c_5)$$

$$v_6 = e_2(1 - c_6)$$

$$v_7 = r(1 - c_7)$$

where $c_i \in (0, 1) \in \mathbb{R}$, $i = 1, 2, 5, 6, 7$ are unknown constants, we can upper bound (B–4) as follows:

$$\left\| \frac{\partial N(\sigma_1, \dot{q}_d, \ddot{q}_d, \dddot{q}_d, 0, 0, 0)}{\partial \sigma_1} \Big|_{\sigma_1 = v_1} \right\| \leq \rho_1(e_1)$$

$$\left\| \frac{\partial N(q, \sigma_2, \ddot{q}_d, \dddot{q}_d, 0, 0, 0)}{\partial \sigma_2} \Big|_{\sigma_2 = v_2} \right\| \leq \rho_2(e_1, e_2)$$

$$\left\| \frac{\partial N(q, \dot{q}, \ddot{q}_d, \dddot{q}_d, \sigma_5, 0, 0)}{\partial \sigma_5} \Big|_{\sigma_5 = v_5} \right\| \leq \rho_5(e_1, e_2)$$

$$\left\| \frac{\partial N(q, \dot{q}, \ddot{q}_d, \dddot{q}_d, e_1, \sigma_6, 0)}{\partial \sigma_6} \Big|_{\sigma_6 = v_6} \right\| \leq \rho_6(e_1, e_2)$$

$$\left\| \frac{\partial N(q, \dot{q}, \ddot{q}_d, \dddot{q}_d, e_1, e_2, \sigma_7)}{\partial \sigma_7} \Big|_{\sigma_7 = v_7} \right\| \leq \rho_7(e_1, e_2, r).$$

The bound on $\tilde{N}(t)$ can be further simplified:

$$\left\| \tilde{N}(t) \right\| \leq \rho_1(e_1) \|e_1\| + \rho_2(e_1, e_2) \|e_2 - \alpha_1 e_1\|$$

$$+ \rho_5(e_1, e_2) \|e_1\| + \rho_6(e_1, e_2) \|e_2\|$$

$$+ \rho_7(e_1, e_2, r) \|r\|.$$

Using the upper bound

$$||e_2 - \alpha_1 e_1|| \leq \|e_2\| + \alpha_1 \|e_1\|.$$

$\tilde{N}(t)$ can be further upper bounded as follows:

$$\left\| \tilde{N}(t) \right\| \leq (\rho_1(e_1) + \alpha_1 \rho_2(e_1, e_2) + \rho_5(e_1, e_2)) \|e_1\|$$

$$+ (\rho_2(e_1, e_2) + \rho_6(e_1, e_2)) \|e_2\| + \rho_7(e_1, e_2, r) \|r\|.$$

Using the definition of $z(t) \in \mathbb{R}^{3n}$ in (4–24), $\tilde{N}(t)$ can be expressed in terms of $z(t)$ as follows:

$$\left\| \tilde{N}(t) \right\| \leq \left(\rho_1(e_1) + \alpha_1 \rho_2(e_1, e_2) + \rho_5(e_1, e_2) \right) \|z(t)\|$$
$$+ \left(\rho_2(e_1, e_2) + \rho_6(e_1, e_2) \right) \|z(t)\|$$
$$+ \rho_7(e_1, e_2, r) \|z(t)\|$$
$$\leq \left(\rho_1(e_1) + \alpha_1 \rho_2(e_1, e_2) + \rho_5(e_1, e_2) \right.$$
$$\left. + \rho_2(e_1, e_2) + \rho_6(e_1, e_2) + \rho_7(e_1, e_2, r) \right) \|z(t)\| .$$

Therefore,

$$\left\| \tilde{N}(t) \right\| \leq \rho\left(\|z\| \right) \|z\|$$

where $\rho\left(\|z\| \right)$ is some positive globally invertible nondecreasing function.

REFERENCES

[1] B. Armstrong -Helouvry, *Control of Machines with Friction*, Kluwer Academic Publishers, Boston, MA, 1991.

[2] B. Armstrong -Helouvry, P. Dupont, and C. Canudas de Wit, "A Survey of Models, Analysis Tools and Compensation Methods for the Control of Machines with Friction," *Automatica*, Vol. 30, No. 7, pp. 1083-1138, 1994.

[3] R. J. Antsaklis and K. M. Passino, eds., *An Introduction to Intelligent and Autonomous Control*, Kluwer Academic Publishers, Norwell, MA, 1993.

[4] N. Barahanov and R. Ortega, "Necessary and Sufficient Conditions for Passivity of the LuGre Friction Model," *IEEE Transactions on Automatic Control*, Vol. 45, No. 4, pp. 830-832, April 2000.

[5] P. A. Bliman and M. Sorine, "Easy-to-use Realistic Dry Friction Models for Automatic Control," in *Proceedings of the 3rd European. Control Conference*, Rome, Italy, pp. 3788-3794, 1995.

[6] F. P. Bowden and D. Tabor, *The Friction and Lubrication of Solids,* Clarendon Press, Oxford, UK, 1950.

[7] Z. Cai, M.S. de Queiroz, and D.M. Dawson, "Robust Adaptive Asymptotic Tracking of Nonlinear Systems with Additive Disturbance," *Proceedings of Conference on Decision and Control, and the European Control Conference*, Seville, Spain, pp. 2877-2882, 2005.

[8] C. Canudas de Wit, H. Olsson, K. J. Astrom, and P. Lischinsky, "A New Model for Control of Systems with Friction," *IEEE Transactions Automatic Control*, Vol. 40, pp. 419-425, March 1995.

[9] C. Canudas de Wit and P. Lichinsky, "Adaptive Friction Compensation with Dynamic Friction Model," *Proceedings of the IFAC World Congress*, San Francisco, CA, pp. 197-202, 1996.

[10] C. Canudas de Wit and P. Lichinsky, "Adaptive Friction Compensation with Partially Known Dynamic Friction Model," *International Journal on Adaptive Control and Signal Processing*, Vol. 11, pp. 65-80, 1997.

[11] C. Canudas de Wit and R. Kelly, "Passivity-Based Control Design for Robots with Dynamic Friction Model," *Proceedings of the IASTED International Conference on Robotics and Manufacturing*, Cancun, Mexico, pp. 84-87, 1997.

[12] Y.-Y. Chen, P.-Y. Huang, and J.-Y. Yen, "Frequency-Domain Identification Algorithms for Servo Systems with Friction," *IEEE Transactions on Control Systems Technology*, Vol. 10, No. 5, pp. 654-665, September 2002.

[13] S.-I. Cho and I.-J. Ha, "A Learning Approach to Tracking in Mechanical Systems with Friction," *IEEE Transactions on Automatic Control*, Vol. 45, No. 1, pp. 111-116, January 2000.

[14] P. Dahl, *A Solid Friction Model*, The Aerospace Corporation, El Segundo, CA, Tech. Rep. TOR-0158(3107-18), 1968.

[15] D. M. Dawson, J. Hu, and T. C. Burg, *Nonlinear Control of Electric Machinery*, Marcel Dekker Inc., New York, NY, 1998.

[16] W. E. Dixon, A. Behal, D. M. Dawson, and S. Nagarkatti, *Nonlinear Control of Engineering Systems: A Lyapunov-Based Approach*, Birkhäuser, Boston, MA, 2003.

[17] W. E. Dixon, Y. Fang, D. M. Dawson, and T. J. Flynn, "Range Identification for Perspective Vision Systems," *IEEE Transactions on Automatic Control*, Vol. 48, No. 12, pp. 2232-2238, 2003.

[18] P. Dupont, V. Hayward, B. Armstrong, and F. Altpeter, "Single State Elastoplastic Friction Models," *IEEE Transactions Automatic Control*, Vol. 47, pp. 683-687, April 2002.

[19] M. R. Elhami and D. J. Brookfield, "Sequential Identification of Coulomb and Viscous Friction in Robot Drives," *Automatica*, Vol. 33, No. 3, pp. 393-401, 1997.

[20] M. Feemster, D. M. Dawson, A. Behal, and W. E. Dixon, "Tracking Control in the Presence of Nonlinear Dynamic Frictional Effects: Robot Extension," *Asian Journal of Control*, Vol. 1, No. 3, pp. 153-168, 1999.

[21] G. Ferretti, G. Magnani, G. Martucci, P. Rocco, V. Stampacchia, *Friction Model Validation in Sliding and Presliding Regimes with High Resolution Encoders*, in Experimental Robotics VIII., B. Siciliano and P. Dario, Eds., Springer-Verlag, New York, NY, pp. 328-337, 2003.

[22] G. Ferretti, G. Magnani, and P. Rocco, " Single and Multistate Integral Friction Models," *IEEE Transactions Automatic Control*, Vol. 49, pp. 2292-2297, December 2004.

[23] B. Friedland and Y. J. Park, "On Adaptive Friction Compensation," *IEEE Transactions on Automatic Control*, Vol. 45, No. 4, pp. 1609-1612, April 2000.

[24] J.A. Greenwood and J.B.P. Williamson, "Contact of Nominally Flat Surfaces," *Proceedings of the Royal Society of London. Series A, Mathematical and Physical Sciences*, Vol. 295, pp. 300-319, 1966.

[25] S. Gupta, D. Aiken, G. Hu, W .E. Dixon, "Lyapunov-Based Range and Motion Identification for a Nonaffine Perspective Dynamic System," *Proceedings of the IEEE American Control Conference*, Minneapolis, Minnesota, June 2006, to appear.

[26] R. H. A. Hensen, G. Z. Angelis, M. J. G. van de Molengraft, A. G. de Jager, and J. J. Kok, "Grey-box modeling of friction: An experimental case study," *European Journal of Control*, Vol. 6, No. 3, pp. 258–267, 2000.

[27] R. H. A. Hensen, M. J. G. van de Molengraft, and M. Steinbuch, "Frequency Domain Identification of Dynamic Friction Model Parameters," *IEEE Transactions on Control Systems Technology*, Vol. 10, No. 2, pp. 191-196, March 2002.

[28] R. M. Hirschorn and G. Miller, "Control of Nonlinear Systems with Friction," *IEEE Transactions on Control Systems Technology*, Vol. 7, No. 5, pp. 588-595, September 1999.

[29] S. Jain, F. Khorrami, N. Ahmad, S. Sankaranarayanan, "Friction Compensation for Drives with and without Transmission Compliance," *Proceedings of the IEEE American Control Conference*, Albuquerque, NM, pp. 2925-2929, 1997.

[30] H. K. Khalil, *Nonlinear Systems*, 3rd ed., Prentice-Hall Inc., Upper Saddle River, NJ, 2002.

[31] S.-J. Kim and I.-J. Ha, "A Frequency-Domain Approach to Identification of Mechanical Systems with Friction," *IEEE Transactions on Automatic Control*, Vol. 46, No. 6, pp. 888-893, June 2001.

[32] S.-J. Kim, S.-Y. Kim, and I.-J. Ha, "An Efficient Identification Method for Friction in Single-DOF Motion Control Systems," *IEEE Transactions on Control Systems Technology*, Vol. 12, No. 4, pp. 555-563, July 2004.

[33] M. Krstic, I. Kanellakopoulos, and P. Kokotovic, *Nonlinear and Adaptive Control Design*, Wiley-Interscience Publications, New York, NY, 1995.

[34] V. Lampaert, J. Swevers, and F. Al-Bender, "Modification of the Leuven Integrated Friction Model Structure," *IEEE Transactions on Automatic Control*, Vol. 47, No. 4, pp. 683-687, April 2002.

[35] F. Lewis, C. Abdallah, and D. Dawson, *Control of Robot Manipulator*, MacMillan Publishing Co., New York, NY, 1993.

[36] F. L. Lewis, J. Campos, and R. Selmic, *Neuro-Fuzzy Control of Industrial Systems with Actuator Nonlinearities*, SIAM, Philadelphia, PA, 2002.

[37] T.-L. Liao and T.-I. Chien, "An Exponentially Stable Adaptive Friction Compensator," *IEEE Transactions on Automatic Control*, Vol. 45, No. 5, pp. 977-980, May 2000.

[38] W. Lin and C. Qian, "Adaptive control of nonlinearly parameterized systems: a nonsmooth feedback framework," *IEEE Transactions on Automatic Control,* Vol. 47, No. 5, pp. 757-774, 2002.

[39] M. Loffler, N. Costescu, and D. Dawson, "Qmotor 3.0 and the Qmotor Robotic Toolkit - An Advanced PC-Based Real-Time Control Platform," *IEEE Control Systems Magazine,* Vol. 22, No. 3, pp. 12-26, June, 2002.

[40] C. Makkar, W. E. Dixon, W. G. Sawyer, G. Hu, "Lyapunov-Based Tracking Control in the Presence of Uncertain Nonlinear Parameterizable Friction," *Proceedings of the IEEE American Control Conference,* Portland, Oregon, pp. 1975-1980, 2005.

[41] C. Makkar, W. E. Dixon, W. G. Sawyer, G. Hu, "Lyapunov-Based Tracking Control in the Presence of Uncertain Nonlinear Parameterizable Friction," *IEEE Transactions on Automatic Control,* submitted.

[42] C. Makkar, W. E. Dixon, W. G. Sawyer, and G.Hu, "A New Continuously Differentiable Friction Model for Control Systems Design," *IEEE/ASME International Conference on Advanced Intelligent Mechatronics,* Monterey, CA, pp. 600-605, 2005.

[43] C. Makkar, W. E. Dixon, W. G. Sawyer, and G. Hu, "A New Continuously Differentiable Friction Model for Control Systems Design," *System and Control Letters,* submitted.

[44] M. McIntyre, W. E. Dixon, D. M. Dawson, and I. D. Walker, "Fault Detection and Identification for Robot Manipulators," *IEEE Transactions on Robotics,* Vol. 21, No. 5, pp. 1028-1034, 2005.

[45] P. M. Patre, W. E. Dixon, C. Makkar, and W. MacKunis, "Asymptotic Tracking for Systems with Structured and Unstructured Uncertainties," *Proceedings of Conference on Decision and Control,* San Diego, CA, 2006, submitted.

[46] Z. Qu, *Robust Control of Nonlinear Uncertain Systems,* Wiley-Interscience Publications, New York, NY, 1998.

[47] S. Sastry and M. Bodson, *Adaptive Control: Stability, Convergence, and Robustness,* Prentice-Hall, Upper Saddle River, NJ, 1989.

[48] T. Schmitz, J. E. Action, J. C. Ziegert, and W. G. Sawyer, "The Difficulty of Measuring Low Friction: Uncertainty Analysis for Friction Coefficient Measurements," *Journal of Tribology,* Vol. 127, pp. 673-678.

[49] A. Serrani, A. Isidori, and L. Marconi, "Semiglobal nonlinear output regulation with adaptive internal model," *IEEE Transactions on Automatic Control,* Vol. 46, pp. 1178–1194, August 2001.

[50] S. Sivakumar and F. Khorrami, "Friction Compensation via Variable Structure Control: Regulation and Low Velocity Tracking," *Proceedings of the IEEE Conference on Control Applications*, Hartford, CT., pp. 645-650, 1997.

[51] J. J. Slotine and W. Li, *Applied Nonlinear Control*, Prentice-Hall, Upper Sadle River, NJ, 1991.

[52] J. Swevers, F. Al-Bender, C. G. Ganseman, and T. Prajogo, "An Integrated Friction Model Structure with Improved Presliding Behavior for Accurate Friction Compensation," *IEEE Transactions Automatic Control*, Vol. 45, pp. 675-686, April 2000.

[53] P. Tomei, "Robust Adaptive Control of Robots with Arbitrary Transient Performance and Disturbance Attenuation," *IEEE Transactions on Automatic Control*, Vol. 44, pp. 654-658, 1999.

[54] P. Tomei, "Robust Adaptive Friction Compensation for Tracking Control of Robot Manipulators," *IEEE Transactions on Automatic Control*, Vol. 45, No. 11, pp. 2164-2169, November 2000.

[55] V. I. Utkin, *Sliding Modes in Control and Optimization*, Springer-Verlag, New York, NY, 1992.

[56] P. Vedagarbda, D. M. Dawson, and M. Feemster, "Tracking Control of Mechanical Systems in the Presence of Nonlinear Dynamic Friction Effects," *IEEE Transactions on Control Systems Technology*, Vol. 7, pp. 446-456, July 1999.

[57] B. Xian, D. M. Dawson, M. S. de Queiroz, and J. Chen, "A Continuous Asymptotic Tracking Control Strategy for Uncertain Multi-Input Nonlinear Systems," *IEEE Transactions on Automatic Control*, Vol. 49, No. 7, pp. 1206-1206, July 2004.

[58] B. Xian, M.S. de Queiroz, D.M. Dawson, and M. McIntyre, "A Discontinuous Output Feedback Controller and Velocity Observer for Nonlinear Mechanical Systems," *Automatica*, Vol. 40, No. 4, pp. 695-700, April 2004.

[59] X. Zhang, A. Behal, D. M. Dawson, and B. Xian, "Output Feedback Control for a Class of Uncertain MIMO Nonlinear Systems With Non-Symmetric Input Gain Matrix," *Proceedings of Conference on Decision and Control, and the European Control Conference*, Seville, Spain, pp. 7762-7767, 2005.

[60] T. Zhang and M. Guay, "Comments on 'An Exponentially Stable Adaptive Friction Compensator'," *IEEE Transactions on Automatic Control*, Vol. 46, No. 11, pp. 1844-1845, November 2001.

BIOGRAPHICAL SKETCH

Charu Makkar was born in New Delhi, the capital city of India. She completed her Bachelor in Technology in the year 2003 from GGS Indraprastha University, Delhi. She worked for a year in Continental Device India Ltd., the leading semi-conductor manufacturing firm in India as a Process RD Engineer. She then joined the nonlinear controls and robotics research group in the University of Florida for Master of Science in mechanical and aerospace engineering in the year 2004.

She will join Deloitte Consulting as a Systems Analyst in July 2006.